

2022

Design and development of 3D printed fins integrated into an instrumented surfboard

Pawel Krzyzanowski

Follow this and additional works at: <https://ro.uow.edu.au/theses1>

University of Wollongong

Copyright Warning

You may print or download ONE copy of this document for the purpose of your own research or study. The University does not authorise you to copy, communicate or otherwise make available electronically to any other person any copyright material contained on this site.

You are reminded of the following: This work is copyright. Apart from any use permitted under the Copyright Act 1968, no part of this work may be reproduced by any process, nor may any other exclusive right be exercised, without the permission of the author. Copyright owners are entitled to take legal action against persons who infringe their copyright. A reproduction of material that is protected by copyright may be a copyright infringement. A court may impose penalties and award damages in relation to offences and infringements relating to copyright material.

Higher penalties may apply, and higher damages may be awarded, for offences and infringements involving the conversion of material into digital or electronic form.

Unless otherwise indicated, the views expressed in this thesis are those of the author and do not necessarily represent the views of the University of Wollongong.

Research Online is the open access institutional repository for the University of Wollongong. For further information contact the UOW Library: research-pubs@uow.edu.au



UNIVERSITY
OF WOLLONGONG
AUSTRALIA

**Design and development of 3D printed fins
integrated into an instrumented surfboard.**

This thesis is presented as part of the requirement for the conferral
of the degree:

Master of Philosophy (Biofabrication)

Faculty of Science, Medicine and Health
School of Chemistry and Molecular Bioscience

By:

Pawel Krzyzanowski

Supervised by:

Professor Marc in het Panhuis

2022

Certification

I, Pawel Krzyzanowski, declare that this thesis submitted in fulfilment of the requirements for the conferral of the degree Master of Philosophy, from the University of Wollongong, is wholly my own work unless otherwise referenced or acknowledged. This document has not been submitted for qualifications at any other academic institution.

Pawel Krzyzanowski

28th February 2022

Contents

Certification.....	1
List of Names or Abbreviations	6
List of Figures	8
List of Tables.....	15
Acknowledgements	18
Abstract	19
Chapter 1: Introduction	21
1.1. Sport of surfing.....	21
1.2. Surfboard fins	22
1.3. Composite materials	23
1.4. Computer Aided Design (CAD).....	26
1.5. Computer Aided Manufacturing (CAM).....	27
1.6. Computational Fluid Dynamics (CFD) analysis	28
1.7. Additive manufacturing (3D printing) techniques	30
1.8. Electronics and signal processing.....	33
1.8.1. Microcontrollers and microprocessors	33
1.8.2. Load cells and Wheatstone bridge.....	34
1.8.3. Gyroscope.....	35
1.8.4. Accelerometer	36
1.8.5. Global Positioning System (GPS)	36
1.8.6. Transceiver	37
1.8.7. Cell phone as everyday measurement tool	37

1.9.	C++ programming language.....	39
1.10.	Polymer heat treatment (annealing).....	40
1.11.	Mechanical testing (three point bend test).....	41
1.12.	Aims	43
Chapter 2: Materials and methods		45
2.1.	Materials and 3D printing technology.....	45
2.2.	CAD.....	46
2.2.1.	Rectangular sample design	46
2.2.2.	Sample design with incorporated sensor.....	46
2.2.3.	Instrumented fin design.....	47
2.2.4.	Pandemic tool design and Shimadzu EZ-S test tool adapter design.....	47
2.2.5.	Electronics box design	54
2.2.6.	Transceiver box design	57
2.2.7.	Tooling design	59
2.2.7.1.	Router templates	59
2.2.7.2.	Mould for samples	61
2.2.7.3.	Fin mould.....	63
2.2.7.4.	Touch probe	65
2.2.7.5.	Dry box filament holder	67
2.3.	3D printer slicer (Cura).....	69
2.4.	CAM	71
2.5.	CNC	72
2.6.	3D printing and modifications.....	74

2.7.	Annealing	80
2.8.	Electronic telemetry system	80
2.9.	Arduino IDE and software solution.....	86
2.10.	Characterisation.....	87
2.10.1.	Sample testing	89
2.10.2.	Fin testing.....	93
Chapter 3: 3D printing and samples results		95
3.1.	3D printer customisation, process optimisation, and accuracy results.....	95
3.2.	Development of tools used for mechanical analysis.	100
3.3.	Samples mechanical analysis results.....	102
3.3.1.	Comparison between pandemic tool and Shimadzu mechanical analyser.	104
3.3.2.	Mechanical characterisation of samples without reinforcement materials	107
3.3.3.	Mechanical characterisation of samples with reinforcement	109
3.3.4.	Analysis of PA6-CF samples	112
3.3.5.	Materials performance parameters analysis	114
3.4.	Heat treatment	117
Chapter 4: Instrumented fins and surfboard results		118
4.1.	Development of the touch probe and an instrumented fin.	118
4.2.	3D printed sensor analysis.....	120
4.3.	Working prototype of an instrumented fin.....	122
4.4.	Comparison between Futures T1 Twin HC and 3D printed fins.....	125
4.5.	Surfboard with inbuilt measurement system and set of instrumented fins.....	129
4.6.	Data telemetry visualisation	139

4.7. Preliminary results of an instrumented surfboard.	140
4.7.1. GPS data.....	141
4.7.2. Accelerometer and gyroscope data.....	144
4.7.3. Instrumented fins.....	146
4.7.4. Temperature.....	147
Chapter 5: Conclusions.....	148
5.1. Future Work.....	151
List of references.....	153
Appendices.....	163
Appendix 1.....	163
Appendix 2.....	162

List of Names or Abbreviations

ABS	Acrylonitrile butadiene styrene
ANSI	American National Standards Institute
AS	Australian Standards
CAD	Computer Aided Design
CAM	Computer Aided Manufacturing
CFD	Computational Fluid Dynamics
CNC	Computer Cumerical Control
CPU	Central processing unit
EPROM	Electrically erasable programmable read-only memory
EPS	Expanded poly(styrene)(EPS)
FDM	Fused deposition modelling
FFF	Fused filament fabrication
FRAM	Ferroelectric random-access memory
GPS	Global Positioning System
HDPE	High-density poly(ethylene)
PC	Inter-integrated circuit
IC	Integrated circuit
ISO	International Organization for Standardization
LiDAR	Light detection and ranging
MEMS	Microelectromechanical system
MRAM	Magnetoresistive random-access memory
PA6-CF	Carbon fibre reinforced Nylon 6

PA12-CF	Carbon fibre reinforced Nylon 12
PA12-GF	Glass fibre reinforced Nylon 12
PETG	Poly(ethylene terephthalate glycol-modified)
PIN	Personal identification number
PLA	Poly(lactic acid)
PNT	Position, navigation and timing
PP	Poly(propylene)
PTC	Positive temperature coefficient
PTFE	Poly(tetrafluoroethylene)
PU	Poly(urethane)
PVA	Poly(vinyl alcohol)
RANS	Reynolds-averaged Navier–Stokes
ROM	Read-only memory
RTC	Real time clock
SEM	Scanning electron microscope
SPI	Serial peripheral interface
TPU	Thermoplastic poly(urethane)
UART	Universal asynchronous receiver-transmitter
USB	Universal serial bus
XPS	Extruded poly(styrene)

List of Figures

- Figure 1.1: Photography of a professional surfer Brett Connellan on a wave ...21
- Figure 1.2: A) Surfboard fin parameters. B) Fins configurations...22
- Figure 1.3: Photography of a Luna Rossa racing yacht competing against Team New Zealand in America's Cup on the Hauraki Gulf, New Zealand in 2020...25
- Figure 1.4: Photography of a prepreg hand layup process...26
- Figure 1.5: Example of a 2D drawing and 3D CAD model...27
- Figure 1.6: Example of a CAM generated simulation of a CNC milling process...28
- Figure 1.7: An example of CFD analysis on a typical surfboard fin (C), with grooves (D) and humpback whale inspired design (E)...28
- Figure 1.8: Schematic of FDM 3D printer...31
- Figure 1.9: An example of a 3D-printed, wireless sensor device...32
- Figure 1.10: A) an example of a ATmega328 single-chip microcontroller by Atmel. B) an example of a load cell schematics...33
- Figure 1.11: Wheatstone bridge schematics...34
- Figure 1.12: A) SEM micrograph of an example of the MEMS gyroscope. B) SEM micrograph of an example of the 3-axis accelerometer...35
- Figure 1.13: A) visualization of the latest GPS III-A satellite, launched in Dec 2018. B) photography of an SparkFun nRF24L01+ transceiver module...36
- Figure 1.14: Photography disassembled cellphone with visible components ...38
- Figure 1.15: Schematic of 3-point bending test...41
- Figure 1.16: Typical load vs deflection response of tested material. A) brittle mechanical behaviour. B) ductile mechanical character...42
- Figure 2.1: CAD model of the rectangular sample. A) side view. B) top view. C) isometric view. Numbers 20, 100, 5 indicate width (mm), length (mm), and height (mm), respectively...46
- Figure 2.2: CAD model of the sample with sensor...46

Figure 2.3: CAD design of instrumented fin. A) top view. B) front view. C) isometric view. Numbers 1-2 in A indicate 3D printed sensor (1), and pocket (2) for commercially obtained Wheatstone bridge, respectively. Numbers 130, 185, 121, 143, 7.2, 3.6, 11, 9.5, 1, 7 indicate height (mm), rake (mm), base (mm), sensor length (mm), sensor top width (mm), sensor bottom width (mm), pocket length (mm), pocket width (mm), sensor thickness (mm), and thickness (mm), respectively...47

Figure 2.4: CAD model of the pandemic tool assembly for three-point bend test. A) front view. B) top view. C) isometric view. D) exploded view. Numbers in D are explained in Table 2.2. Numbers 553, 103, 606, 80, 40 in A-B indicate height (mm), width (mm), length (mm), distance between supporting pins (mm), and distance between loading pin, and supporting pin (mm), respectively...48

Figure 2.5: A) picture of a dial indicator used in pandemic tool [56]. B) picture of a Mijia temperature and humidity meter [57]. C) picture of a Xiaomi Amazfit Pace A1612 smartwatch...50

Figure 2.6: CAD model of the three-point bend test Shimadzu adapter solution. A) side view. B) front view. C) isometric view. D) isometric view of an adapter base. Numbers 1-3 indicate: holes in the Z-axis (1), support cut-outs in the Y-axis (2), and holes in the X-axis (3). E) Exploded view of Shimadzu tool assembly. Numbers depicted in the picture are explained in Table 2.3. Numbers 162, 15, 53, 160, 120, 80 in A-B indicate tool head length (mm), tool head width (mm), base height (mm), base length (mm), base width (mm), and span (mm), respectively...53

Figure 2.7: CAD model of the electronic box with components solution. A) side view. B) front view. C) top view. D) isometric view. E) Exploded view of an electronic box. Numbers depicted in E are explained in Table 2.4. Numbers 20, 27, 130, 186, 98 indicate base height (mm), height (mm), width (mm), length (mm), and base width (mm), respectively...55

Figure 2.8: CAD model of the data receiver system. A) side view. B) front view. C) isometric view. D) exploded view of a data receiver system. Numbers in D are explained in Table 2.5. Numbers 217, 108, 22, 93 in A-B indicate, length (mm), antenna length (mm), height (mm), and width (mm), respectively...58

Figure 2.9: CAD model of a router templates for electronic box. A) side view. B) top view. C) isometric view. D) Exploded view of a electronic box templates. Numbers depicted in D explained in Table 2.5. Numbers 3.1, 239, 295 indicate height (mm), width (mm), and length (mm), respectively...60

Figure 2.10: CAD model of a mould for rectangular samples. A) side view. B) front view. C) top view. D) isometric view. E) Exploded view of a rectangular sample mould. Numbers depicted in E are explained in Table 2.7. Numbers 9, 120, 40, 5, 19 in A-C indicate cover height (mm), length (mm), width (mm), resin overflow port width (mm), and height (mm), respectively...62

Figure 2.11: CAD model of a mould for surfboard fin. A) side view. B) top view. C) isometric view. D) Exploded view of a mould for surfboard fin. Numbers depicted in D are explained in Table 2.8. Numbers 20, 177, 210 in A-B indicate height (mm), length (mm), and width (mm), respectively...64

Figure 2.12: CAD model of a touch probe used to design fin. A) top view. B) side view. C) isometric view. D) exploded view of a touch probe solution. Numbers depicted in D are explained in Table 2.9. Numbers 72, 42 in A-B indicate length (mm), and case length (mm), respectively...66

Figure 2.13: CAD model of a dry box solution. A) side view. B) top view. C) isometric view. D) Exploded view of a filament dry box. Numbers depicted in D are explained in Table 2.10. Numbers 127, 265, 240 in A-B indicate height (mm), length (mm), and width (mm), respectively...68

Figure 2.14: Screenshot of an Ultimaker Cura slicer software work space...70

Figure 2.15: Example of a CAM generated simulation of a CNC milling process...71

Figure 2.16: Picture of a 3018 CNC mill...73

Figure 2.17: Picture of customized 3D printer...74

Figure 2.18: A) picture of E3D NozzleX. B) E3D Hemera extruder...75

Figure 2.19: A) picture of SKR V1.4 turbo. B) FYSETC TMC-2130 StepStick stepper motor driver...77

Figure 2.20: A) picture of FYSETC spring steel build plate surface. B) PVA glue used for first layer adhesion...79

Figure 2.21: A) picture of an Arduino Mega 2560. B) picture of a DFRobot μ SD card reader...81

Figure 2.22: A) picture of a Sparkfun NEO-M9N GPS module. B) picture of a DFRobot MPU6050 gyro and accelerometer module...82

Figure 2.23: A) picture of a Sparkfun HX711 load cell amplifier. B) picture of a full bridge Wheatstone bridge...84

Figure 2.24: A) picture of a Sparkfun nRF24L01+ transceiver module. B) picture of a Sparkfun 2.4GHz Duck Antenna RP-SMA...85

Figure 2.25: Screenshot of an Arduino IDE work space...86

Figure 2.26: Picture of the Shimadzu EZ-S mechanical tester...87

Figure 2.27: A) picture of a Agilent 34410A digital multimeter. B) picture of a Powertech MP-3087 power supply...88

Figure 2.28: CAD model of pandemic tool head position relative to sample. A) top view. B) isometric view. C) photography of 3D printed three-point bend test solution. Numbers 1-4 in A depicts base, tool head, dial indicator, and sample, respectively. Numbers 50, 5, 30, and 606 in A indicate midpoint of the sample (mm), distance between sample, and pins (mm), pins length (mm), and length (mm), respectively. Numbers 1-7 in C indicate depth gauge, tool head, tool base, basket for weights, timer, thermometer and hygroscope, and 500 g weights, respectively...90

Figure 2.29: A) CAD model of Shimadzu adapter probe position relative to sample. B) picture of the Shimadzu EZ-S mechanical analyser with 3D printed adapter. Numbers 1-4 in A depicts sample, adapter base, press tool, and sample positioner, respectively. Numbers 160, 80, 80, 40, 50 in A indicate length (mm), midpoint length (mm), span (mm), distance between supporting pin and loading pin (mm), sample midpoint (mm), respectively. Number 1-4 in C indicate adapter base, press tool, 500 N load cell, and Shimadzu mechanical analyser, respectively...92

Figure 2.30: CAD model of Shimadzu EZ-S probe position relative to fin. A) side view. B) top view. C) isometric view. D) Picture of the Shimadzu EZ-S mechanical analyser with sensor fin setup. Numbers 4, 35, 94, and 120 indicate vertical distance between a 3D printed sensor and a tool (mm), horizontal distance between a 3D printed sensor and a tool (mm), vertical distance between a Wheatstone bridge, and a tool (mm), horizontal distance between a Wheatstone bridge and a tool (mm), respectively. Numbers 1-7 in D indicate: instrumented fin, surfboard, 10 mm press tool, 500 N load cell, mechanical analyser, PC, and digital multimeter, respectively...94

Figure 3.1: Photography of one of a 3D printed rectangular sample (A). Photography of a nozzle front opening after 3D printing of around 1 kg of abrasive materials (B)...96

Figure 3.2: Photography of samples of Nylon 12 with carbon fibre filament with different Cura slicer software flow rates parameters, 100 % (A), 80 % (B), 70 % (C), and close up photography of a side wall of a 3D printed rectangular sample...98

Figure 3.3: Photography of a 3D printed adapter base with PA12-CF...102

Figure 3.4: Response of a sample to loading-unloading cycle conducted on a 3D printed pandemic tool. Letters A-E indicate loading sequence: no load (A), 5 kg load (B), 9.5 kg load (C), 18.5 kg load (D), and 20 kg load (E) respectively. Letters F-I indicate unloading cycle: 18.5 kg (F), 9.5 kg (G), 5 kg (H), and no-load (I) respectively...103

Figure 3.5: Presents characterisation data of the pandemic tool. A) stress-strain behaviour of the loading part of three cycles for Clariti - 1 (sample number 1). B) stress-strain behaviour of the loading part of three cycles for PLA - 1 (sample number 4). C) Obtained mean flexural modulus values with ± 1 Standard Deviation error...104

Figure 3.6: Presents comparison between so-called pandemic tool and Shimadzu mechanical apparatus. A) stress-strain behaviour of the loading part of the cycle for PETG-CF - 1 (sample number 3). B) stress-strain behaviour of the loading part of the cycle for PLA - 1 (sample number 4). C) Obtained flexural modulus using both tools up to about 5 GPa. D) Difference between determined Flexural modulus. For samples details check appendix 2. Orange and blue lines indicate testing concluded using the pandemic tool and the Shimadzu EZ-S, respectively...106

Figure 3.7: Stress-strain behaviour of the loading part of the cycle of as-prepared composite materials determined using the Shimadzu EZ-S (500N load cell). PA6-CF - 5, and PA6-CF - 7 indicate PA6-CF 3D printed with 35 % infill rate, and PA6-CF 3D printed with 100 % infill rate, respectively. PA12-CF - 5, and PA12-CF - 18 indicate PA12-CF 3D printed with 100 % infill, and heat-treated PA12-CF 3D printed with 100 % infill rate, respectively. PETG - 4 indicates a sample of PETG 3D printed with a 35 % infill rate. PETG-CF - 5, PETG-CF - 7, and PETG-CF - 10 indicate heat-treated PETG-CF 3D printed with 35 % infill rate, PETG-CF 3D printed with 100 % infill rate, and PETG-CF 3D printed with 35 % infill rate, respectively. PLA - 3 indicates PLA 3D printed with a 100 % infill rate...108

Figure 3.8: Stress-strain behaviour of the loading part of the cycle of reinforced composite materials tested using the Shimadzu EZ-S (500N load cell). Basalt fibre - 1 indicate 25 layers of basalt fibre, and West System epoxy resin. PA6-CF - 12, and PA6-CF - 16 indicate heat-treated 3D printed with 100 % infill rate prepreg reinforced PA6-CF, and heat-treated 3D printed with 35 % infill rate prepreg reinforced PA6-CF, respectively. PA12-CF - 3, PA12-CF - 26, and PA12-CF - 29 indicate 3D printed with 100 % infill rate carbon fibre reinforced PA12-CF, heat-treated 3D printed with 35 % infill rate prepreg reinforced PA12-CF, and indicate heat-treated 3D printed with 100 % infill rate prepreg reinforced PA12-CF, respectively. Kinetix R118 - 5, and Kinetix R118 - 6 indicate basalt fibre reinforced Kinetix R118 epoxy resin, and carbon fibre reinforced Kinetix R118 epoxy resin, respectively...110

Figure 3.9: Typical mechanical response of 3D printed PA6-CF rectangles samples tested using Shimadzu EZ-S (500N load cell). A) loading-unloading cycle force-deflection. B) stress-strain behaviour of the loading part of the cycle. PA6-CF - 1, PA6-CF - 2, PA6-CF - 5, PA6-CF - 7, PA6-CF - 12, and PA6-CF - 16 indicate 3D printed with 35 % infill rate water-saturated PA6-CF, 3D printed with 100 % infill rate water-saturated PA6-CF, 3D printed with 35 % infill rate PA6-CF, 3D printed with 100 % infill rate PA6-CF, heat-treated 3D printed with 100 % infill rate prepreg reinforced PA6-CF, and heat-treated 3D printed with 35 % infill rate prepreg reinforced PA6-CF, respectively...113

Figure 3.10: Prepreg datasheet optimal curing cycle...117

Figure 4.1: Photography of a typical touch probe set up used to measure discrete points of the Futures Twin T1 surfboard fin surface. An example of rectangular sample measurements. A) Touch probe was not touching the object, therefore the resistance of the circuit could be measured. B) Touch probe was touching the object, and the

resistance of the circuit could not be measured which indicated breaking the electrical circuit, and machine coordinates could be registered...119

Figure 4.2: Charts of a typical response of an rectangular samples with 3D printed sensors for a loading-unloading cycle. A) stress vs strain. B) force vs time. C) Δ resistance vs time for tension. D) Δ resistance vs time for compression...121

Figure 4.3: Image of the working prototype of an instrumented fin with visible 3D printed flex sensor (1), and commercial Wheatstone bridge (2)...123

Figure 4.4: Charts of a typical response of an instrumented fin for a loading-unloading cycle. A) stroke vs time. B) force vs time. C) force vs stroke. D) resistance vs stroke. E) voltage vs stroke. F) average voltage vs fin flex response. Dotted lines are linear fits of the data. Arrows in C-F indicate the direction of loading and unloading of the instrumented fin...124

Figure 4.5: Charts of a response of an instrumented fin for a three loading-unloading cycles. A) voltage vs time for Wheatstone bridge. B) resistance vs time for a 3D printed sensor. C) force vs time. D) force vs time...125

Figure 4.6: Picture of commercial and 3D printed fins. A) CNC machined pocket for a sensor. B) close up of two sensors. C) both fins...126

Figure 4.7: Charts of a typical response of a Futures T1 Twin HC and 3D printed fins equipped with Wheatstone bridge for a loading-unloading cycle. A) force vs stroke for tension. B)) force vs stroke for compression. C) force vs time for tension. D) force vs time for compression. E) stroke vs time for tension. F) stroke vs time for compression. Arrows in A-B indicate the direction of loading and unloading of the fins...127

Figure 4.8: Charts of a typical response of a Futures T1 Twin HC and 3D printed fins equipped with Wheatstone bridge for a loading-unloading cycle. A) force vs stroke for tension. B)) force vs stroke for compression. C) force vs time for tension. D) force vs time for compression. E) stroke vs time for tension. F) stroke vs time for compression. Arrows in A-B indicate the direction of loading and unloading of the fins...129

Figure 4.9: Pictures of subsequent stages of an instrumented surfboard prototype development. Letters A-F indicate: sketching of cut-outs (A), installing templates and cutting the surfboard (B), electronic box fitting (C), sealing cables hole with resin (D), coating box with a layer of epoxy resin (E), creating gasket (F), respectively...131

Figure 4.10: Pictures of subsequent stages of an instrumented surfboard prototype development. Letters A-F indicate: leak testing (A, B), soldering cables (C), installing a layer of fibreglass (D), electronic box gluing (E), compressing electronic box and fibreglass (F)), respectively...133

Figure 4.11: Pictures of subsequent stages of an instrumented surfboard prototype development. Letters A-F indicate: connecting electronics (A), testing telemetry system (B), custom fit of fibreglass and carbon fibre tapes (C, D), glueing fibre tapes with epoxy resin (E, F)), respectively...135

Figure 4.12: Photography of a surfboard, and instrumented fins prototypes with inbuilt data telemetry unit. A) top view. B) bottom view...136

Figure 4.13: A) instrumented surfboard prototype electronics. B) photography of an assembled 3D printed transceiver. C) instrumented surfboard with a mounted set of “Jimi” and “Hendrix” instrumented fins...138

Figure 4.14: A) photography of a transceiver unit mounted on a data collection computer. B) typical data visualisation created in Telemetry Viewer software...139

Figure 4.15: A) Path of the first GPS test. B) junction 1. C) junction 2. Red, yellow, and green solid lines indicate paths obtained using GoPro, Poco F3, and surfboard telemetry, respectively...141

Figure 4.16: Speed vs time response of benchmarked devices. GoPro, Poco F3, and Telemetry indicate GoPro Hero 10 action camera, Poco F3 cell phone, and the telemetry unit built into the surfboard, respectively...142

Figure 4.17: A) GPS path of the ocean test. B) event 1. C) event 2. Red, yellow, and green solid lines indicate paths obtained using GoPro, Poco F3, and surfboard telemetry, respectively...143

Figure 4.18: Speed vs time response of benchmarked devices. GoPro, Poco F3, and Telemetry indicate GoPro Hero 10 action camera, Poco F3 cell phone, and the telemetry unit built into the surfboard, respectively...144

Figure 4.19: A typical response of an accelerometer and a gyroscope sensors. A) acceleration + gravity vs time response in Z-axis. B) gyro vs time response in Z-axis. C) acceleration + gravity vs time response in Y-axis. D) gyro vs time response in Y-axis. E) acceleration + gravity vs time response in X-axis. F) gyro vs time response in X-axis. GoPro_accZ, GoPro_accY, GoPro_accX, GoPro_gyroZ, GoPro_gyroY, GoPro_gyroX, indicate GoPro Hero 10 action camera. Poco_F3_accZ, Poco_F3_accY, Poco_F3_accX, Poco_F3_gyroZ, Poco_F3_gyroY, Poco_F3_gyroX, indicate Poco F3 cell phone. Telemetry_accZ, Telemetry_accY, Telemetry_accX, Telemetry_gyroZ, Telemetry_gyroY, Telemetry_gyroX, indicate telemetry unit inbuilt into surfboard...145

Figure 4.20: Load vs time response of instrumented fins sensors. Sensor 1, and Sensor 3 indicate commercial Wheatstone bridge in the first fin, and commercial Wheatstone bridge in the second, respectively...146

Figure 4.21: Temperature vs time response of benchmarked devices. A) the first test. B) the second test. GoPro and Telemetry indicate GoPro action camera, and telemetry unit built into the surfboard, respectively...147

List of Tables

Table 2.1: Filament materials, and fabrics used to produce rectangular samples and instrumented fins. 200 gsm, 240 gsm, and 265 gsm indicate 200 grams per square metre, 240 grams per square metre, and 265 grams per square metre, respectively. Cubic Technologies indicates an Australian shop with 3D printing accessories...45

Table 2.2: List of parts used for the pandemic tool. Parts indicated as 3D printed were manufactured in-house on a customised Creality CR10-S. Bunnings and Maker Store indicate names of Australian shops, respectively. eBay indicates the name of the American shop...49

Table 2.3: List of parts used for Shimadzu adapter tool. Parts indicated as 3D printed were manufactured in-house on customised the Creality CR10-S. Maker Store indicates the name of an Australian shop...54

Table 2.4: List of parts used for electronic box Parts indicated as 3D printed were manufactured in-house on customised the Creality CR10-S. Barnes and Core electronics indicate the names of Australian shops, respectively. eBay indicates the name of the American shop...56

Table 2.5: List of parts used for the electronic box. Parts indicated as 3D printed were manufactured in-house on customised the Creality CR10-S. Core electronics indicates the name of an Australian shop. eBay indicates the name of the American shop...59

Table 2.6: List of parts used for router templates. Parts indicated as 3D printed were manufactured in-house on customised the Creality CR10-S...61

Table 2.7: List of parts used for sample mould. Parts indicated as 3D printed, and CNC machined were manufactured in-house on customised the Creality CR10-S, and CNC mill, respectively...63

Table 2.8: List of parts used for fin mould. Parts indicated as 3D printed were manufactured in-house on customised the Creality CR10-S...65

Table 2.9: List of parts used for touch probe. Parts indicated as 3D printed were manufactured in-house on customised the Creality CR10-S. Bunnings indicates the name of an Australian shop. eBay indicates the name of the American shop...67

Table 2.10: List of parts used for the dry box solution. Parts indicated as 3D printed were manufactured in-house on customised the Creality CR10-S. Bunnings and Woolworths indicate the names of an Australian shops. eBay indicates the name of the American shop...69

Table 2.11: Parameters for used materials...	70
Table 2.12: Parameters of chosen operations used for HDPE milling...	72
Table 2.13: Parameters of chosen operations used for XPS foam milling...	72
Table 2.14: General specification of mini CNC machine...	73
Table 2.15: General specification of a chosen nozzle...	75
Table 2.16: General specification of a chosen extruder...	76
Table 2.17: General specification of a used motherboard...	77
Table 2.18: General specification of a used stepper driver StepStick...	78
Table 2.19: General specification of a Arduino Mega 2560 development board...	81
Table 2.20: General specification of a used GPS module...	82
Table 2.21: General specification of used gyro/accelerometer module...	83
Table 2.22: General specification of used load cell amplifier module...	84
Table 2.23: General specification of used transceiver module...	85
Table 2.24: General specification of used Shimadzu EZ-S...	87
Table 2.25: General specification of used Agilent 34410A...	88
Table 2.26: General specification of used Powertech MP-3087...	89
Table 3.1: Summary of flow rate calibration sample parameters for PA12-CF...	99
Table 3.2: Summary of mean values of rectangular samples dimensions. PA6-CF indicates as prepared Nylon 6 with carbon fibre additives material. PA12-CF indicates as prepared Nylon 12 with carbon fibre additives material. PA12-GF indicates as prepared Nylon 12 with glass fibre additives material. PETG indicates as prepared poly(ethylene terephthalate glycol-modified) material. PETG-CF indicates as prepared PETG with carbon fibre additives material. PLA indicates as prepared poly(lactic acid) material...	100

Table 3.3: Summary of obtained results. Samples refer to table in appendix 2. PA6-CF – 5, and PA6-CF - 7 indicate PA6-CF 3D printed with 35 % infill rate, and PA6-CF 3D printed with 100 % infill rate, respectively. PA12-CF – 5, and PA12-CF – 18 indicate PA12-CF 3D printed with 100 % infill, and heat treated PA12-CF 3D printed with 100 % infill rate, respectively. PETG – 4 indicates a sample of PETG 3D printed with a w35 % infill rate. PETG-CF – 5, PETG-CF – 7, and PETG-CF – 10 indicate heat-treated PETG-CF 3D printed with 35 % infill rate, PETG-CF 3D printed with 100 % infill rate, and PETG-CF 3D printed with 35 % infill rate, respectively. PLA – 3 indicates PLA 3D printed with a 100 % infill rate...108

Table 3.4: Summary of obtained results Samples refer to table in appendix 2. Basalt fibre – 1 indicate 25 layers of basalt fibre, and West System 105 epoxy resin. PA6-CF – 12, and PA6-CF - 16 indicate heat-treated 3D printed with 100 % infill rate prepreg reinforced PA6-CF, and heat-treated 3D printed with 35 % infill rate prepreg reinforced PA6-CF, respectively. PA12-CF – 3, PA12-CF – 26, and PA12-CF – 29 indicate 3D printed with 100 % infill rate carbon fibre reinforced PA12-CF, heat-treated 3D printed with 35 % infill rate prepreg reinforced PA12-CF, and indicate heat-treated 3D printed with 100 % infill rate prepreg reinforced PA12-CF, respectively. Kinetix R118 – 5, and Kinetix R118 – 6 indicate basalt fibre reinforced Kinetix R118 epoxy resin, and carbon fibre reinforced Kinetix R118 epoxy resin, respectively...110

Table 3.5: Summary of obtained results for PA6-CF. Samples refer to table in appendix 2. PA6-CF – 1, PA6-CF – 2, PA6-CF – 5, PA6-CF – 7, PA6-CF – 12, and PA6-CF - 16 indicate 3D printed with 35 % infill rate water-saturated PA6-CF, 3D printed with 100 % infill rate water-saturated PA6-CF, 3D printed with 35 % infill rate PA6-CF, 3D printed with 100 % infill rate PA6-CF, heat-treated 3D printed with 100 % infill rate prepreg reinforced PA6-CF, and heat-treated 3D printed with 35 % infill rate prepreg reinforced PA6-CF, respectively...113

Table 3.6: Summary of obtained results. Samples refer to table in appendix 2. Basalt fibre – 1, PA6-CF – 7, PA6-CF – 11-15, PA6-CF – 16-20, PA12-CF – 18, PA12-CF – 29 – 33, and PLA - 3 indicate 25 layers of basalt fibre, and West System 105 epoxy resin, PA6-CF 3D printed with 35 % infill rate, heat-treated 3D printed with 100 % infill rate prepreg reinforced PA6-CF, and heat-treated 3D printed with 35 % infill rate prepreg reinforced PA6-CF, heat treated PA12-CF 3D printed with 100 % infill rate, heat treated 3D printed with 100 % infill rate prepreg reinforced PA12-CF, and PLA 3D printed with a 100 % infill rate, respectively...115

Acknowledgements

I would like to thank the following people for their time, guidance, resources supply and support throughout this project: Prof Marc in het Panhuis, and Osama Al Takhayneh.

Abstract

Surfing is a highly competitive sport, to which additive manufacturing technology can be applied to develop new solutions to improve knowledge.

The main focus of this study was to design, prototype and test 3D printed surfboard fins with incorporated sensors interfaced with an instrumented surfboard prototype. Specific aim 1 (customisation of a 3D printer in order to 3D print with carbon fibre composites) was addressed by changing the nozzle, extruder, motherboard, stepper drivers, heat bed surface, and introduction of the dry box to the Creality CR-10S 3D printer. Introduced modifications resulted in successful 3D printing using abrasive and hygroscopic filament materials. Specific aim 2 (3D printing of model samples and instrumented fins) was achieved by using a customised 3D printer to fabricate 101 rectangular samples and six instrumented fins. The surfboard fin was designed in CAD and inspired by Futures T1 Twin HC (Futures Fins). Two sensors were incorporated into the fin. The first was 3D printed in-house out of conductive PLA, and TPU filaments while the second one was a commercially obtained 350 Ω full Wheatstone bridge. Specific aim 3 (design, and manufacturing of moulds and tools used for mechanical analysis and data collection unit) was addressed by the development of the so-called pandemic tool, a Shimadzu EZ-S mechanical analyser adapter, touch probe, fin mould, mould for rectangular samples (produced from high-density poly(ethylene) (HDPE) material), and router templates. The comparison between the so-called pandemic tool and the Shimadzu EZ-S laboratory tool showed an excellent accuracy of around 20 % in a range of 0 to around 5 GPa of calculated flexural modulus. The accuracy above 5 GPa was exponentially lower. Specific aim 4 (mechanical analysis of model samples and fins) was achieved using the pandemic tool during Covid-19 pandemic related lockdowns, and the Shimadzu EZ-S between lockdowns.

Mechanical analysis of rectangular samples concluded that carbon fibre reinforced Nylon 6 (CF-PA6) with prepreg composite exhibited the highest flexural modulus value (12 ± 1 GPa). The final aim (laboratory and field-testing of instrumented fins) was addressed by laboratory testing of an instrumented fin using a universal mechanical analyser. The results of a tested prototype of an instrumented fin indicated that under tension the commercial Wheatstone bridge exhibited a linear response to applied stroke in a range of up to 7.7 ± 0.1 % of a fin flex. Field-testing was achieved in two trials. The first field test involved driving with a car that had the instrumented surfboard and fins mounted onto it. The second field test involved paddling and walking the instrumented surfboard and fins in a waveless part of the ocean (Gunnamatta Bay, NSW, Australia). The preliminary data results indicate the excellent GPS accuracy of the telemetry unit. Data from sensors installed in the surfboard and fins were saved on the μ SD card, while it was simultaneously transferred in real-time between the surfboard's electronics and the transceiver connected to the laptop with a 13 Hz sampling rate.

The main outcome of this project was the development of a working prototype of a surfboard with inbuilt electronics and a set of instrumented fins.

Chapter 1: Introduction

1.1. Sport of surfing

The sport of surfing is growing significantly in participants with around 12 % - 16 % more surfers per year [1,2]. In 2002 there were over 10 million surfers (Figure 1.1) around the World [2]. Along with the increase in surfing popularity, the market is expanding to the value of around US\$ 10 billion per year [2]. The companies continue to develop the technical solutions implemented in their surfboards and fins. The development process requires cooperation between surfers and surfboard shapers. For example, Firewire Surfboards company utilises CAD and computer numerical control (CNC) machining of their boards [3]. Surfboards and fins are products based on composite materials including a combination of foam, e.g. poly(urethane)(PU), extruded poly(styrene)(XPS), expanded poly(styrene)(EPS), plywood, fibre cloths such as fibreglass, carbon fibre and, basalt fibre, and resins (poly(ester), epoxy). Figure 1.1 presents an example of a surfer on a wave [4].



Figure 1.1: Photography of a professional surfer Brett Connellan on a wave [4].

1.2. Surfboard fins

A surfboard fin is a hydrofoil mounted at the tail of a surfboard. The surfer uses fins for stability, direction control, and gaining speed. Without them, control of the surfboard would be impossible. They are characterized by parameters including base, height, rake, area, cant, flex, toe or foil shape (see Figure 1.2A). Flat foil, or inside foil are used on side fins, and a symmetrical foil shape is used for central fins. Foil shape determines the characteristic of lift to drag ratio.

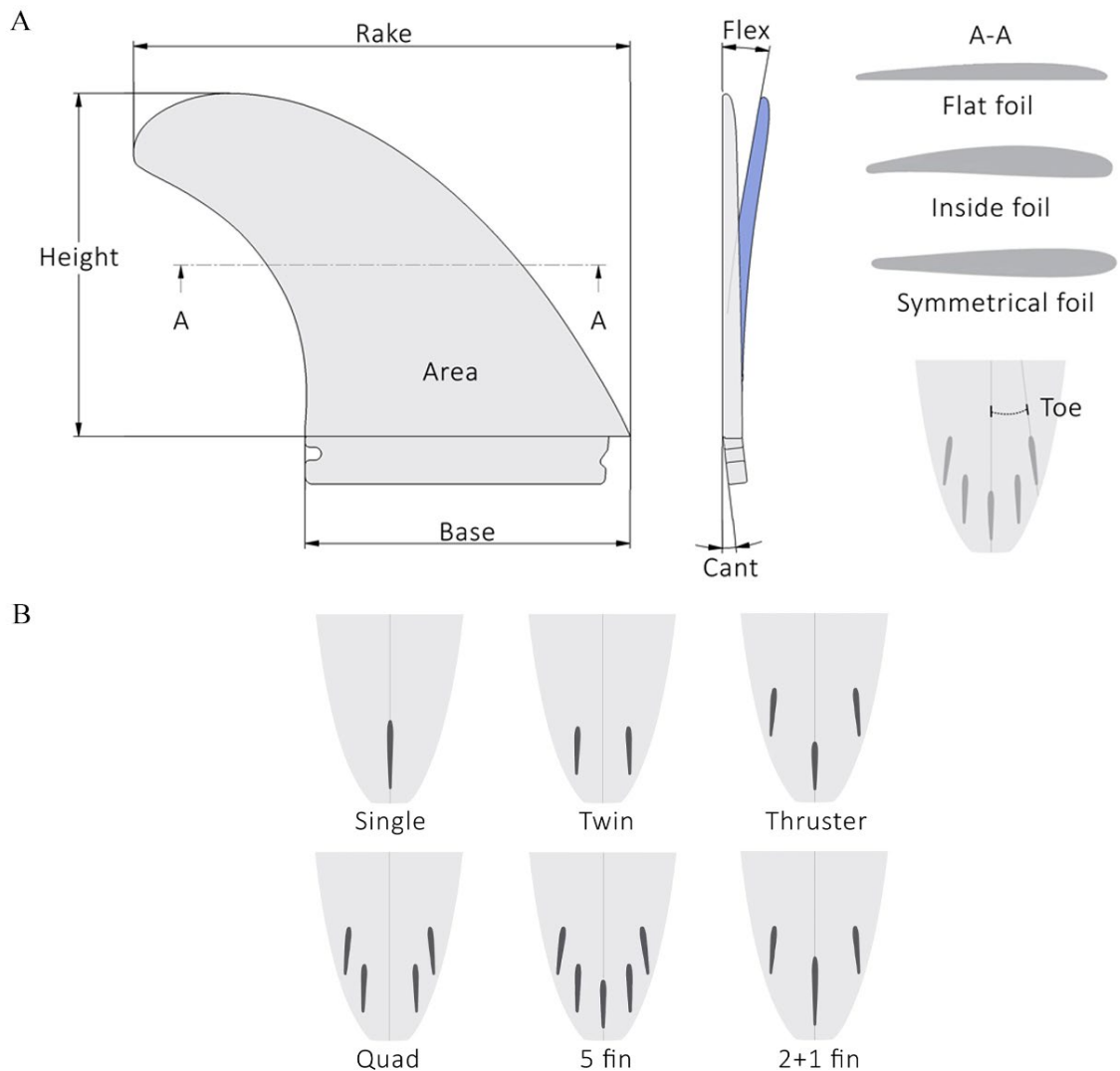


Figure 1.2: A) Surfboard fin parameters. B) Fins configurations

Fins are made with different fibres and resins composites. Additionally, they can have wooden cores or be made out of plastic. They can be produced with the use of resin transfer moulding, CNC machining, hand lay-up or 3D printing techniques. Moreover, there are six main fin configuration setups which influence the performance of the surfboard. Single, twin, thruster, quad, 5 fins or 2+1 (see Figure 1.2B). The last one has a bigger central fin box and allows to change the position of a centre fin. Other configurations have fixed fins positions. In the presented project, a twin configuration was used as it consists of two fins and required the mounting of four sensors.

1.3. Composite materials

In 2014 the advanced composite materials market expansion rate was 6.3 % reaching around US\$ 8.2 billion in value (2.5 billion kg in the amount of material). Economic indicators predicted a 4.9 % expansion to around US\$ 8.6 billion in value (2.63 billion kg in material) of annual shipments. The most popular reinforcement composite material was fibreglass, and poly(ester) resin was the most popular resin. In the surfing industry, this combination represents around 80 % of all surfboards and fins manufactured. It is estimated that the American market alone for end products based on composite materials was around US\$ 21 billion in 2014. Furthermore, composite materials and end products combined together created a market worth US\$ 30 billion. Further calculations suggest that the market will reach around US\$ 38 billion p.a. by 2023 [5].

China is the largest market for composite materials in terms of total volume consumption. The USA is second followed by Germany. However, per capita, the American market is the largest with around 7.3 kg per person. Germany is second with approximately 3.9 kg per person. In comparison, in China consumption per capita is around 2.2 kg [5].

The industrial use of composite materials helped to develop new applications in fields such as transportation, construction, corrosion-resistance, marine, infrastructure, consumer products, electrics, aerospace, appliances, and business equipment. Composites are used to manufacture an abundance of products that can be divided into three broad categories: consumer, industrial and advanced [5].

For example, the aerospace industry is a well-known end-user of composite materials. Future aircraft programs, such as the Boeing 787 and Airbus A350XWB, utilise more than 50 % by weight of advanced composite components. In addition, there is a lot of focus on optimising the rate and economy of composite manufacturing to meet the set goals. Advanced uses of composite materials include parts such as inlet duct in F-18 E/F or stabilator pivot in F22 Raptor jet fighters [6].

A composite material is manufactured with the use of two or more materials. Constituent materials impart different chemical or physical parameters. When merged together, they create a material with a set of properties, unlike the individual constituents. Examples of composite materials include reinforced rubber, filled polymers, mortar and concrete, alloys, porous and cracked media, aligned, chopped fibre composites or prepreg. The latter composite (prepreg) is a state-of-the-art component used in high-performance sports such as Formula 1 cars and racing yachts.

Prepregs are laminate composites of fibre sheets that are impregnated with polymer resins (thermoplastic or thermosets). Figure 1.3 presents an example of the use of prepreg for the America's Cup race yacht [7]. Fibre sheets are often fibreglass, carbon fibre, or aramid (Kevlar). Prepreg cloths when not cured are called B-staged. These are made by creating layered soft and flexible sheets of materials. Prepregs are tacky and remain flexible and can be cut into any shape. The most common way to make a composite part from prepreg reinforcement is to lay-up layers of the

prepreg reinforcement cloth into or onto a mould. Subsequently, vacuum the mould and laminate in a bag, and finally cure it. The curing process is done with a specific heating curve depending on the composition of the prepreg in an oven or an autoclave. Many prepregs are based on epoxy or phenolic resin, but also thermosets can be used including materials such as poly(imide) [8].



Figure 1.3: Photography of a Luna Rossa racing yacht competing against Team New Zealand in America's Cup on the Hauraki Gulf, New Zealand in 2020 [7].

The production process with the use of prepreg is highly demanding and requires highly skilled experts with a lot of experience as the composite materials lay-up process is conducted manually. Different weaves patterns and thicknesses of the cloths are used to meet set requirements. Figure 1.4 presents an example of a typical hand lay-up process with the use of mould [9]. The moulds used for parts production are created with the use of CNC machining, sculpted by hand or with the use of additive manufacturing process. Moreover, additive manufacturing techniques such

as 3D printing can be utilised to produce plugs to reduce the cost of production of the parts.

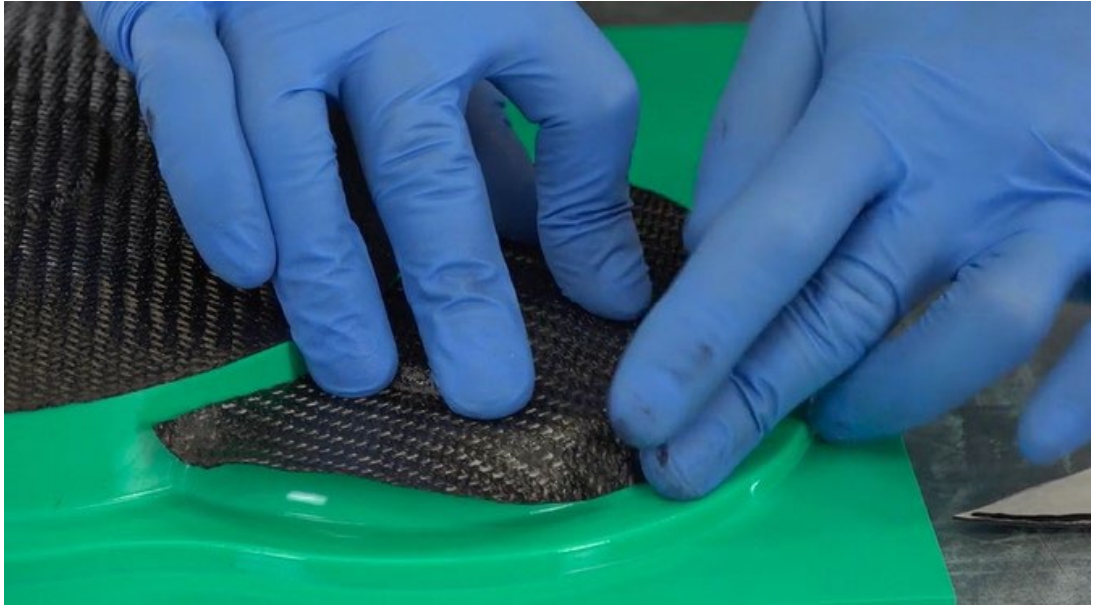


Figure 1.4: Photography of a prepreg hand layup process [9].

1.4. Computer Aided Design (CAD)

CAD is a software tool that utilises computers in order to optimise, modify, create, analyse a design. It contributes to raising design quality, productivity, documentation flow. It uses vector-based graphics to presents design in 2D documentation or may produce raster graphics to depict the virtual 3D model of the designed solution. Technical documentation consists of information about used materials, production processes, dimensions and tolerances accordingly to a chosen standard organisation such as Australian Standards (AS), International Organization for Standardization (ISO), American National Standards Institute (ANSI). CAD tools are widely used in industries including mechanical engineering, construction, architecture, medical, special effects. Nowadays, the majority of commercially available products were designed with

the use of CAD software [10]. Figure 1.5 presents an example of a 2D drawing and 3D CAD model.

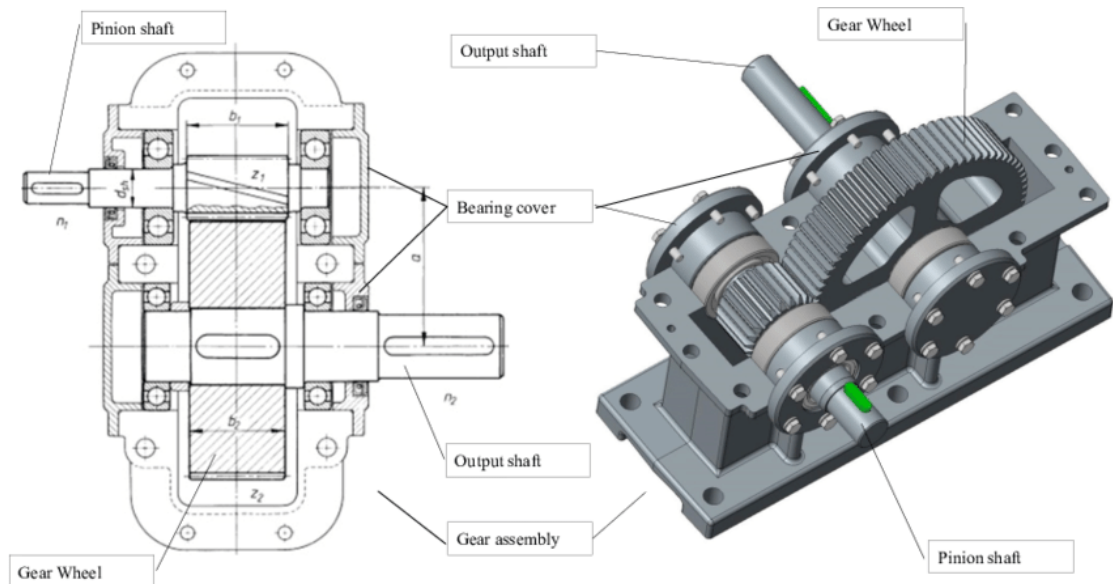


Figure 1.5: Example of a 2D drawing and 3D CAD model [11].

1.5. Computer Aided Manufacturing (CAM)

CAM is a software tool that utilises computers in order to generate programs for CNC machines. It can be used in manufacturing processes such as multi-axis milling, turning, laser control, and 3D printer control. Users for instance can specify the type of operation, tools, tool-paths, machine parameters, operation parameters, and tool changes. It is widely used in industries such as automotive, mechanical machining to produce parts. Figure 1.6 presents an example of a CAM generated simulation [12].

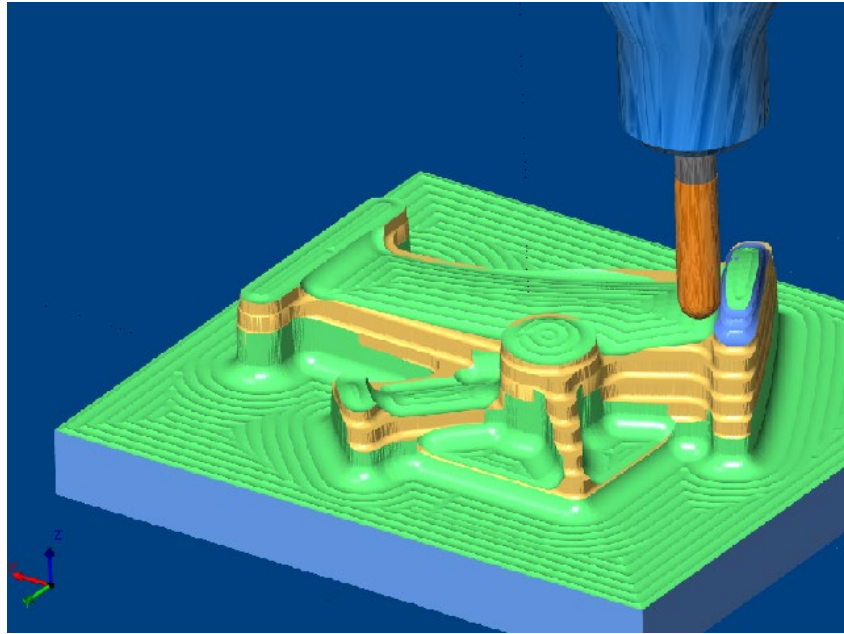


Figure 1.6: Example of a CAM generated simulation of a CNC milling process [13].

1.6. Computational Fluid Dynamics (CFD) analysis

CFD is a powerful tool that can be utilised in the design process of new solutions implemented in many areas of engineering products. For example, case studies in maritime CFD include sail shapes [14], hydrodynamic analysis of super and mega yachts [15], and the design of lifeboats [16]. The main advantages of CFD are rapid solutions analysis, lower expense compared to traditional physical test models, access to many simulations areas, high spatial and temporal resolutions. Figure 1.18 represents an example of CFD analysis of surfboard fins [17].

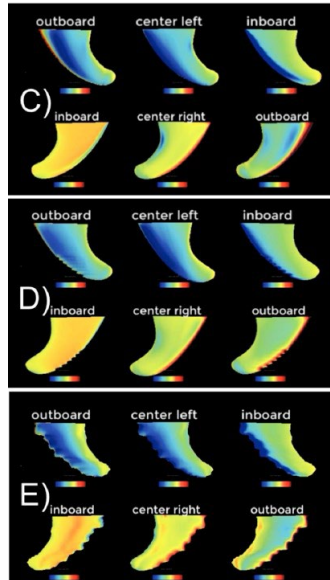


Figure 1.7: An example of CFD analysis on a typical surfboard fin (C), with grooves (D) and humpback whale inspired design (E) [17].

While CAD and computer-aided manufacturing (CAM) such as CNC machining are standard tools used in surfboards and fins production process [3], CFD support is fairly novel, and only a few studies have employed it effectively [18]. The reported research work can be divided into simulations of fin models without a surfboard (FIN), surfboard models without fins (BOARD) and case studies including both surfboard and fins [19,20]. Additionally, FIN group studies can be subdivided into the application of laminar and turbulent flow models. Reynolds-Averaged Navier–Stokes equations (RANS) can be employed to simulate the fluid flow. Lavery [21] assumed laminar flow boundary conditions while investigating the impact of the fillet and un-fillet fins on the lift, drag forces at variable flow rates, and angles of attack. Turbulent flow models based on RANS were researched by Gudimetla [22], Sakellariou [23], and Macneill [24]. 3D printed fins were simulated to compute longitudinal and tangential forces. In the BOARD group, studies on 3D models were conducted [25,26]. Barnett and Miravete [27] researched a 2D simplified surfboard model.

A comparison between a surfboard and an Alaia was conducted by Oggiano [25]. In their work Oggiano and Pierella [26] researched contemporary surfboard solutions with different tails and rockers. The most complex CFD analysis with the use of surfboards and fins were reported by Shormann, in het Panhuis, and Oggiano [19,20].

1.7. Additive manufacturing (3D printing) techniques

3D printing is an additive manufacturing process by which components are fabricated directly from computer models by selectively curing, depositing or consolidating materials in successive layers [28]. In past years 3D printing was used to manufacture visualization of products only, but in recent years this technology evolved and proved that it can be used for the fabrication of a range of functional end-use components [28].

Recently it has been shown that 3D printing is suitable for rapid prototyping custom fins for surfboards [29]. The research demonstrated that materials such as acrylonitrile butadiene styrene (ABS), carbon fibre and, fibreglass can be used for manufacturing fins. The authors reported that the mechanical properties of 3D printed fins are similar to commercially used solutions [29].

Fused filament fabrication (FFF), also known as fused deposition modelling (FDM), is an additive manufacturing 3D printing process that uses a continuous filament of a thermoplastic material. The filament is fed from a spool through a moving, heated printer extruder head. Under a CNC controller, the print head usually moves in a 2D XY plane to define the printed shape [30]. Subsequently, the printed part or the print head is moved vertically by a preconfigured value to begin a new layer. The feed rate of the extruder may be controlled to prevent over deposition which could

cause stringing or dribbling between sections [30]. Figure 1.8 presents an example of a typical FDM 3D printer schematic.

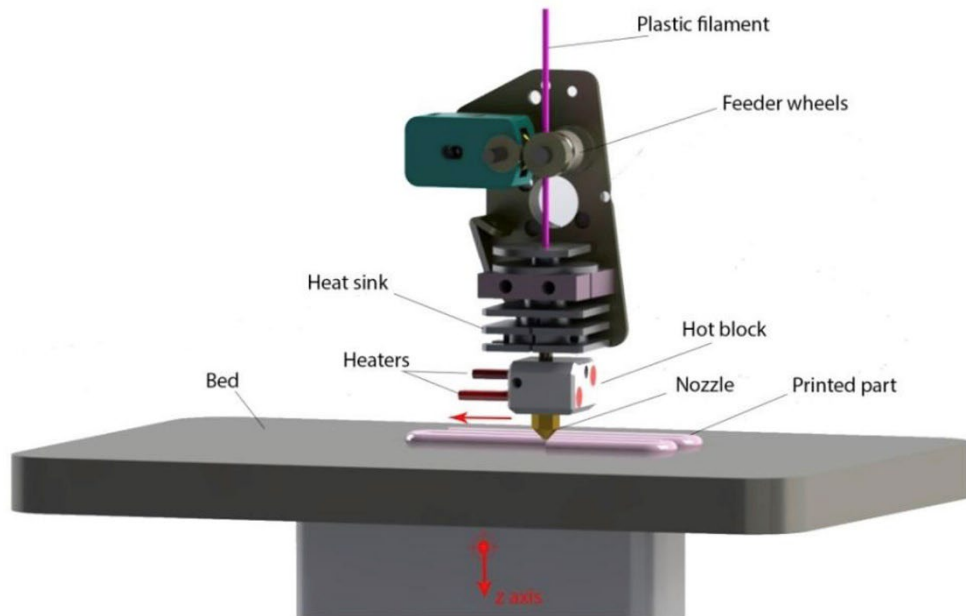


Figure 1.8: Schematic of FDM 3D printer [31].

FDM 3D printing technology requires the use of thermoplastic filaments. They vary in properties, printing temperatures, and speed or feeding rate. Parameters such as density, heat distortion, tensile strength, flexural strength, flexural modulus, UV resistance and water resistance differentiate materials. Most commonly used materials are: poly(lactic acid) (PLA), ABS, poly(ethylene terephthalate glycol-modified) (PETG), Nylon, thermoplastic poly(urethane) (TPU), and poly(vinyl alcohol) (PVA). They can be mixed with additives such as carbon fibres, glass fibre, graphene, wood powder to create composite materials with different chemical and physical parameters. For instance, the addition of graphene can be used to design filaments with conductive parameters. That can be utilised for printing electronic components such as sensors.

The use of 3D printed sensors applications has been reported in a number of other studies. For example, researchers [32] using a poly(propylene) (PP)-based electroconductive filament demonstrated low volume resistivity of their material of $5 \times 10^{-3} \Omega\text{m}$ by adding 30 % by weight of carbon black filler to a poly(propylene) base. Moreover, they reported a Positive Temperature Coefficient (PTC) effect, in which an increase in temperature leads to an increase in electrical resistance. Commercially available filaments include graphene PLA composite with a reported volume resistivity of $6 \times 10^{-3} \Omega\text{m}$ were used in the flex sensor connected to an Arduino interface [33]. Figure 1.9 presents an example of a 3D printed sensor device [34].

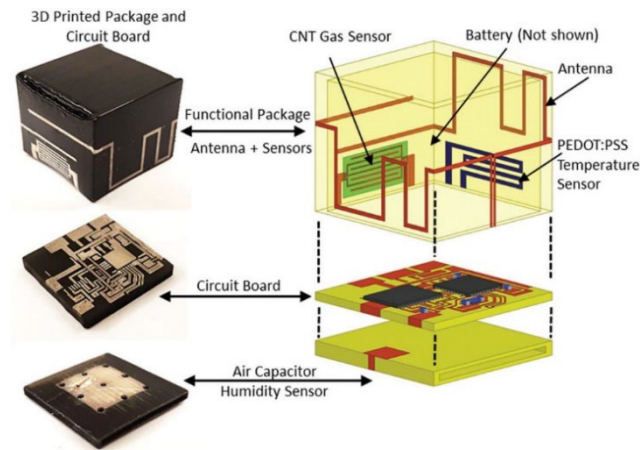


Figure 1.9: An example of a 3D-printed, wireless sensor device [34].

The use of additive manufacturing requires designing objects using CAD software (e.g. Autodesk Inventor). These objects can then be simulated and used to optimise designs with computational fluid dynamics (CFD).

1.8. Electronics and signal processing

1.8.1. Microcontrollers and microprocessors

A microcontroller is a simple computer based on an integrated microprocessor system implemented as a single integrated circuit (IC) containing a central processing unit (CPU), RAM memory, extensive input/output circuits, timers and counters, and interrupt controllers. It can be equipped with programable memory such as FRAM, MRAM, ROM or Flash. It can perform a series of arithmetic or logical operations in a loop. Therefore it is widely used in automation. A microcontroller can optionally be equipped with serial communication controllers (universal asynchronous receiver-transmitter (UART), serial peripheral interface (SPI), inter-integrated circuit (I²C), and universal serial bus (USB)), simple analog-to-digital or digital-to-analog converters, electrically erasable programmable read-only memory (EEPROM), real-time clock (RTC), watchdog timer, and internal sensors of non-electrical quantities, such as temperature sensor [35]. Figure 1.10A presents an example of a microcontroller chip.

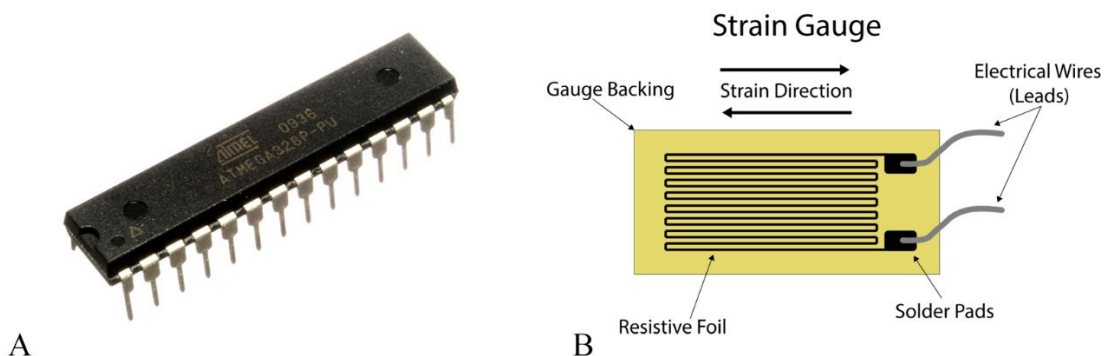


Figure 1.10: A) an example of a ATmega328P single-chip microcontroller by Atmel [36]. B) an example of a load cell schematics [37].

1.8.2. Load cells and Wheatstone bridge

A load cell is a force transducer used to measure tension. In practice, the deformation of a sensor is measured and the stress is calculated based on the assumed physical relationship. For example, Hooke's law can be used. Strain gauges are also used indirectly to measure non-electrical quantities such as force, pressure, acceleration, and mass [38]. Figure 1.9B presents an example of a strain gauge schematics.

Wheatstone bridge is a system consisting of four balanced resistors. There are three configurations, the first is called quarter-bridge with one strain gauge, the second is half-bridge with two load cells and the third is full-bridge with four strain gauges. Figure 1.10 presents Wheatstone bridge schematics. Known excitation voltage V_{EX} is applied to the bridge and output voltage V_O is measured. When a bridge is balanced then V_O is equal to zero. If resistance in any of the resistors changes, then a bridge is no longer in balance and output voltage can be measured and analysed with the use of Ohm's law [38].

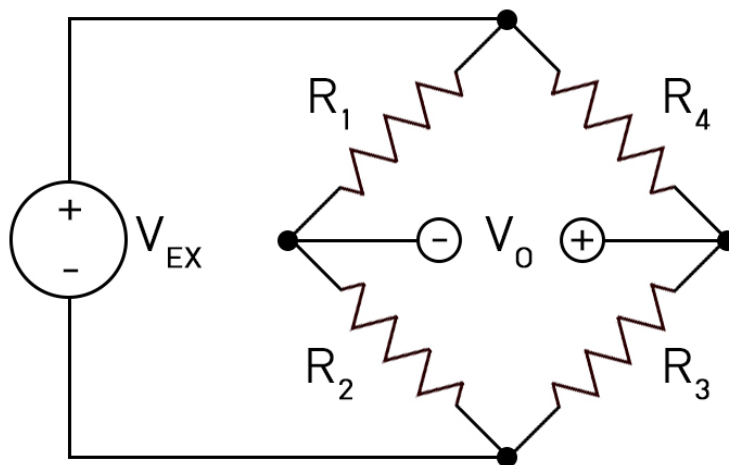


Figure 1.11: Wheatstone bridge schematics [39].

$$V_O = \left(\frac{R_2}{R_1 + R_2} - \frac{R_3}{R_3 + R_4} \right) V_{EX}, \quad (\text{eq. 1})$$

where V_O , V_{EX} , R_1 , R_2 , R_3 , R_4 indicate measured output voltage (V), applied excitation voltage (V), resistors and/or load cells resistance (Ω), respectively.

1.8.3. Gyroscope

In electronics, a gyroscope, or gyro is a device used to control or calculate rotational motion. It is a microelectromechanical system (MEMS) which makes it a compact and economical solution. The measured speed of rotation or angular velocity is in revolutions (RPS) or degrees per second ($^\circ/\text{s}$). Figure 1.12A presents a scanning electron microscope (SEM) micrograph of an example of the MEMS gyroscope [40].

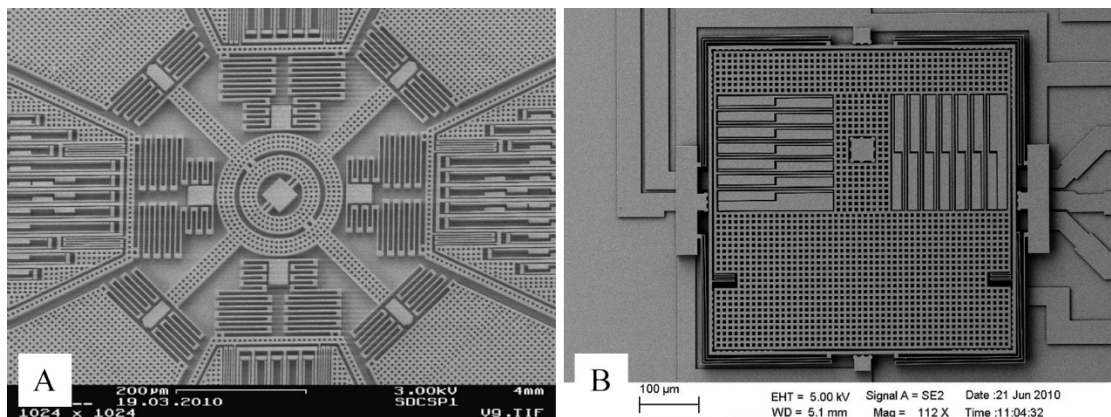


Figure 1.12: A) SEM micrograph of an example of the MEMS gyroscope [41]. B) SEM micrograph of an example of the 3-axis accelerometer [44].

In 2015 major producers of the global MEMS gyroscope market were companies such as Analog Devices Inc., Bosch Sensortec, InvenSense Inc. and STMicroelectronics NV. For instance, MEMS gyroscopes are widely used in wearable electronics, cell phones, mobile devices, and gaming consoles [41].

1.8.4. Accelerometer

An accelerometer is another MEMS device widely used in the electronic industry. It is one of the first devices created with micromachining technology [42]. As the name suggests it is designed to measure the acceleration of the object in meters per second squared (m/s^2) or in gravitational force equivalent (g). They are used to detect vibrations, orientation or acceleration [43]. Figure 1.11B presents an SEM image of an example of a MEMS accelerometer.

1.8.5. Global Positioning System (GPS)

The Global Positioning System (GPS) is a system that allows determining position, navigation and timing (PNT). GPS system can be divided into three sections, the space system, the control segment, and the user section. First, consist of a constellation of thirty-one satellites orbited at 20,180 km height. Second is the network of sixteen ground control stations. The user interface consists of around 6.4 billion units [45]. It is owned by the United States of America (USA). GPS is operated, maintained and developed by the USA Space Force [46]. To determine the location, the user interface device receives GPS signals from the satellites, obtain pseudoranges and compute the navigation calculations to determine coordinates and time [45]. Radiofrequency used in the system is in a range from 1.1 to 1.5 GHz. Figure 1.12A presents the visualization of the latest GPS III-A satellite.

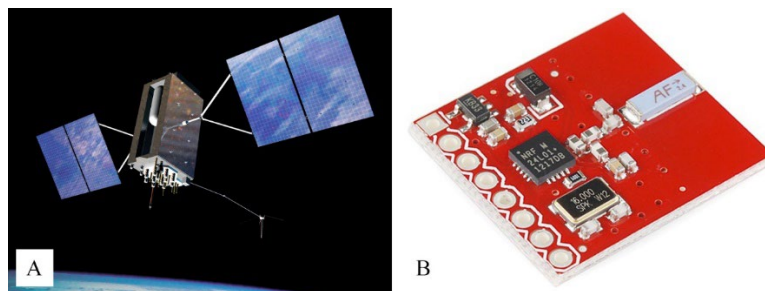


Figure 1.13: A) visualization of the latest GPS III-A satellite, launched in Dec 2018 [46]. B) photograph of an SparkFun nRF24L01+ transceiver module [48].

1.8.6. Transceiver

A transceiver is a widely used electronic device designed for radio communication. It consists of a transmitter and a receiver. As a combination of both, it can send and receive radio waves. One example of a transceiver device can be a cell phone which enables people to have a long-distance conversation. A radio signal is sent from one cell phone to a network of cell towers and then to another cell phone on the other side. Another use of transceivers is a wireless modem. Routers allow to sending and receive digital data. In the aircraft industry, they are called transponders and they are used to identify planes by air traffic control radar. For example, in mechatronics, transceivers can be used to send data from sensors, telemetry, trigger functions from the distance, communicate with the master device, and receive commands [47]. Figure 1.12B presents an example of a transceiver breakout module with a built-in antenna.

1.8.7. Cell phone as everyday measurement tool

Nowadays, every smartphone has several sensors which can be used to track users activity, and navigation. For example, Snapchat application developers check if somebody is moving by gathering data from the use of the phone's accelerometer. Fitness applications also use this sensor to count a number of steps. With the development of augmented reality applications, the accelerometer has an invaluable role in determining the way cell phone is pointing. Another sensor used in mobile phones is a gyroscope [49]. It is widely used in games, where for instance user can pretend that the phone is a steering wheel, by tilting the device, a gyroscope can sense the orientation of the phone and provide necessary data to the game and software will translate it to direction and speed of the driven vehicle. In smartphones, a magnetometer is used for compass applications as well as it is responsible in combination with gyro and accelerometer for determining where in space the device is. Moreover, it can

be used as a metal detector. GPS system in smartphones is used to give users directions, and positions in the world. It is designed in a way that does not need mobile data to operate. There is a possibility to download the map of the region of interest and GPS will work without a network connection. Biometric sensors are used to recognize the owner of the device. It can be a fingerprint sensor or facial recognition system. They provide more protection and convenience than personal identification number (PIN) codes. For example, biometric sensors can be used to log in to a bank account. In high-end phones, light detection and ranging (LiDAR) or Soli sensors are used to recognize the motion around the device. For example, the Google Pixel 4 phone can detect if a user is reaching for the phone and trigger face recognition before a user will touch the device. Another is the proximity sensor which switches off the screen when the user has the phone up to ear during the conversation. An ambient light sensor can measure the intensity of the light in a given environment and adjust the brightness of the screen. [49]. Figure 1.13 presents an example of disassembled mobile phone with visible electronics.



Figure 1.14: Photography disassembled cellphone with visible components [49].

Modern cellphones are versatile measuring devices that can provide benchmark data in certain conditions. With a dedicated application, users can access all sensors of the device and record their measurements. MEMS technology allows the production of small yet accurate sensors [49].

1.9. C++ programming language

C++ is a programming language developed by Bjarne Stroustrup from the C programming language. Over the years language evolved and has object-oriented, generic and functional features. It can be used for low-level memory manipulation. In most cases, it is implemented as a compiled language. Companies such as Free Software Foundation, LLVM, Microsoft, Intel, Oracle, and IBM, provide the necessary software to compile the programs [50].

C programming language is part of the family which include ALGOL and FORTRAN languages. They are characterized by programs consisting of sequences of operations using a nomenclature resembling algebraic representation. Lines of code are performed based on a logical conditions. The majority of data has its type such as character, integer, real number, and name [51]. By 1980 language was used in many applications and in 1984 ANSI set up a committee called X3J11 to standardize C. In this time the role of C as the most prominent programming language was established. Bjarne Stroustrup of AT&T Bell Laboratories designed a C language expansion named C with Classes. His major aim was to develop more useful language with higher-level abstractions. The introduction of classes was the biggest improvement. It is characterized by implementing an object-oriented programming style, where code is written in a way to create software objects resembling real-world objects. In 1985 C with Classes evolved into C++, and started to be applied outside

of AT&T Bell Laboratories. In 1987 ISO and ANSI created separate committees called Working Group 21 and X3J16 respectively to introduce a standard for C++. ISO standard ISO/IEC 14882-1998 was introduced in 1998 [51].

1.10. Polymer heat treatment (annealing)

Studies in the past proved that 3D printed composites demonstrate orthotropic nature with significantly reduced interlayer mechanical parameters [52]. Researchers proved that annealing can be a viable option in order to improve the tensile strength of FDM printed parts. In one of the studies two thermoplastic polymers were tested, a semi-crystalline PLA and an amorphous PETG [52]. For PLA annealing temperature was determined as above glass transition but no higher than cold-crystallization. Crystals growth have an impact on the diffusion of the polymer chains between layers. In the case of the PETG, annealing temperature above glass transition proved to be a viable option. Research work concluded that the rheological and thermal behaviour of tested polymers have an impact on interlayer mechanical parameters. Moreover, research work reported that annealing is effective in improving tensile strength between layers. PLA reinforced with carbon fibre (PLA-CF) exhibits two times and PETG reinforced with carbon fibre (PETG-CF) three times higher interlayer tensile strength hence to the annealing process. Additionally, the use of the heat treatment process improved Young's modulus and ductility of the extrusion printed materials. PLA-CF showed 1.48 times and PETG-CF exhibited a 1.65 times rise of Young's modulus in comparison to unannealed samples of the same materials. Finally, 49 % for PLA-CF and 64 % for PETG-CF increase in interlayer strain-to-failure was observed [52]. One of the methods of determining mechanical parameters of thermoplastic materials can be the three-point bending testing.

1.11. Mechanical testing (three point bend test)

The three-point bending test is used to evaluate the modulus of elasticity in bending E_f , flexural stress σ_f , flexural strain ε_f and the flexural stress–strain response of the materials (equations 2, 3, and 4, respectively). The test is usually performed on a universal testing machine (tensile testing machine or tensile tester) with a three-point bend fixture. Figure 1.14 presents a schematic of the three-point bend test [53].

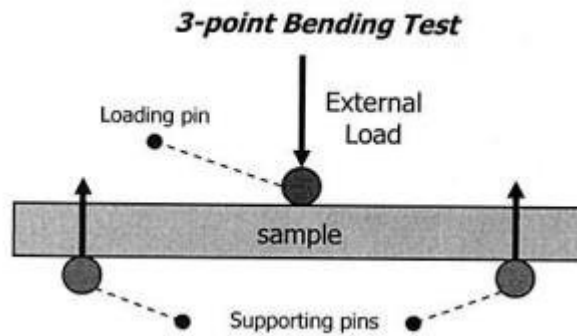


Figure 1.15: Schematic of 3-point bending test [53].

Calculation of the flexural stress σ_f :

$$\sigma_f = \frac{3 FL}{2bd^2}, \quad (\text{eq. 2})$$

where F, L, b, d indicate load at a given point on the load deflection curve (N), support span (mm), the width of test beam (mm), and the thickness of tested beam (mm), respectively.

Calculation of the flexural strain ε_f :

$$\varepsilon_f = \frac{6Dd}{L^2}, \quad (\text{eq. 3})$$

where D indicates maximum deflection of the centre of the beam (mm).

Calculation of the flexural modulus E_f :

$$E_f = \frac{L^3 m}{4bd^3}, \quad (\text{eq. 4})$$

where m indicates the gradient (i.e., slope) of the initial straight-line portion of the load deflection curve.

The test is characterised by applying force to a sample with a single load pin positioned in the midpoint between two supporting pins. The typical load vs deflection response differ depending if researched material is characterised by brittle (Figure 1.15A), or ductile (Figure 1.15B) mechanical behaviour.

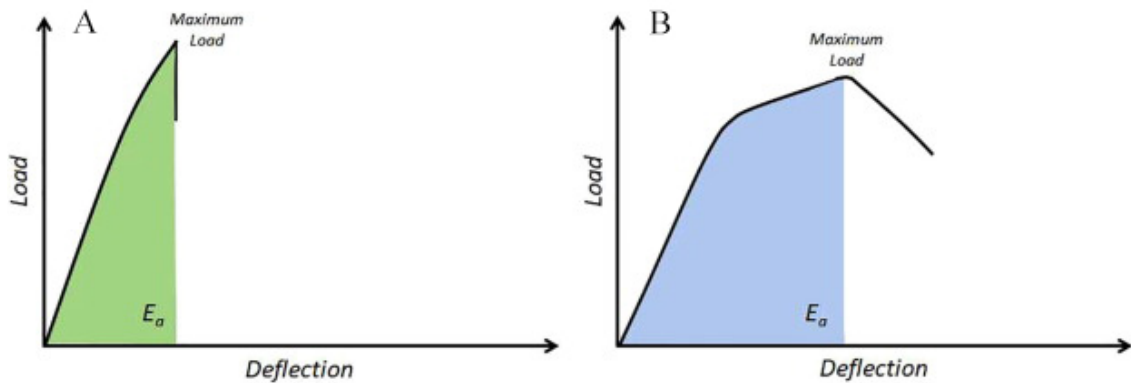


Figure 1.16: Typical load vs deflection response of tested material. A) brittle mechanical behaviour. B) ductile mechanical character [54].

Then data can be analysed to calculate various parameters of material's performance mentioned above. The absorbed energy E_a can be determined by calculating area below load vs deflection graph [54]. Typically, the test is used to better understand material's behaviour where a simple uniaxial tension, or compression tests do not provide enough information. During flexing, specimen is introduced to a combination of loads (tension, compression, and shear) [55].

1.12. Aims

The main aim of this research project is to design, test, validate and develop an instrumented fin that is interfaced to a measuring and data collection unit built into a surfboard. Collection of data is necessary to determine behaviour and mechanical parameters of researched design. Typically, the surfboard equipment development process is based on verbal feedback gathered from surfers participating in field tests. The approach presented in this study focus on obtaining measurable and objective data which can be potentially compared with data gathered from different trials. Therefore, human factors and potential prejudice towards new designs can be eliminated. Additionally, the presented approach allows collecting parameters such as vibration frequency and amplitudes, fin flex, and forces which are impossible to convey verbally by trials participants.

The specific aims are as follows:

- **Aim 1.** Customisation of a 3D printer in order to 3D print with carbon fibre composites - in order to use a broader spectrum of materials, changes such as hardened steel nozzle, and parts of the hot end are necessary. 3D printer customisation steps and details are presented in Chapter 2.6,
- **Aim 2.** 3D printing of model samples and instrumented fins - the first step of the presented goal is to produce a number of samples from various materials. The second phase of the aim is to determine the 3D printing process combined with sensors introduction into instrumented fins. For details see Chapter 2.1 and Chapter 3,
- **Aim 3.** Design, and manufacturing of moulds and tools used for mechanical analysis and data collection unit - this phase of the project consists of the development of rectangular samples, instrumented fin, electronic box,

transceiver, two three-point bend test tools, router templates, mould for samples, touch probe, and a dry box (see Chapter 2.2 and Chapter 3.2).

Designs were used to meet requirements set in Aim 4 and Aim 5,

- **Aim 4.** Mechanical analysis of model samples and fins - performed on previously designed and developed solutions (see Aim 3). Obtained data was used to determine the mechanical parameters of researched materials. (see Chapter 2.10 and Chapter 3.3),
- **Aim 5.** Laboratory and field-testing of instrumented fins - the final goal of the project is the characterisation of the instrumented fin and integration with data collection unit. Parameters are required to be able to accurately analyse field-collected data (see Chapter 2.10 and Chapter 4).

Chapter 2: Materials and methods

2.1. Materials and 3D printing technology

The following filament materials (Table 2.1) were used in a 3D printer to produce fins and rectangular samples. The presented filaments were obtained in a 1 kg spool rolls. All filaments used were 1.75 mm in diameter.

Table 2.1: Filament materials, and fabrics used to produce rectangular samples and instrumented fins. 200 gsm, 240 gsm, and 265 gsm indicate 200 grams per square metre, 240 grams per square metre, and 265 grams per square metre, respectively. Cubic Technologies indicates an Australian shop with 3D printing accessories.

Material	Source
Poly(lactic acid) (PLA)	Cubic Technologies
Poly(ethylene terephthalate glycol-modified) (PETG)	Cubic Technologies
Carbon fibre reinforced PETG (PETG-CF)	PrintMe (Poland)
Bamboo fibre reinforced PLA (Bamboo PLA)	Cubic Technologies
Cork fibre reinforced PLA (Cork PLA)	Cubic Technologies
Carbon fibre reinforced Nylon 12 (PA12-CF)	Cubic Technologies
Carbon fibre reinforced Nylon 6 (PA6-CF)	Cubic Technologies
Glass fibre reinforced Nylon 12 (PA12-GF)	Cubic Technologies
PA12-CF	PrintMe (Poland)
High temperature PLA (HT PLA)	PrintMe (Poland)
Conductive PLA	PrintMe (Poland)
Conductive TPU	PrintMe (Poland)
Fibreglass (plain weave fabric, 265 gsm)	Beyond Materials
Carbon fibre (twill weave fabric, 200 gsm)	Beyond Materials
Basalt fibre (plain weave fabric, 200 gsm)	Beyond Materials
Kevlar/carbon fibre (h weave fabric, 200 gsm)	Beyond Materials
Carbon fibre prepreg (twill weave fabric, 240 gsm)	Beyond Materials

Samples and instrumented fins were 3D printed with the use of a modified Creality3D CR-10S (FDM) 3D printer. Modifications included changes of the nozzle, extruder, motherboard, stepper drivers, build plate, creating dry chamber for Nylon-based materials, and incorporating PTFE tubing.

2.2. CAD

2.2.1. Rectangular sample design

A rectangular sample of 20 mm width, 100 mm length, and 5 mm height was designed using an extrusion tool in Autodesk Inventor software (Figure 2.1).

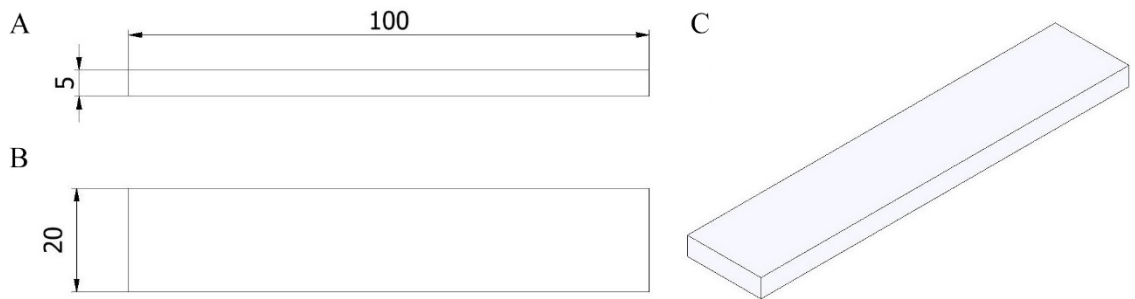


Figure 2.1: CAD model of the rectangular sample. A) side view. B) top view. C) isometric view. Numbers 20, 100, 5 indicate width (mm), length (mm), and height (mm), respectively.

2.2.2. Sample design with incorporated sensor

A rectangular sample with a sensor was developed in order to research conductive filaments. It is 20 mm width, 110 mm length, and 5 mm height. The sensor has a trapezoid cross-section with 3.6 mm bottom width, 7.2 mm top width, and 1 mm height. Figure 2.2 depicts a CAD model of the rectangular sample with a sensor.

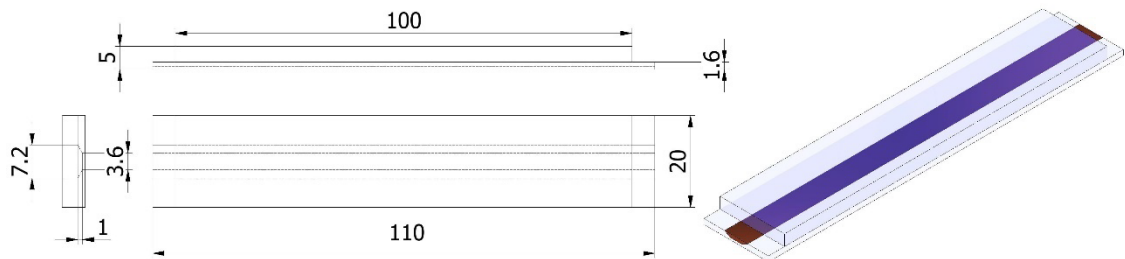


Figure 2.2: CAD model of the sample with sensor.

2.2.3. Instrumented fin design

The outer shape of an instrumented fin was inspired and measured from commercially available Futures T1 Twin HC fin (Futures Fins). The design was conducted with the Autodesk Inventor software. Tools such as extrude, loft, chamfer, fillet were used. Figure 2.3 presents the design of the instrumented fin. Designed sensor indicated as number 1 (Figure 2.3A) has dimensions of 143 mm length, 7.2 mm top width of a trapezoid, 3.6 mm bottom width of trapezoid and 1 mm height, respectively.

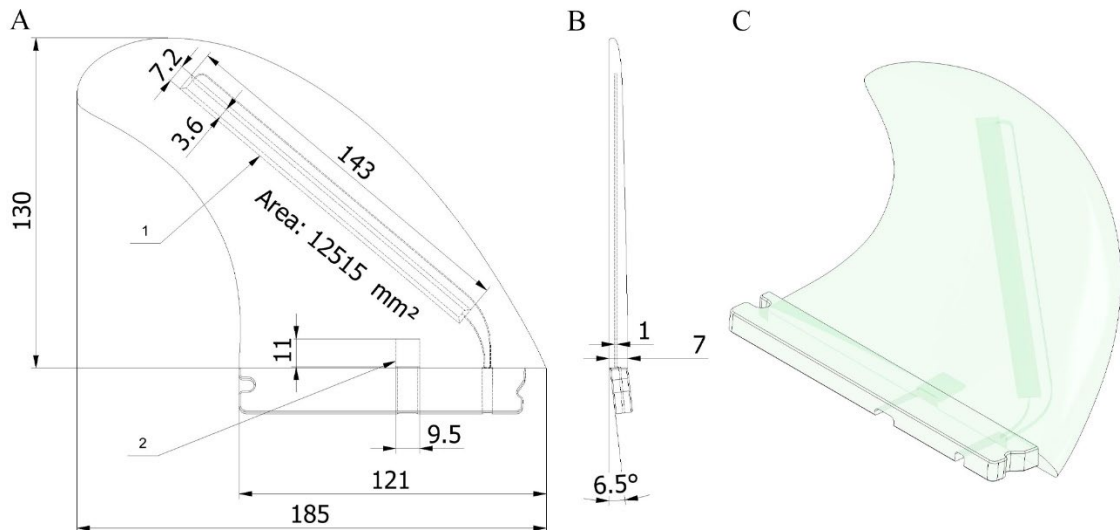


Figure 2.3: CAD design of instrumented fin. A) top view. B) front view. C) isometric view. Numbers 1-2 in A indicate 3D printed sensor (1), and pocket (2) for commercially obtained Wheatstone bridge, respectively. Numbers 130, 185, 121, 143, 7.2, 3.6, 11, 9.5, 1, 7 indicate height (mm), rake (mm), base (mm), sensor length (mm), sensor top width (mm), sensor bottom width (mm), pocket length (mm), pocket width (mm), sensor thickness (mm), and thickness (mm), respectively.

2.2.4. Pandemic tool design and Shimadzu EZ-S test tool adapter design

Two three-point bend test tools were designed. Both of them utilise an 80 mm span between supports. The tool head, as well as supporting pins, have 8 mm in diameter. The design was conducted with the Autodesk Inventor. Figure 2.4 presents the so-called pandemic tool solution and Figure 2.6 depicts the Shimadzu adapter tool design.

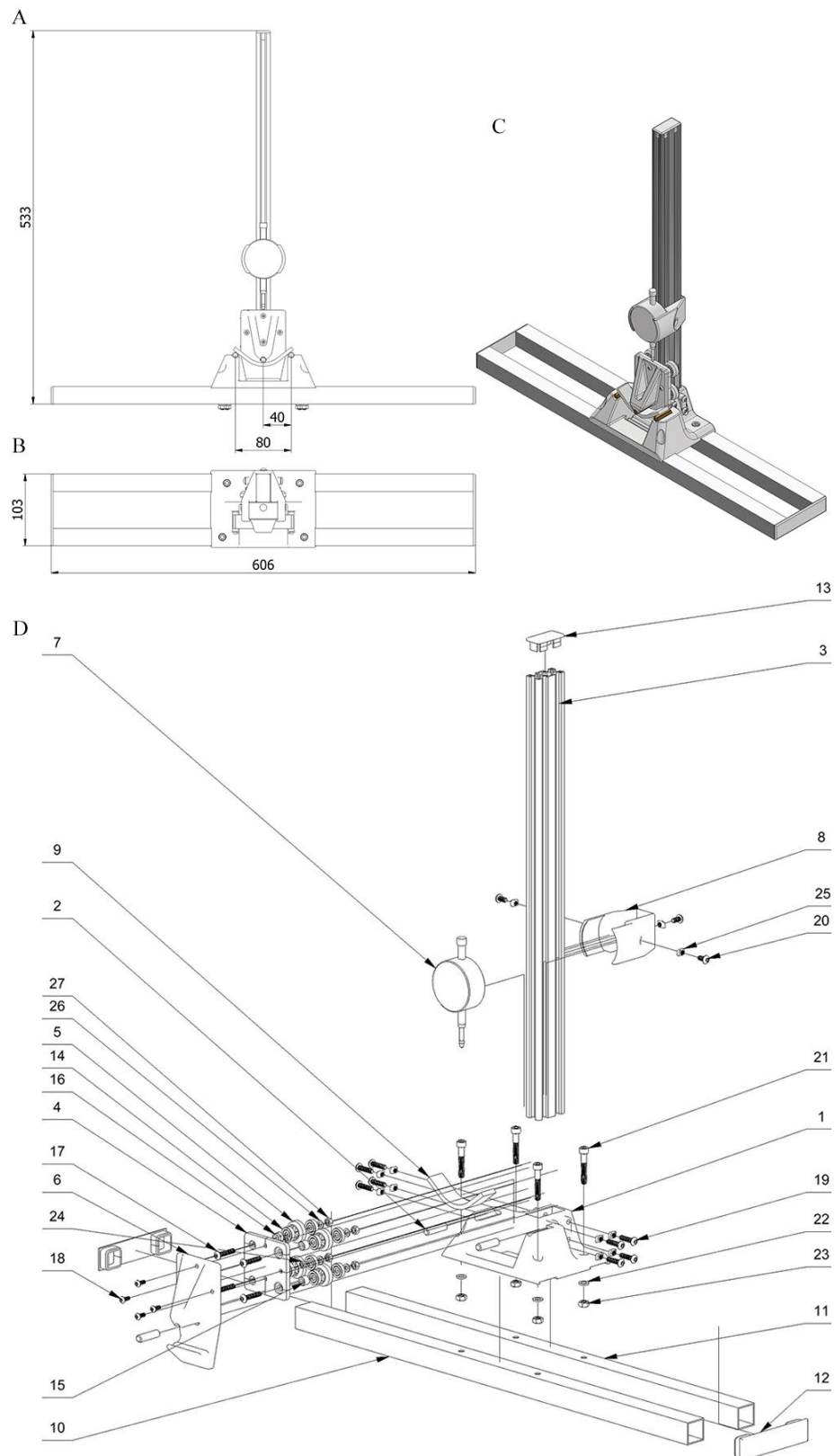


Figure 2.4: CAD model of the pandemic tool assembly for three-point bend test. A) front view. B) top view. C) isometric view. D) exploded view. Numbers in D are explained in Table 2.2. Numbers 553, 103, 606, 80, 40 in A-B indicate height (mm), width (mm), length (mm), distance between supporting pins (mm), and distance between loading pin, and supporting pin (mm), respectively.

The design of the pandemic tool consists of twenty-seven parts listed in Table 2.2. Figure 2.4D. depicts exploded view of a developed solution. In the design, the 2040 V-slot linear rail aluminium extrusion profile (number 3 in Figure 2.3D) was used in conjunction with the V-slot gantry assembly (numbers 4, 5, 6, 9, 14, 15, 16, 17, 18, 24, 26, 27 in Figure 2.5D, respectively). It utilises four V shaped rolls (number 4 in Figure 2.4D) with two 625ZZ bearings (number 14 in Figure 2.4D) per wheel. The solution provides a firm and backlash-free fit. It allows to position the gantry and top pin (number 2 in Figure 2.4D) above the sample. The design provides accurate and repetitive positioning of samples between three pins. Subsequently, the dial indicator (number 7 in Figure 2.4D) was set to zero and measuring of deflection could occur. The gantry top plate (number 6 in Figure 2.4D) design is equipped with a hook to be able to hang wire mesh bin with weights.

Table 2.2: List of parts used for the pandemic tool. Parts indicated as 3D printed were manufactured in-house on a customised Creality CR10-S. Bunnings and Maker Store indicate names of Australian shops, respectively. eBay indicates the name of the American shop.

Part #	Pcs	Name	Material	Source
1	1	Base	PLA	3D printed
2	3	Brass pin (8 mm)	Brass	Bunnings
3	1	4020 v-slot extrusion	Aluminium	Maker Store
4	1	Top plate	PLA	3D printed
5	4	Double bearings wheel	TPE	Maker Store
6	1	Tool	PLA	3D printed
7	1	Dial gauge	N/A	eBay
8	1	Dial gauge holder	PLA	3D printed
9	1	Sample	N/A	3D printed
10	1	Base profile	Aluminium	Bunnings
11	1	Base profile 2	Aluminium	Bunnings
12	2	Side cover	PLA	3D printed
13	1	4020 v-slot plug	PLA	3D printed
14	8	DIN 625 - 625-2Z ball bearing	Chrome steel	eBay
15	2	Plate stand	Aluminium	Maker Store
16	2	Plate stand (off centre)	Aluminium	Maker Store

17	4	ISO 7380 – M5x25 screw	Stainless steel (A2)	eBay
18	4	ISO 7380 – M4x10 screw	Stainless steel (A2)	eBay
19	8	ISO 7380 – M5x20 screw	Stainless steel (A2)	eBay
20	3	ISO 7380 – M5x10 screw	Stainless steel (A2)	eBay
21	4	ISO 4762 – M6x35 screw	Stainless steel (A2)	eBay
22	4	ISO 7092 – ST6 washer	Stainless steel (A2)	eBay
23	4	ISO 4032 – M6 nut	Stainless steel (A2)	eBay
24	4	ISO 4032 – M4 nut	Stainless steel (A2)	eBay
25	11	ISO 299 – M5 nut	Stainless steel	eBay
26	4	ISO 7092 – ST5 washer	Stainless steel (A2)	eBay
27	4	ISO 4032 – M5 nut	Stainless steel (A2)	eBay

For measuring deflection digital dial indicator was used (Figure 2.5A). The comparison between the 3D printed tool utilising presented dial gauge, and the laboratory tool (Shimadzu EZ-S) is depicted in chapter 3 of this work.



Figure 2.5: A) picture of a dial indicator used in pandemic tool [58]. B) picture of a Mijia temperature and humidity meter [59]. C) picture of a Xiaomi Amazfit Pace A1612 smartwatch [60].

The range, resolution, operating voltage, dimensions, and weight of the digital dial indicator are 0 - 12.7 mm, 0.01 mm, 1.5 V, 57 (width mm) x 125 (length mm) x 26 (height mm), and 0.144 kg, respectively. The Mijia temperature and humidity meter was used to collect environmental data during experiment (Figure 2.5B). The brand, model, range of temperature, range of humidity, type of communications, dimensions, and weight of the meter are Mijia, LYWSDCGQ/01ZM, 0 - 60 °C, 0 – 99 %, Bluetooth, 60 (width mm) x 60 (length mm) x 23 (height mm), and 0.055 kg, respectively. The Xiaomi smartwatch was used to track time (Figure 2.5C). The brand, model, CPU type, RAM, eMMC Flash, functions, and weight of the smartwatch are Xiaomi, Amazfit Pace A1612, Ingenic XBurst M200S (2 core, 1.2 GHz + 300 MHz), 512 MB, 4 GB, GPS, heart rate sensor, accelerometer, stopwatch, and 0.055 kg, respectively.

The second designed device used for the three-point bend test was Shimadzu EZ-S adapter. To improve stiffness, 304 stainless steel rods (8 mm in diameter) were incorporated inside the design. The adapter design consists of nine intersecting holes, three in the X-axis, and six in the Z-axis, in which reinforcing rods are glued together with sample support rods (Y-axis). Figure 2.5D presents an isometric view of an adapter base design. Figure 2.6AB presents a CAD model with general dimensions of the proposed adapter solution.

Figure 2.6E is the exploded view showing components of the Shimadzu adapter assembly. The adapter was designed to accommodate Shimadzu tooth-shape press B (part number 346-51814-02) depicted in Figure 2.6E as number 6. The three-point bend test (presented in 1.10) requires accurate positioning between supporting pins and a loading pin. In order to align the adapter base with supporting pins (numbers 2 and 1 in Figure 2.6E, respectively) with the tool with a loading pin (numbers 5 and 1 in Figure 2.5E, respectively), the positioner (number 7 in Figure 2.6E) was designed.

The developed solution was to mount mechanical analyser adapter base with supporting pins (numbers 2 and 1 in Figure 2.6E, respectively), and then lower the Shimadzu EZ-S arm equipped with a tool with a loading pin (numbers 5 and 1 in Figure 2.5E, respectively). The base design consisting of four slots was then finely aligned with tool pin. Subsequently, all four bolts could be tightened. The presented solution consists of a second positioner (number 8 in Figure 2.6E), which was used to align the sample in the middle of the tool and perpendicular to tool pins. Shimadzu press tool (part number 346-51814-02) is tangent with a top pin (number 1 in Figure 2.6E) . During the three-point bend testing, the press is pushing the stainless steel pin. Table 2.3 depicts the list of parts used for the Shimadzu adapter tool.

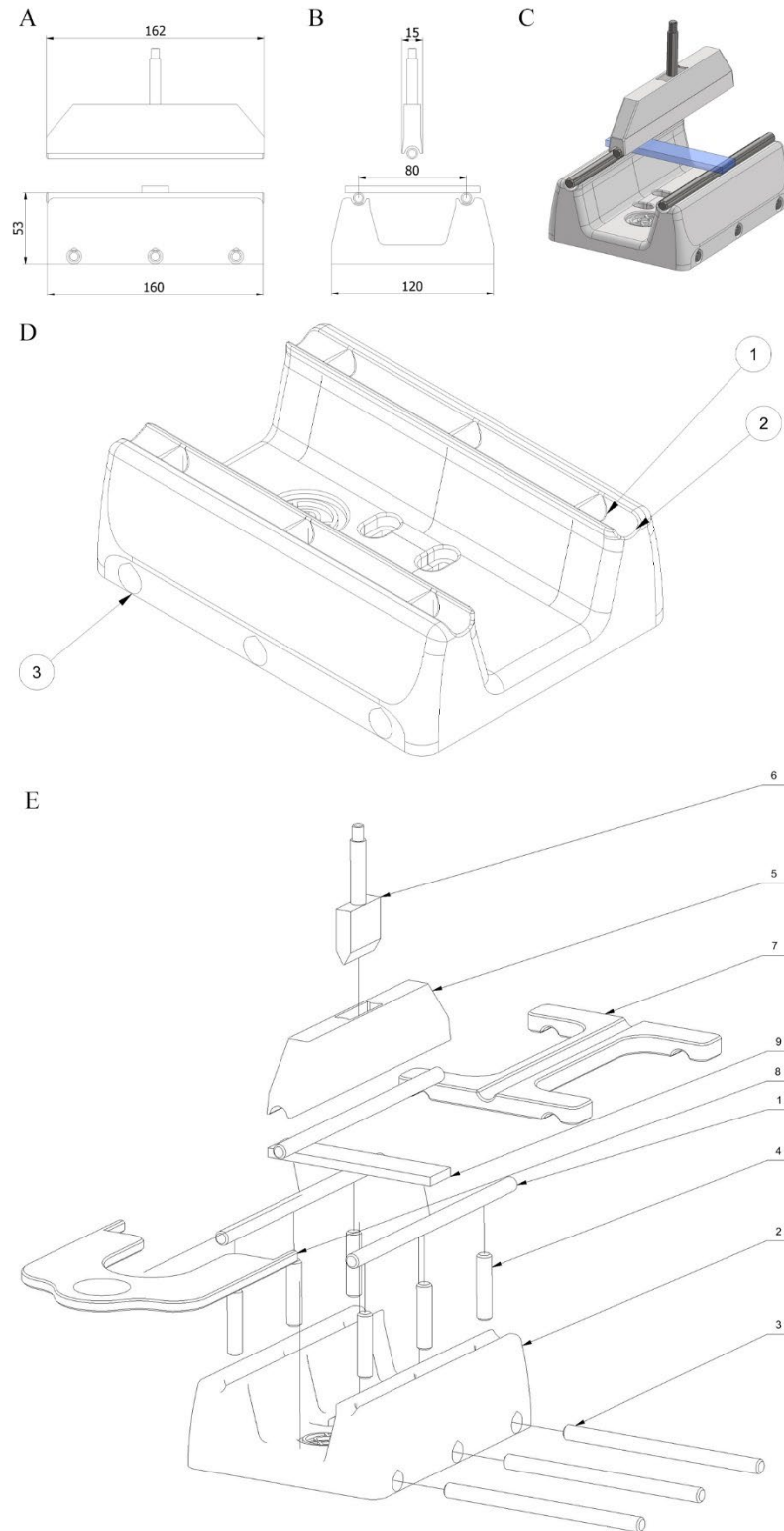


Figure 2.6: CAD model of the three-point bend test Shimadzu adapter solution. A) side view. B) front view. C) isometric view. D) isometric view of an adapter base. Numbers 1-3 indicate: holes in the Z-axis (1), support cut-outs in the Y-axis (2), and holes in the X-axis (3). E) Exploded view of Shimadzu tool assembly. Numbers depicted in the picture are explained in Table 2.3. Numbers 162, 15, 53, 160, 120, 80 in A-B indicate tool head length (mm), tool head width (mm), base height (mm), base length (mm), base width (mm), and span (mm), respectively.

Table 2.3: List of parts used for Shimadzu adapter tool. Parts indicated as 3D printed were manufactured in-house on customised the Creality CR10-S. Maker Store indicates the name of an Australian shop.

Part #	Pcs	Name	Material	Source
1	3	Stainless steel pin (Ø8, 160 mm)	Stainless steel (304)	Maker Store
2	1	Base	PA12-CF	3D printed
3	3	Stainless steel pin (Ø8, 120 mm)	Stainless steel (304)	Maker Store
4	6	Stainless steel pin (Ø8, 35 mm)	Stainless steel (304)	Maker Store
5	1	Shimadzu tool sock	PA12-CF	3D printed
6	1	Shimadzu tool	Stainless steel	Shimadzu
7	1	Tool positioner	PLA	3D printed
8	1	Sample positioner	PLA	3D printed
9	1	Sample	N/A	3D printed

2.2.5. Electronics box design

To accommodate all electronic components inside the surfboard, an electronic box with an acrylic lid (number 16 in Figure 2.7E) were designed and developed. To provide an efficient water-tight seal between both parts, a gasket (number 15 in Figure 2.7E) was produced in-house (Barnes M4642 silicone rubber). The idea was to level electronic box on a 3D printer's heat bed and pour silicon rubber (enough material to create a convex meniscus). The whole assembly was then custom fit to the surfboard. Figure 2.7ABC presents a CAD model with general dimensions of the whole assembly.

Figure 2.7E depicts an exploded view of the presented solution with visible electronic components. It consists of twenty-four different parts indicated in Table 2.4. The casing (number 9 in Figure 2.7E), and some internal components were intended to be 3D printed with the use of PLA filament. All fastenings proposed in the solution were made from stainless steel (A2), due to intended exposure to saltwater during deployment.

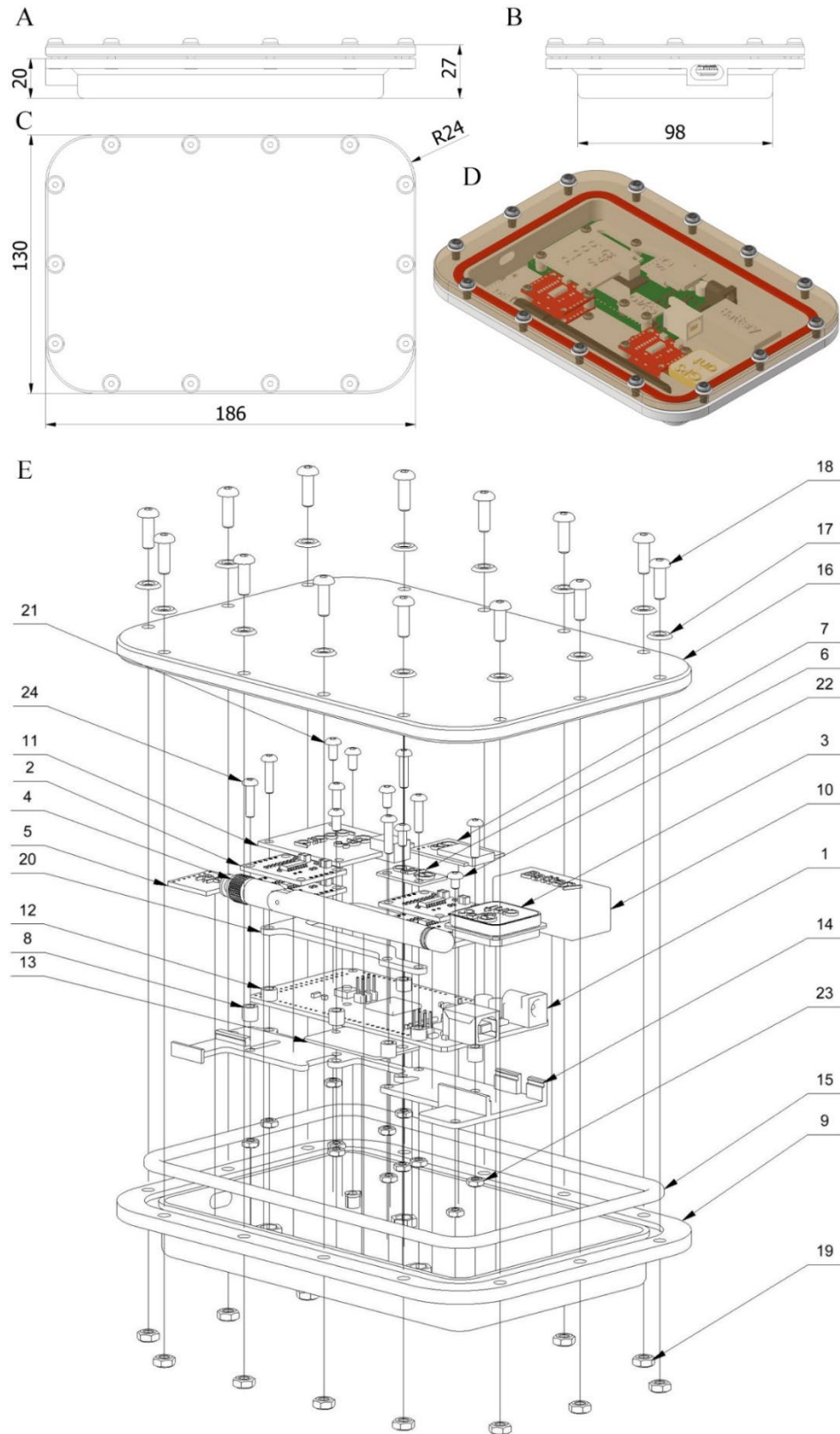


Figure 2.7: CAD model of the electronic box with components solution. A) side view. B) front view. C) top view. D) isometric view. E) Exploded view of an electronic box. Numbers depicted in E are explained in Table 2.4. Numbers 20, 27, 130, 186, 98 indicate base height (mm), height (mm), width (mm), length (mm), and base width (mm), respectively.

Table 2.4: List of parts used for electronic box. Parts indicated as 3D printed were manufactured in-house on customised the Creality CR10-S. Barnes and Core electronics indicate the names of Australian shops, respectively. eBay indicates the name of the American shop.

Part #	Pcs	Name	Material	Source
1	1	Arduino Mega 2560	N/A	Core electronics
2	4	HX711 load cell amplifier	N/A	Core electronics
3	1	GPS antenna	N/A	Core electronics
4	1	Transceiver antenna	N/A	Core electronics
5	1	nRF24L01L+ transceiver	N/A	Core electronics
6	1	MPU6050 gyro/accelerometer	N/A	Core electronics
7	1	µSD card reader	N/A	Core electronics
8	4	Stand (5mm)	PLA	Core electronics
9	1	Electronic casing	PLA	Core electronics
10	1	Battery pack	N/A	Core electronics
11	1	NEO-M9N GPS	N/A	Core electronics
12	3	Stand (4mm)	PLA	3D printed
13	1	Bridge board	N/A	Core electronics
14	1	Electronic holder	N/A	Core electronics
15	1	Gasket	Silicone rubber	Barnes
16	1	6mm cover	Acrylic	eBay
17	14	Casing washer	PLA	3D printed
18	14	ISO 7380 – M4x12 screw	Stainless steel (A2)	eBay
19	14	ISO 4032 – M4 nut	Stainless steel (A2)	eBay
20	1	Electronic holder top	PLA	3D printed
21	5	ISO 7380 – M3x6 screw	Stainless steel (A2)	eBay
22	1	ISO 7380 – M3x4 screw	Stainless steel (A2)	eBay
23	12	ISO 4032 – M3 nut	Stainless steel (A2)	eBay
24	7	ISO 7380 – M3x12 screw	Stainless steel (A2)	eBay

2.2.6. Transceiver box design

An electronic system inbuilt into the surfboard communicates with the laptop or PC via a transceiver. Figure 2.8AB presents a CAD model of transceiver assembly with general dimensions.

The design was obtained with the use of extrude and chamfer tools in Autodesk Inventor CAD software. Figure 2.8D presents an exploded view of a data transceiver solution. Assembly consists of ten different components depicted in Table 2.5. The designed mount (number 6 in Figure 2.8D) allows to hang the transceiver box on the top of the laptop, which helps with antenna (number 2 in Figure 2.8D) positioning. Moreover, two LED diodes (number 10 in Figure 2.8D) are installed and delegated to blink every time data is received. This solution provides visual information when the signal is lost.

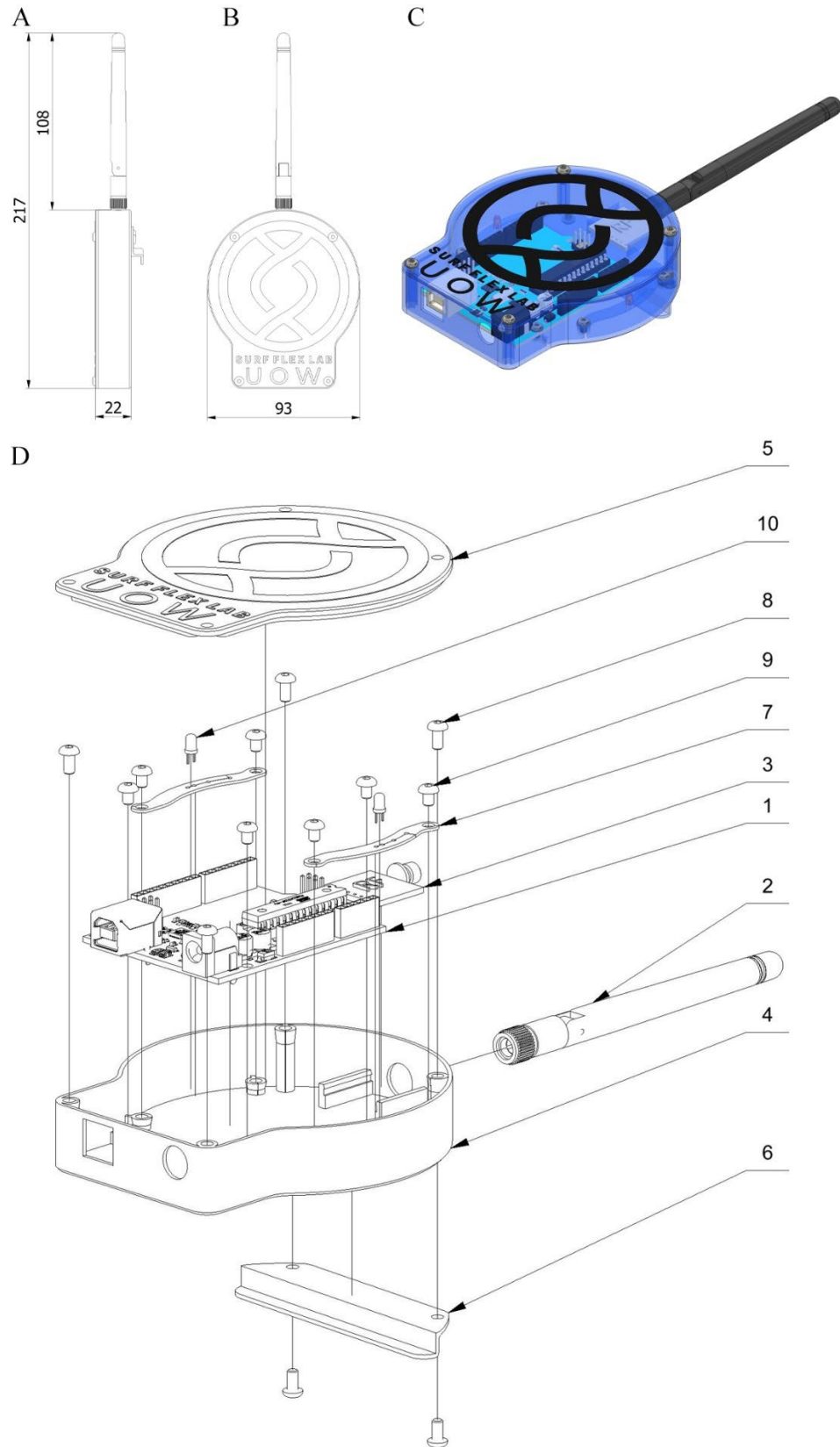


Figure 2.8: CAD model of the data receiver system. A) side view. B) front view. C) isometric view. D) exploded view of a data receiver system. Numbers in D are explained in Table 2.5. Numbers 217, 108, 22, 93 in A-B indicate, length (mm), antenna length (mm), height (mm), and width (mm), respectively.

Table 2.5: List of parts used for the electronic box. Parts indicated as 3D printed were manufactured in-house on customised the Creality CR10-S. Core electronics indicates the name of an Australian shop. eBay indicates the name of the American shop.

Part #	Pcs	Name	Material	Source
1	1	Arduino Uno	N/A	Core electronics
2	1	Transceiver antenna	N/A	Core electronics
3	1	nRF24L01L+ transceiver	N/A	Core electronics
4	1	Case	PLA	3D printed
5	1	Cover	PLA	3D printed
6	1	Laptop mount	PLA	3D printed
7	2	LED holder	PLA	3D printed
8	6	ISO 7380 – M3x6 screw	Stainless steel (A2)	eBay
9	7	ISO 7380 – M3x4 screw	Stainless steel (A2)	eBay
10	2	Red LED diode	N/A	eBay

2.2.7. Tooling design

2.2.7.1. Router templates

The researched surfboard was equipped with an electronic box with components. To be able to achieve that goal, a set of templates were designed. They were necessary to provide stability and path for the used Makita DRT50Z router tool. Three different router bits were used in this process. Figure 2.9AC depicts CAD model with general dimensions of used templates.

Templates consist of two elements presented in exploded view (Figure 2.9D). A two-stage process was developed in order to be able to sink electronic box assembly (number 3 in Figure 2.9D) into the surfboard. Table 2.6 depicts designed elements. Inner shape template (number 1 in Figure 2.9D) acts as a fence for router bit equipped with top-mounted bearing. The outer template (number 2 in Figure 2.9D) provides a barrier for the router base plate. Two-step templates were necessary as the electronic box design consist of a 16 mm flange and it was designed to be situated shallower

in a surfboard. That solution was designed with a condition to limit interference in the structural construction of a surfboard as much as possible.

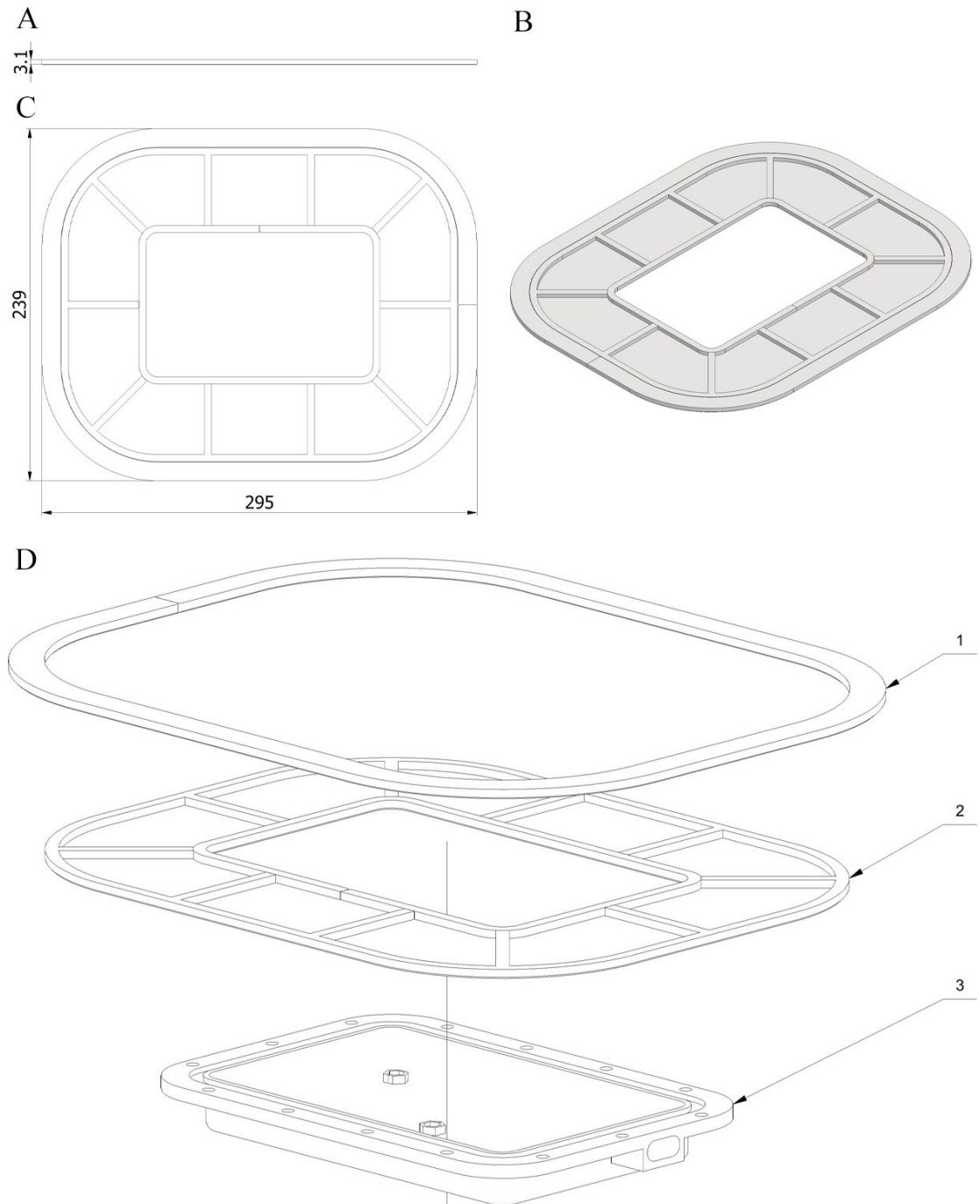


Figure 2.9: CAD model of a router templates for electronic box. A) side view. B) top view. C) isometric view. D) Exploded view of a electronic box templates. Numbers depicted in D explained in Table 2.5. Numbers 3.1, 239, 295 indicate height (mm), width (mm), and length (mm), respectively.

Table 2.6: List of parts used for router templates. Parts indicated as 3D printed were manufactured in-house on customised the Creality CR10-S.

Part #	Pcs	Name	Material	Source
1	1	Router template outer shape	PLA	3D printed
2	1	Router template inner shape	PLA	3D printed
3	1	Electronic case	PLA	3D printed

2.2.7.2. Mould for samples

Sample mould was CNC machined with the use of high-density poly(ethylene) (HDPE) material. Figure 2.10 depicts the CAD model of the solution.

The design consist of two parts, the bottom (number 2 in Figure 2.10E) where wrapped sample was situated and a top part (number 1 in Figure 2.10E) was used as a lid. The solution was designed to be used with 3D printed inserts and different fabric materials such as carbon fibre, fibre glass, or basalt fibre. Then the sample was wrapped in one of the mentioned materials, and was saturated with an epoxy resin. The sample made this way was then placed in the mould and the top part was assembled. C-clamp was then applied to introduce pressure and to help compress layers of fabric and 3D printed inserts. HDPE material was chosen as an epoxy resin cannot stick to it. Figure 2.10E presents an exploded view of a chosen solution.

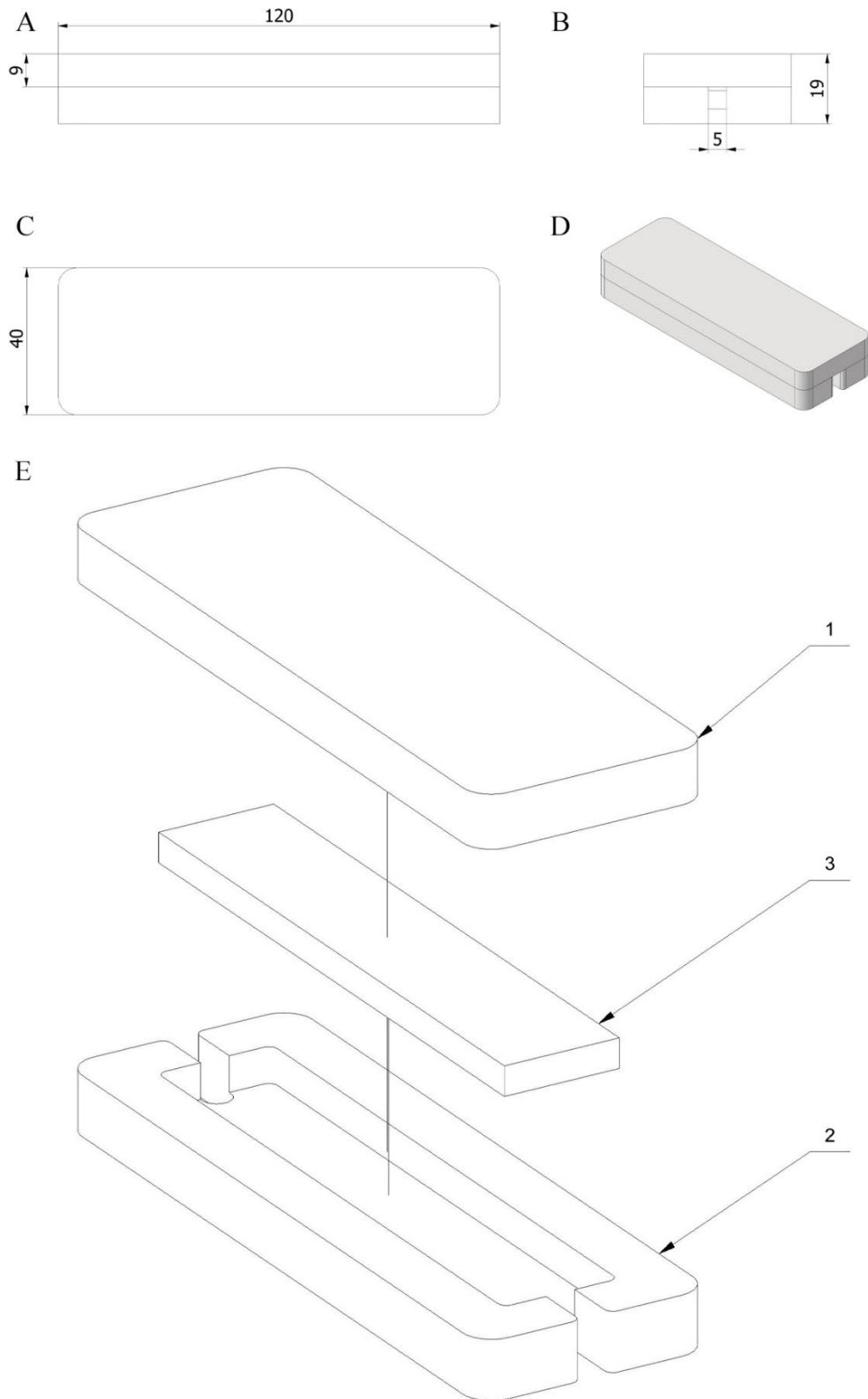


Figure 2.10: CAD model of a mould for rectangular samples. A) side view. B) front view. C) top view. D) isometric view. E) Exploded view of a rectangular sample mould. Numbers depicted in E are explained in Table 2.7. Numbers 9, 120, 40, 5, 19 in A-C indicate cover height (mm), length (mm), width (mm), resin overflow port width (mm), and height (mm), respectively.

Table 2.7: List of parts used for sample mould. Parts indicated as 3D printed, and CNC machined were manufactured in-house on customised the Creality CR10-S, and CNC mill, respectively.

Part #	Pcs	Name	Material	Source
1	1	Mould top	HDPE	CNC machined
2	1	Mould bottom	HDPE	CNC machined
3	1	Rectangular sample	N/A	3D printed

2.2.7.3. Fin mould

Surfboard fin mould was designed in Autodesk Inventor CAD software. Tools such as extrude, loft, combine, fillet, chamfer were used. It was used to produce fins wrapped into fabric materials such as carbon fibre, fibre glass, or basalt fibre with 3D printed inserts. Figure 2.11AB presents a CAD model of the surfboard fin mould assembly with general dimensions.

The design consists of four elements presented on exploded view in Figure 2.11E. The bottom element (number 1 in Figure 2.11D) of the mould was meant to accommodate fabric, resin, and 3D printed insert (number 2 in Figure 2.11D). Mould middle part (number 3 in Figure 2.11D) was designed to be able to compress fabric and to give an opportunity to add top layers of fabric through the cut-out. The mould top (number 4 in Figure 2.11D) was designed to fit the cut-out and help to compress layers of the fabric. The whole assembly was then inserted into the vacuum bag and air was removed. This process helped to squeeze all materials together. The whole process of fin production was designed to be finished with only one set of applied epoxy resin.

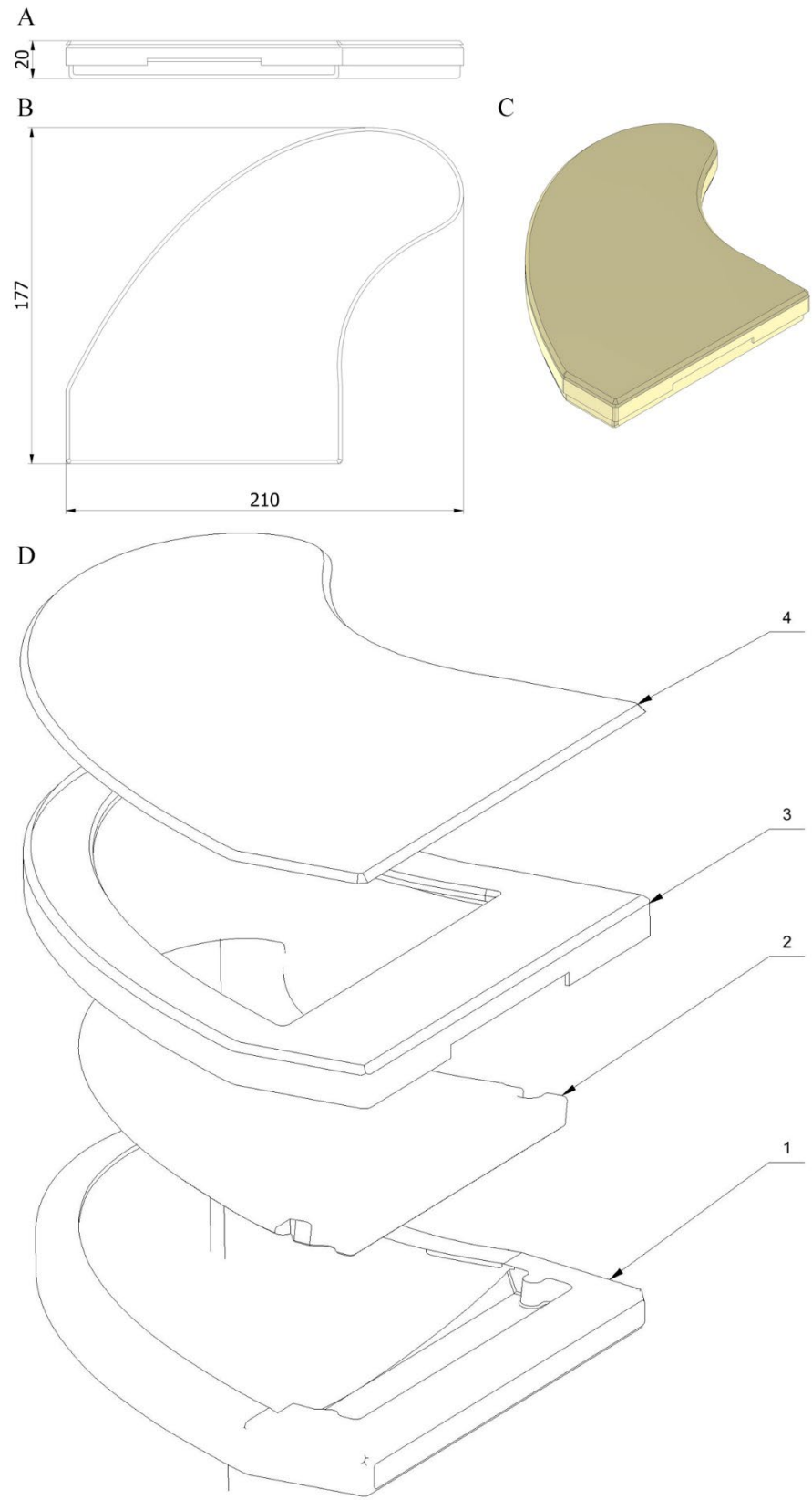


Figure 2.11: CAD model of a mould for surfboard fin. A) side view. B) top view. C) isometric view. D) Exploded view of a mould for surfboard fin. Numbers depicted in D are explained in Table 2.8. Numbers 20, 177, 210 in A-B indicate height (mm), length (mm), and width (mm), respectively.

Table 2.8: List of parts used for fin mould. Parts indicated as 3D printed were manufactured in-house on customised the Creality CR10-S.

Part #	Pcs	Name	Material	Source
1	1	Mould bottom	PLA	3D printed
2	1	Fin insert	PA12-CF / PA6-CF / PLA	3D printed
3	1	Mould middle	PLA	3D printed
4	1	Mould top	PLA	3D printed

2.2.7.4. Touch probe

Touch probe design was inspired by Renishaw touch probes. Figure 2.12AB depicts CAD model and general dimensions of designed solution.

The touch probe consists of nine different elements. The probe (number 6 in Figure 2.12D) depicted in the exploded view has 4 mm in diameter. The principle of the device is that whenever the probe touches the measured object, it breaks the electrical circuit consisting of set of elements (numbers 5, and 7 in Figure 2.12D, respectively) and connected cables. When the probe does not touch the object, the spring (number 8 in Figure 2.12D) compress mentioned elements and current can flow through the circuit. The device was used to measure Futures T1 Twin HC dimensions, and it was designed to fit used CNC machine. Data was collected from the machine coordinates and introduced to Inventor Professional CAD software.

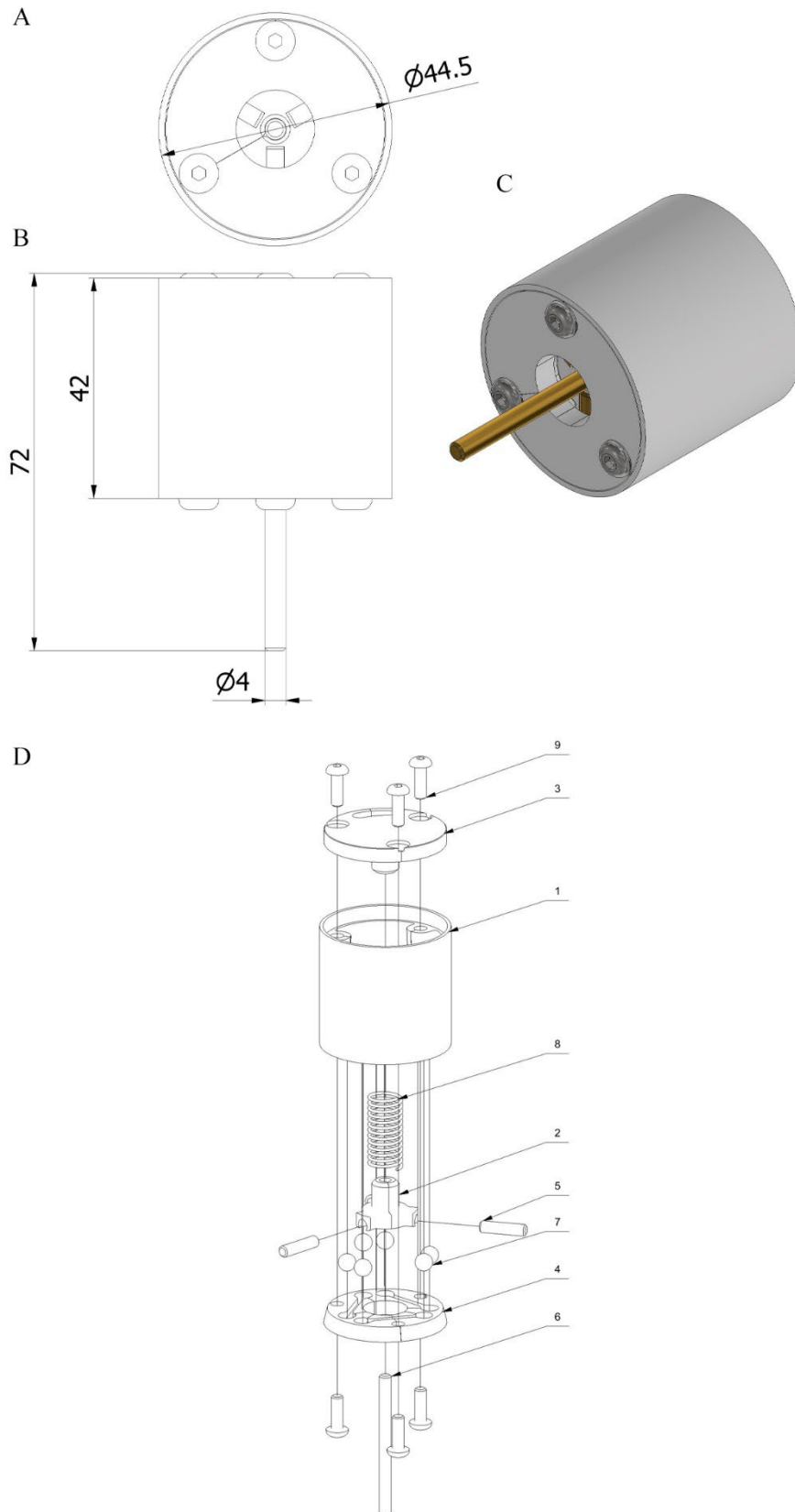


Figure 2.12: CAD model of a touch probe used to design fin. A) top view. B) side view. C) isometric view. D) exploded view of a touch probe solution. Numbers depicted in D are explained in Table 2.9. Numbers 72, 42 in A-B indicate length (mm), and case length (mm), respectively.

Table 2.9: List of parts used for touch probe. Parts indicated as 3D printed were manufactured in-house on customised the Creality CR10-S. Bunnings indicates the name of an Australian shop. eBay indicates the name of the American shop.

Part #	Pcs	Name	Material	Source
1	1	Touch probe case	PLA	3D printed
2	1	Pin holder	PLA	3D printed
3	1	Touch probe top lid	PLA	3D printed
4	1	Touch probe bottom lid	PLA	3D printed
5	3	Pin	Brass	Bunnings
6	1	Probe	Brass	Bunnings
7	6	6mm ball	Chrome steel	eBay
8	1	Spring C-676	Hard drawn carbon steel	Bunnings
9	6	ISO 7380 – M4x12 screw	Stainless steel (A2)	eBay

2.2.7.5. Dry box filament holder

The filament dry box design was based on Sistema 5 l food container. Figure 2.13AB depicts the CAD model of the solution and general dimensions of the system.

The design consists of twelve different components presented in exploded view (Figure 2.13D). To lower air humidity inside the box, silica gel desiccant was used as well as calcium chloride granules. The proposed solution allowed to use of hygroscopic materials such as Nylon-based filaments. For ease of movement, the filament spool roll (number 3 in Figure 2.13D) was equipped with two 6201-2RS bearings (number 12 in Figure 2.13D). The box (number 6 in Figure 2.13D) was connected with a 3D printer's extruder via pneumatic connectors and PTFE tubing.

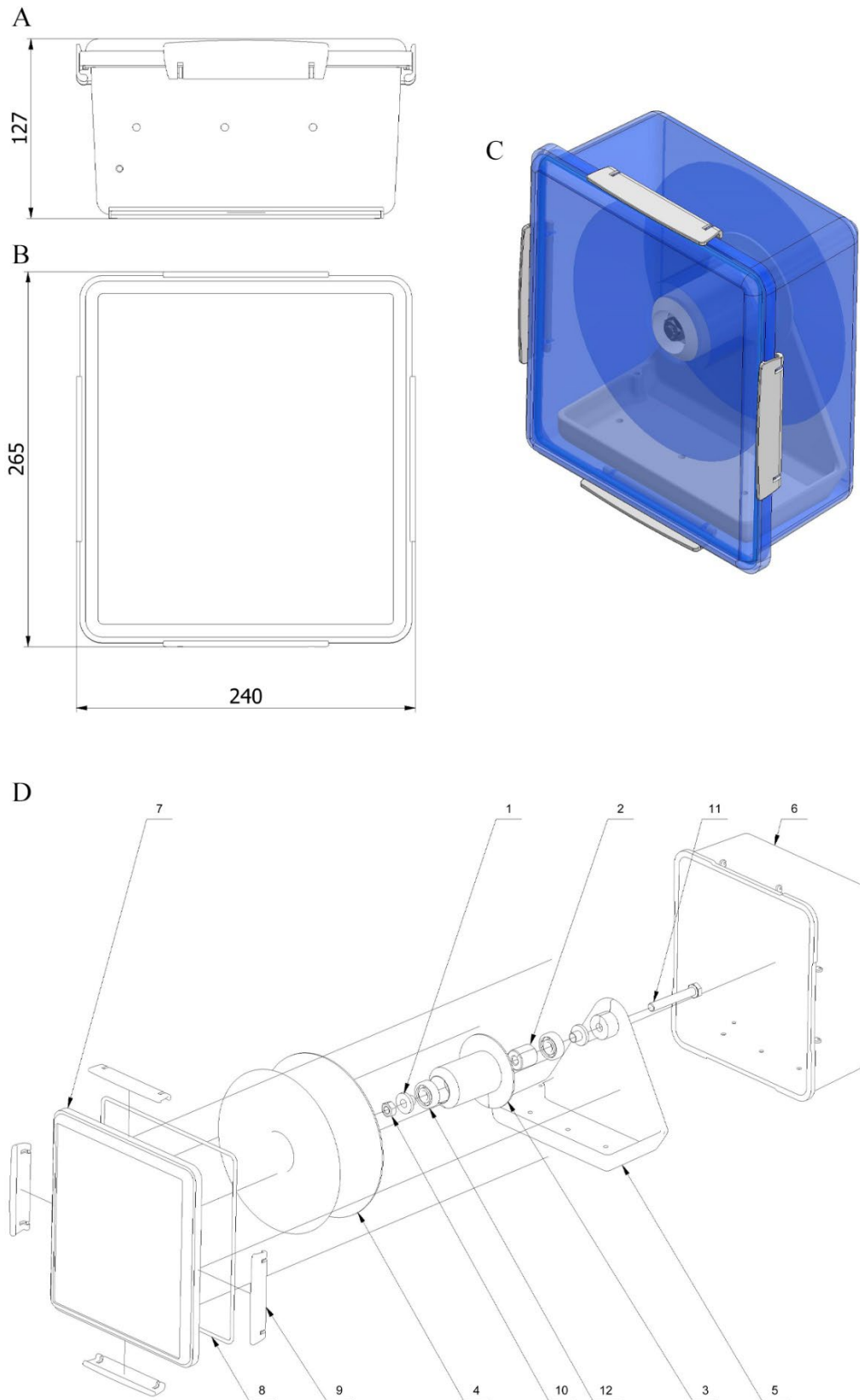


Figure 2.13: CAD model of a dry box solution. A) side view. B) top view. C) isometric view. D) Exploded view of a filament dry box. Numbers depicted in D are explained in Table 2.10. Numbers 127, 265, 240 in A-B indicate height (mm), length (mm), and width (mm), respectively.

Table 2.10: List of parts used for the dry box solution. Parts indicated as 3D printed were manufactured in-house on customised the Creality CR10-S. Bunnings and Woolworths indicate the names of an Australian shops. eBay indicates the name of the American shop.

Part #	Pcs	Name	Material	Source
1	2	Bearing/screw adapter	PLA	3D printed
2	1	Distance	PLA	3D printed
3	1	Spool roll	PLA	3D printed
4	1	Spool	N/A	N/A
5	1	Spool holder	PLA	3D printed
6	1	5l food container	PP	Woolworths
7	1	5l food container lid	PP	Woolworths
8	1	5l food container gasket	Silicone rubber	Woolworths
9	4	5l food container clips	PP	Woolworths
10	1	ISO 4032 – M10 nut	Stainless steel (A2)	eBay
11	1	ISO 4014 – M10 x 70 screw	Stainless steel (A2)	eBay
12	2	DIN 625 – 6201-2RS bearing	Chrome steel	Bunnings

2.3. 3D printer slicer (Cura)

Slicing software works by generating machine movements for each pre-configured layer height layer of produced element. It creates a specific g-code for every machine. Moreover, it consists of printer parameters such as nozzle temperature, heat bed temperature, cooling fan speed, extrusion flow and many more. In this project, Ultimaker Cura software was used for slicing all 3D printed parts. Figure 2.14 depicts the general workspace window of the application. Table 2.11 presents parameters used for 3D printing. They differ accordingly to the used material.

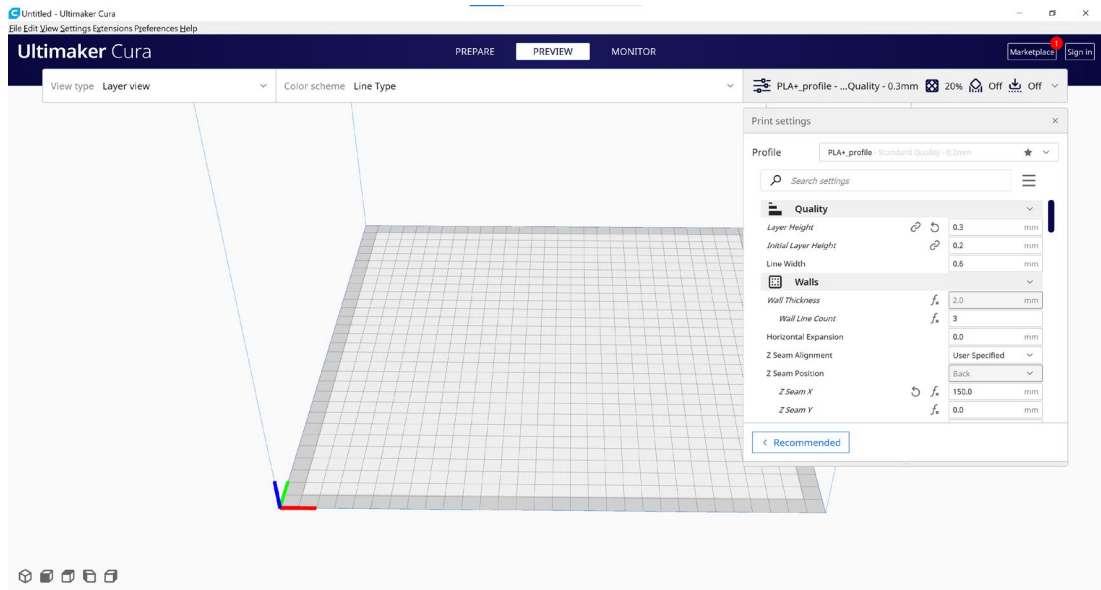


Figure 2.14 Screenshot of an Ultimaker Cura slicer software work space.

Table 2.11: Parameters for used materials.

	PLA / HT PLA / Cork PLA / Bamboo PLA	PETG / PETG-CF	PA6-CF	PA12-CF / PA12-GF
Layer height	0.3 mm	0.3 mm	0.3 mm	0.3 mm
Line width	0.8 mm	0.8 mm	0.8 mm	0.8 mm
Wall line count	2	2	2	2
Top/bottom pattern	concentric	concentric	concentric	concentric
Infill density	35-100 %	35-100 %	35-100 %	35-100 %
Infill pattern	concentric / gyroid	concentric / gyroid	concentric / gyroid	concentric / gyroid
Nozzle temperature	210 °C	240 °C	270 °C	245 °C
Bed temperature	50 °C	70 °C	70 °C	70 °C
Heated chamber	no	no	no	no
Flow	97 %	100 %	75 %	80 %
Print speed	40 mm/s	40 mm/s	40 mm/s	40 mm/s
Print acceleration	500 mm/s ²	500 mm/s ²	500 mm/s ²	500 mm/s ²
Print Jerk	8 mm/s	8 mm/s	8 mm/s	8 mm/s
Retraction distance	1.2 mm	1.2 mm	1.2 mm	1.2 mm
Retraction speed	40 mm/s	40 mm/s	40 mm/s	40 mm/s
Cooling fan speed	100 %	70 %	0 %	0 %
Min. layer time	10 s	10 s	10 s	10 s
Bed adhesion type	skirt	skirt	skirt	skirt
Skirt line count	1	1	1	1
Skirt distance	10 mm	10 mm	10 mm	10 mm

2.4. CAM

In the presented project, the Inventor Professional CAM module was used to generate paths and set parameters for the CNC machine. For all milling purposes, 3 mm in diameter flat endmill was used. For example, to produce an HDPE sample mould, three operations were chosen, first was face milling which allowed flattening the used stock. In the subsequent step, 2D adaptive and 2D contour operations were used. Figure 2.15 depicts a simulation of a 3D parallel milling operation used to produce foam plugs for surfboard fins. Table 2.12 and 2.13 present operation parameters used in the CNC milling process for HDPE, and XPS foam materials respectively.

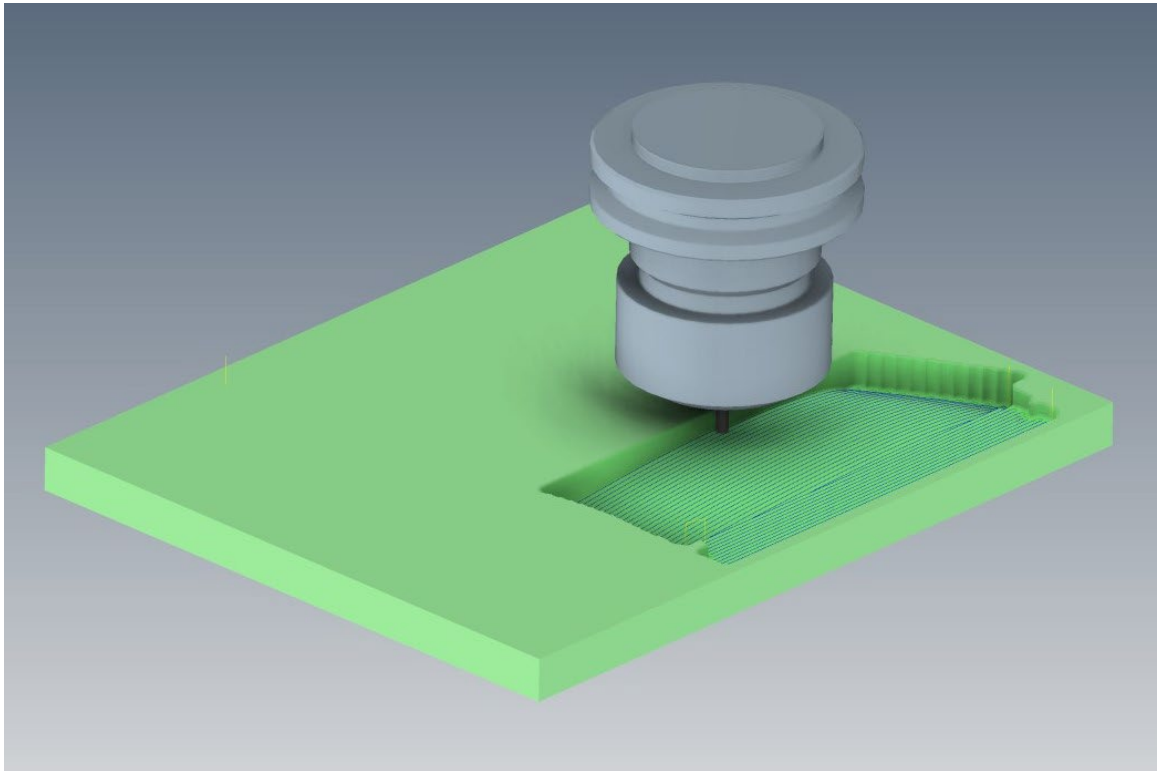


Figure 2.15: Example of a CAM generated simulation of a CNC milling process.

Table 2.12: Parameters of chosen operations used for HDPE milling.

Specification	Face milling	2D adaptive	2D contour
Spindle speed	7000 rpm	7000 rpm	7000 rpm
Surface speed	94.25 m/min	94.25 m/min	94.25 m/min
Ramp spindle speed	7000 rpm	7000 rpm	7000 rpm
Cutting feedrate	1500 mm/min	1500 mm/min	1500 mm/min
Feed per tooth	0.050 mm	0.050 mm	0.050 mm
Lead-in feedrate	1500 mm/min	1500 mm/min	1500 mm/min
Lead-out feedrate	1500 mm/min	1500 mm/min	1500 mm/min
Ramp feedrate	1500 mm/min	1500 mm/min	1500 mm/min
Plunge feedrate	30 mm/min	1500 mm/min	1500 mm/min
Feed per revolution	0.003 mm	0.15 mm	0.15 mm

Table 2.13: Parameters of chosen operations used for XPS foam milling.

Specification	3D parallel	2D contour
Spindle speed	1500 rpm	1500 rpm
Surface speed	14.14 m/min	14.14 m/min
Ramp spindle speed	1500 rpm	1500 rpm
Cutting feedrate	400 mm/min	400 mm/min
Feed per tooth	0.067 mm	0.067 mm
Lead-in feedrate	400 mm/min	400 mm/min
Lead-out feedrate	400 mm/min	400 mm/min
Ramp feedrate	400 mm/min	400 mm/min
Plunge feedrate	30 mm/min	30 mm/min
Feed per revolution	0.02 mm	0.02 mm

2.5. CNC

The CNC mill used for the project was 3018 style generic machine. CNC mill was used in order to manufacture sample mould with the use of HDPE material. The same machine was used for surfboard fin insert production from XPS foam. Moreover, touch probe was design in a way to fit the spindle holder of presented tool. It was used to measure the dimensions of fin (Futures T1 Twin HC - Futures Fins) used as an inspiration for the instrumented one. Figure 2.16 depicts machine used in the project.

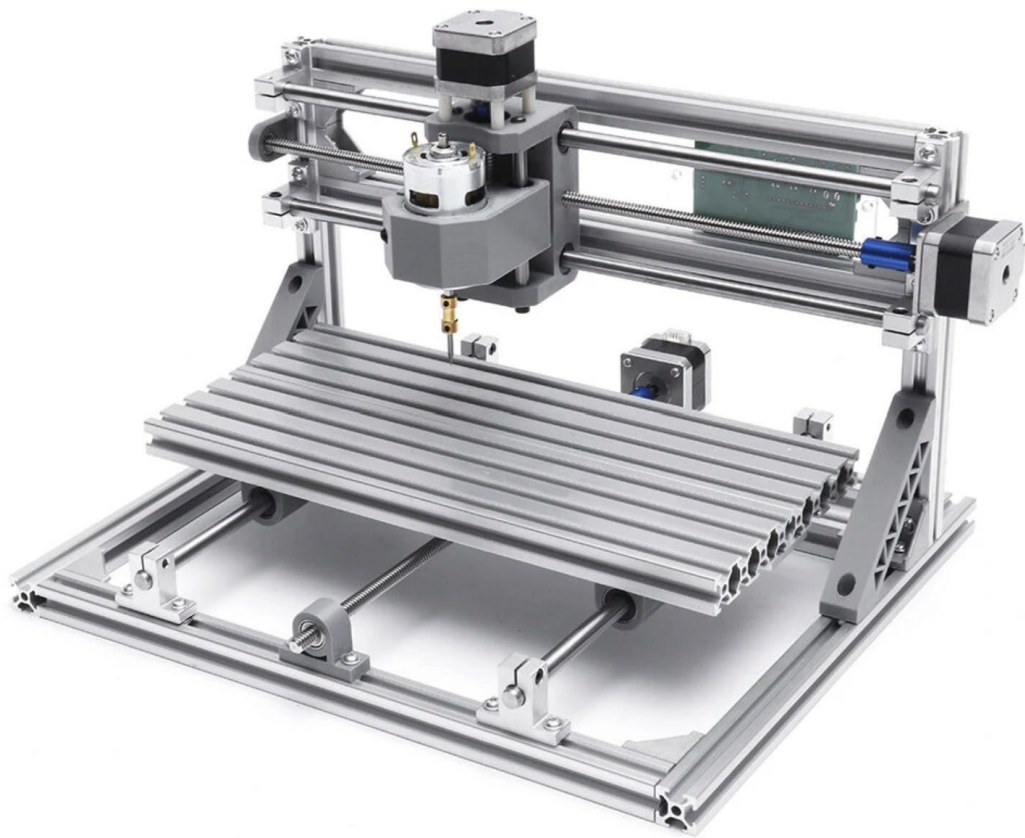


Figure 2.16: Picture of a 3018 CNC mill [61].

Table 2.14: General specification of mini CNC machine.

Specification	
Model	CNC3018
Frame material	Aluminium Alloy
Working Area	340x160x40 mm
Weight	7.5 kg
Control Software for Spindle	GrblControl
Stepper Motor2	NEMA 17, Phase Current 1.3 A, Torque 0.25 Nm
Spindle Motor	24 V, 7000 r/min
Spindle Motor Shaft Diameter	5 mm

2.6. 3D printing and modifications

One of the first aims of the project was to modify the Creality CR-10 3D printer in order to be able to 3D print abrasive and hygroscopic materials such as PA12-CF. The changes included nozzle, hot-end with all metal parts, Bowden type extruder to dual gear direct driver extruder, magnetic bed with spring steel sheet, auto levelling system with a touch probe, stepper drivers for TMC 2130 for a quiet operation and better micro-stepping and 32-bit motherboard for more computing power which resulted in faster printing of complex shapes. Figure 2.17 presents a modified 3D printer.

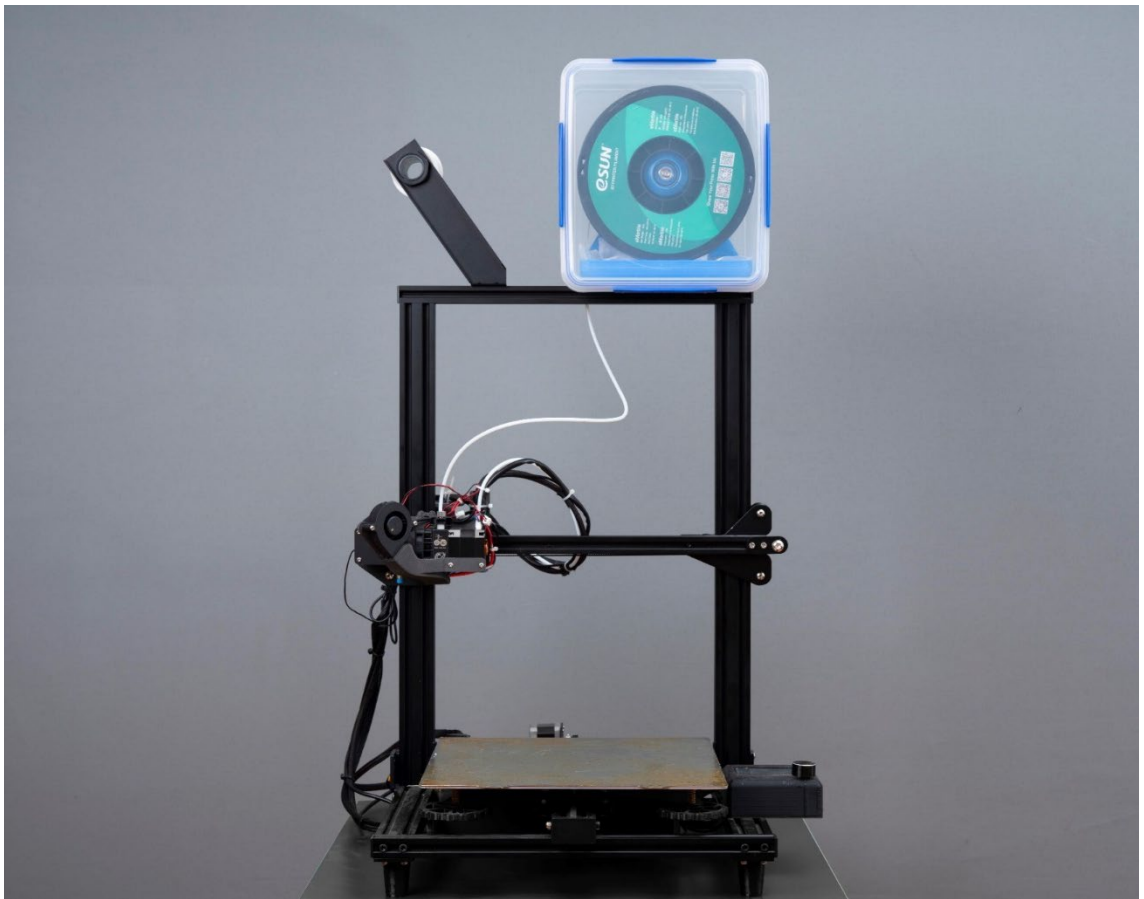


Figure 2.17: Picture of customized 3D printer.

Usually, stock 3D printers are equipped with a nozzle made from brass and they have 0.4 mm in diameter. In order to print abrasive materials, it had to be changed to a different material such as hardened tool steel, stainless steel, or brass with ruby insert. Moreover, 0.4 mm in diameter of the nozzle leads to clogging as filament additives such as carbon fibre or graphene are long enough to group together and stuck at the end of the nozzle. In the presented project, the nozzle was changed to 0.6 mm in diameter nozzle X from the E3D company. Figure 2.18A presents the used nozzle. Specification of the used solution is presented in Table 2.15.

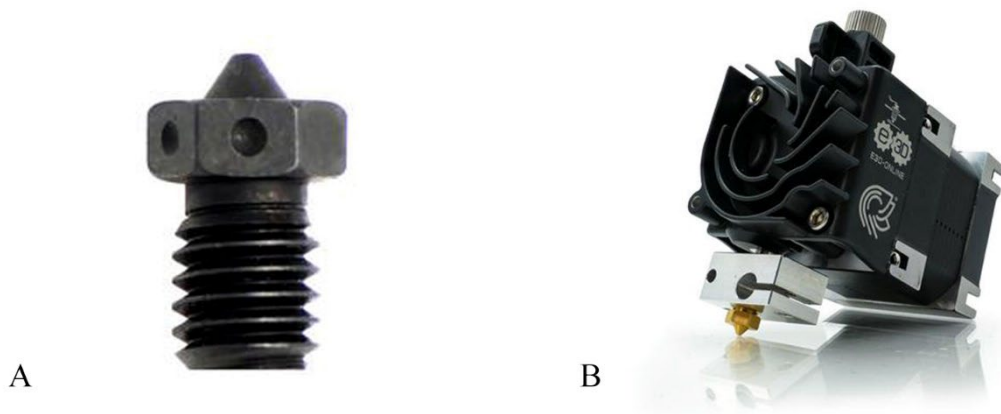


Figure 2.18: A) picture of E3D NozzleX [62]. B) E3D Hemera extruder [63].

Table 2.15: General specification of a chosen nozzle.

Specification	
Brand	E3D
Model	NozzleX
Diameter	0.6 mm
Material	Hardened tools steel base, Nickel plated and Tungsten Disulfide (WS2) coated
Work temperature	Up to 500 °C

Creality 3D printer was equipped in Bowden style extruder with a single drive gear pushing filament against a bearing. This solution has the advantage of being lightweight, but it is not optimal when it comes to 3D printing flexible materials. Moreover, retraction settings are greater which leads to extended printing time and fine

control of the printing process is challenging. Therefore extruder was changed to a dual gear direct drive Hemera extruder from E3D company. It has the advantage of having two gears pushing filament through a nozzle and retraction settings can be tweaked precisely. Distance for the filament to travel between gears and nozzle end is very short, therefore it is suitable to print flexible filaments such as conductive TPU. Retraction distance can be reduced from approximately 6 mm in Bowden style extruder to around 1 mm. It has an impact on printing speed and the consistency of extrusion. Figure 2.18B presents the used Hemera extruder. Table 2.16 depicts the general specification of the device.

Table 2.16: General specification of a chosen extruder.

Specification	
Brand	E3D
Model	Hemera
Filament diameter	1.75 mm
Filament pushing force	100 N
Drive type	Direct, dual drive
Work temperature	Up to 285 °C
Stepper motor step angle	1.8 °
Stepper motor current	1.33 A
Stepper motor voltage	12 V
Heater cartridge power	30 W
Thermistor Cartridge	Semitec 104NT
Dimensions	77x44x83 mm
Weight	0.388 kg

Standard Creality 3D printer is equipped with an 8-bit motherboard based on an ATmega2560 microchip microcontroller with built-in Allegro A4988 stepper motor drivers. It does not allow for stepper motor driver exchange. Moreover, 8-bit architecture does not provide enough computing power to be able to print fast, organic objects such as surfboard fin. Therefore it was necessary to improve the motherboard to 32-bit one with the possibility to introduce new stepper motor drivers. Figure 2.19A

depicts used BIGTREETECH's motherboard. Table 2.17 describe the parameters of the chosen solution.

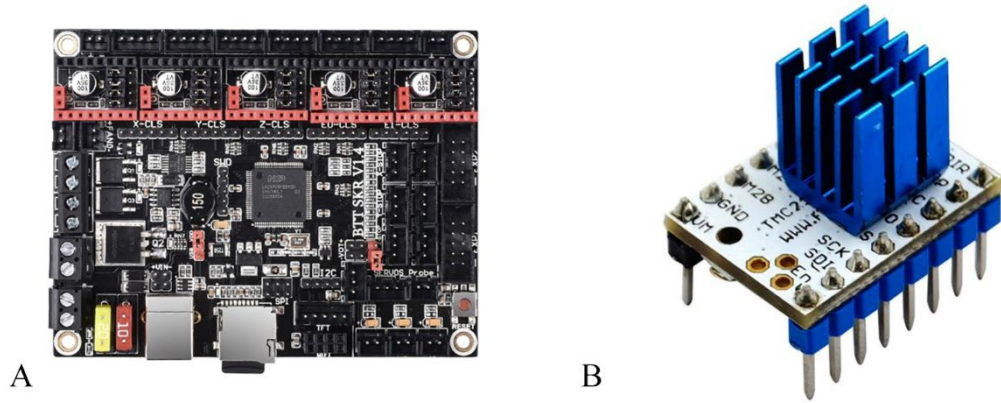


Figure 2.19: A) picture of SKR V1.4 turbo [65]. B) FYSETC TMC-2130 StepStick stepper motor driver [66].

Table 2.17: General specification of a used motherboard.

Specification	
Brand	BIGTREETECH
Model	SKR V1.4 Turbo
Microprocessor	32-bit ARM Cortex-M3
Frequency	120 MHz
Input voltage	12-24 VDC
Logic voltage	3.3 V
Communication	USB, SPI, I ² C, UART
Supported kinematics	XYZ, delta, kossel, corexy
Number of stepper motors	Up to 5
Display interfaces	Serial touch screen, SPI touch screen, and LCD display
Firmware support	Marlin, RepRap
Dimensions	110 x 85 x 22 mm
Weight	0.089 kg

Stepper drivers used for customised 3D printer consist of the Trinamic TMC-2130 stepper driver chips. In comparison to standard A4988 drivers, TMC-2130 are optimised for quiet operation, they have higher motor phase current, and higher resolution microstepping. Figure 2.19B depicts the stepper motor driver in form

of StepStick used in the project. Table 2.18 consists of the parameters of the TMC-2130 device.

Table 2.18: General specification of a used stepper driver StepStick.

Specification	
StepStick brand	FYSETC
Chip brand	Trinamic
Model	TMC-2130
Interface	Step/Dir or SPI
Configuration	CFG pins or SPI
Microstep resolution	Up to 1/256
Logic voltage	3-5 V
Stepper motor voltage	5.5 – 46 V
Motor phase current	1.2 A RMS, 2.5 A peak
Functions	stealthChop, spreadCycle, coolStep, stallGuard, dcStep
Dimensions with radiator	20.2 x 15.4 x 22 mm
Weight with radiator	0.003 kg

Another modification was printing surface from glass platform to spring steel sheet. It was mounted via a set of rare earth magnets. The used 3D printer is a cartesian coordinate system based on an X, Y, and Z-axis. Build surface travels along Y-axis. During the printing process bed is moving, therefore its mass has an impact on the ghosting effect caused by vibrations occurring with every change of movement direction. The weight of the glass bed surface is around 1 kg in contrast to the approximately 0.4 kg spring steel set. Another advantage of introduced modification is that after printing is finished, it is easier to remove the part from the surface. With used Poly(vinyl acetate) (PVA) glue as the first layer surface bond, removing an object from the not flexible surface could be challenging and could potentially lead to shattering glass build plate. Figure 2.20A presents the used spring steel solution. The brand, material, dimensions, and weight of the heat bed surface are FYSETC,

spring steel, 310 (length mm) x 310 (width mm) x 0.8 (height mm), and 0.379 kg, respectively.

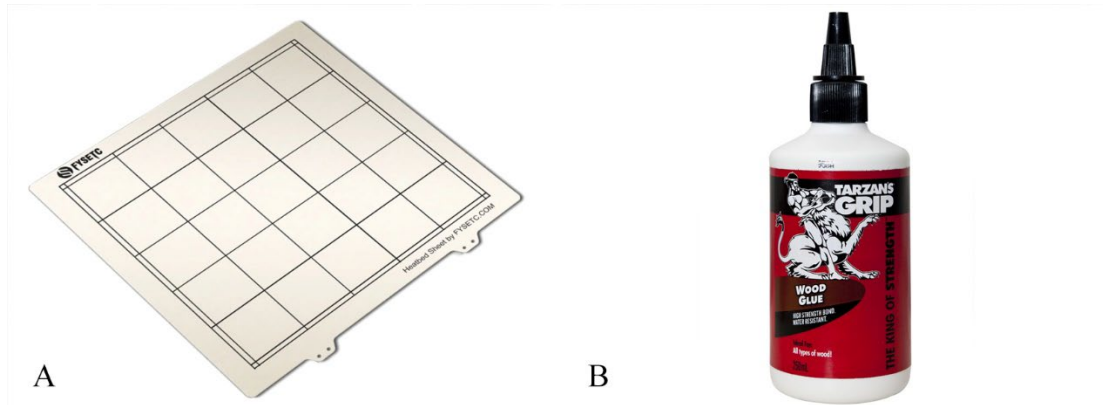


Figure 2.20: A) picture of FYSETC spring steel build plate surface [64]. B) PVA glue used for first layer adhesion [67].

PVA glue was used to improve first layer adhesion. Filaments such as PA6-CF, PA12-CF or PETG-CF can shrink during printing and it can lead to lifting and detaching of the object from the build plate. Therefore, first layer adhesion is crucial for successful 3D printing. Glue was spread on the spring steel sheet with the use of a rubber brayer. It allowed for even distribution of the product. Figure 2.20B depicts used PVA glue. The brand, model, and heat resistance of the PVA glue are Tarzan's Grip, PVA wood glue, and up to 110 °C, respectively.

The last upgrade to the printer was related to Nylon-based composite as they are hygroscopic, its mechanical parameters are affected by moisture. The higher the air humidity, the faster the rate of absorption. Full saturation in 20 °C and 80 % air humidity is reached within 24 h. To compare dry material with fully saturated, samples marked as “WET” were produced and left in environmental conditions for 24 h prior to measuring.

Attempt to 3D print with saturated material caused a decrease in overall quality and occasional nozzle clogs. Water trapped inside the filament was heated beyond

boiling point and was evaporating through the nozzle causing artefacts in samples and disrupting the manufacturing process. In order to prevent Nylon-based composite materials from absorbing the water, a dry box mentioned in 2.2.7.5 of this work was developed. A 5 l food container filled with calcium chloride and silica gel proved to be an optimal solution for the issue. To create a closed and sealed connection with a 3D printer, PTFE tubing was used.

All changes opened the possibility of 3D printing organic shapes faster with the use of abrasive, and hygroscopic materials. Also improvement in flow characteristics and overall quality was feasible.

2.7. Annealing

Annealing was used to modify the physical or chemical properties of some 3D printed materials. It improved layers bonding leading to a change in mechanical parameters. Some samples produced from PLA were heat-treated in a furnace for 1 h (110 °C) and PETG, Nylon 12 and Nylon 6 for 1 h (140 °C, 150 °C, or 240 °C).

2.8. Electronic telemetry system

The electronic telemetry system used in the project was based on an 8-bit Arduino Mega 2560 microcontroller board connected to breakout boards from various vendors. The system made in this way was characterised by modularity and it was highly flexible in use.

The main component of the system was the Arduino Mega2560 development board depicted in Figure 2.21A. It allowed to connect of all components of the system and collect data from sensors. Specification of the part is presented in Table 2.19. Its main disadvantage is size, which required designing a bigger electronic box. In future iterations of the solution, a smaller development board or dedicated electronics will be the main improvement.

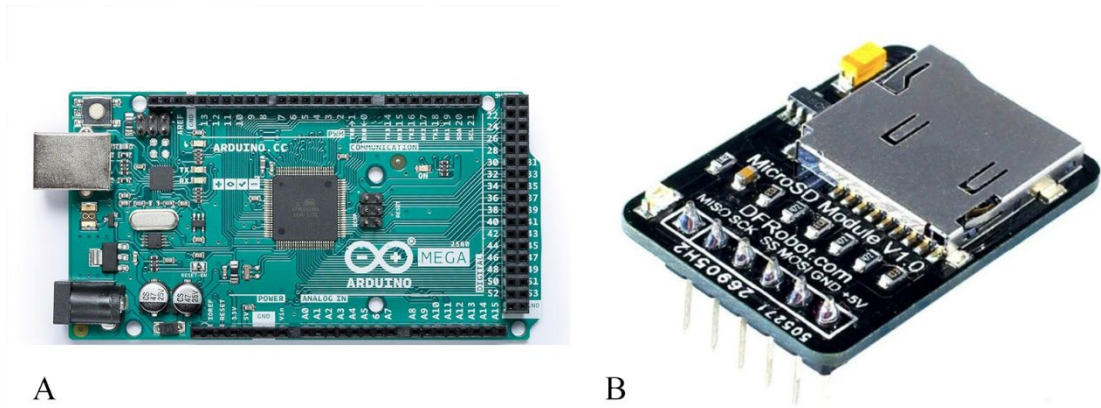


Figure 2.21: A) picture of an Arduino Mega 2560 [68]. B) picture of a DFRobot μ SD card reader [69].

Table 2.19: General specification of a Arduino Mega 2560 development board.

Specification	
Brand	Arduino
Model	Mega 2560
Microcontroller	8-bit ATmega 2560
Operating voltage	5 V
Input voltage	7-12 V
Digital I/O pins	54 (15 PWM)
Analog input pins	16
DC current per I/O pins	20 mA
DC current for 3.3V Pin	50 mA
MemoryFlash memory	256 KB Flash, 8 KB SRAM, 4 KB EEPROM
Clock frequency	16 MHz
Communication	USB, UART, SPI, I ² C
Dimensions	101.5 x 53 mm
Weight	0.037 kg

The first module connected to the Arduino was the DFRobot μ SD card reader which provided an opportunity to record all collected data internally. As radio transfer of information in the ocean could be interrupted by waves and other circumstances, μ SD card reader was mounted as a backup device. Figure 2.21B presents a chosen solution. The brand, working voltage, communication type, compatible cards,

dimensions, and weight of the μ SD card reader are DFRobot, 5 V, SPI, MicroSD (TF), 28 (length mm) x 20 (width mm) x 5 (height mm), and 0.004 kg, respectively.

Subsequently, the Sparkfun NEO-M9N GPS breakout board was connected. It was used to collect velocity, acceleration, altitude, direction, date, and time data. The specification is depicted in Table 2.20. Figure 2.22A presents a chosen solution. The main advantage of the unit was the 25 Hz update rate. It is one of the fastest updating GPS breakout board available on the market. Fast data sampling is vital for the high accuracy representation of sensors.

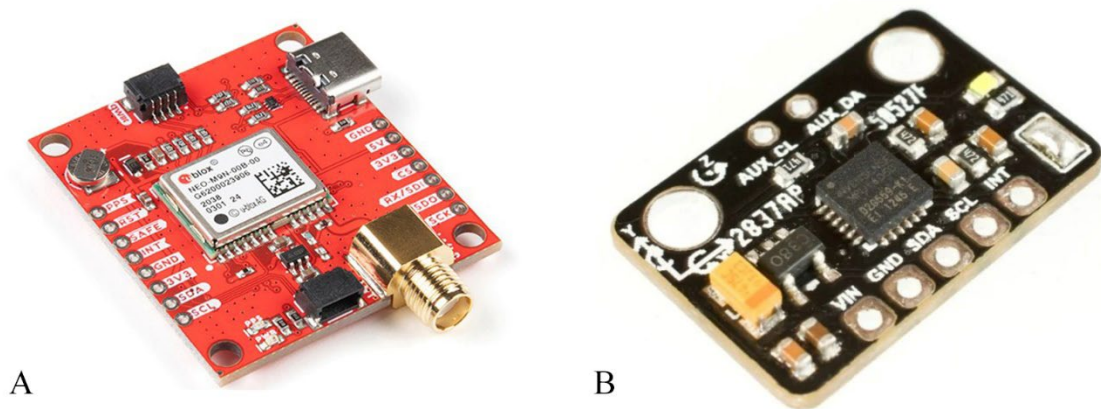


Figure 2.22: A) picture of a Sparkfun NEO-M9N GPS module [70]. B) picture of a DFRobot MPU6050 gyro and accelerometer module [71].

Table 2.20: General specification of a used GPS module.

Specification	
Brand	Sparkfun
Model	NEO-M9N
Antenna interface	SMA
Receiver	92-channel GNSS
Horizontal accuracy	1.5 m
Update rate	Up to 25 Hz
Max working altitude	80000 m
Maximum G	4
Max velocity	500 m/s
Velocity accuracy	0.05 m/s
Heading accuracy	0.3 degrees

Time pulse accuracy	30 ns
Input voltage	3.3 V
Current consumption	31 mA
Tracking	GPS, GLONASS
Communication	UART, I ² C
Dimensions	40.6 x 36.8 mm
Weight	0.012 kg

Accelerometer combined with gyroscope was another device used in the telemetry system. DFRobot MPU6050 is a MEMS device that was used to collect three-axis acceleration, rotation, angles, and temperature. Figure 2.22B depicts the used solution. Furthermore, Table 2.21 presents the specification of the unit.

Table 2.21: General specification of used gyro/accelerometer module.

Specification	
Brand	DFRobot
Model	MPU6050
Accelerometer range	±2, ±4, ±8, and ±16 g
Angular rate sensor range	±250, ±500, ±1000, and ±2000 dps
Data format	Rotation matrix, quaternion, Euler angle, or raw data
Communication	I ² C
Dimensions	21 x 14 mm
Weight	0.0011 kg

To be able to measure loads from commercial and 3D printed Wheatstone bridges, Sparkfun HX711 were used. The device is an amplifier and it contains a filter to help reduce noise coming from the system. Figure 2.23A depicts photography of the used device. Moreover, Table 2.22 consist of the specification of the unit. The main advantage of the HX711 is the 80 Hz sampling rate. For example, in the telemetry system, there is a possibility to switch off the GPS module which would result in a higher data transfer rate from the amplifier breakout board.

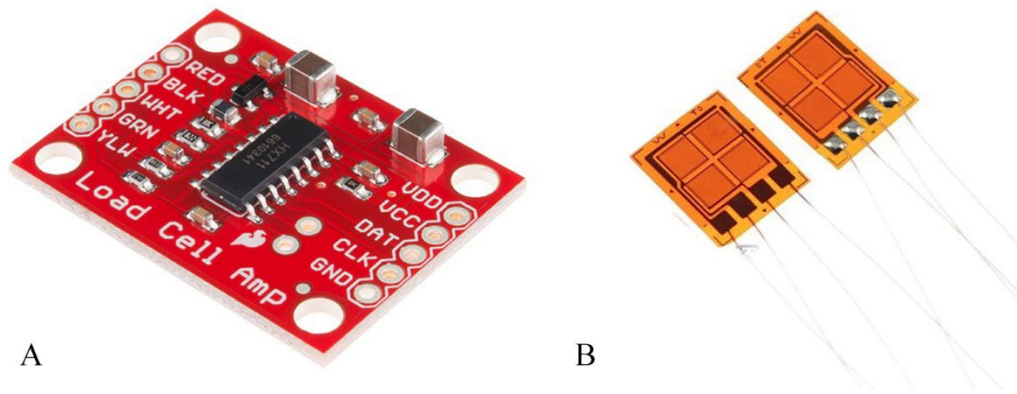


Figure 2.23: A) picture of a Sparkfun HX711 load cell amplifier [72]. B) picture of a full bridge Wheatstone bridge [73].

Table 2.22: General specification of used load cell amplifier module.

Specification	
Brand	Sparkfun
Model	HX711
Operating voltage	2.7-5 V
Operation current	1.5 mA
Sampling rate	Up to 80 Hz
Analog to digital converter	Avia Semiconductor 24-bit
Programable gain amplifier	32, 64, and 128
Operation temperature range	-40 to 85 °C
Dimensions	30.5 x 22.9 mm
Weight	0.00284 kg

The Wheatstone bridge used in the prototype surfboard is presented in Figure 2.23B. For the purpose of the experiment, it was a generic brand. The focus was emphasised on the proof of concept of design rather than high accuracy, expensive device. The model, cover material, sensor material, nominal resistance value, applicable temperature, and mechanical lag of the load cell are BF350 - 3EB, phenolic-epoxy, etched resistance foil, 350 Ω , -30 to 60 °C, and 1.2, respectively.

Electronic system inbuilt into the surfboard communicates with the laptop or PC via a set of transceivers, first mounted inside the surfboard electronics and another

connected to Arduino Uno and computer. Data is transferred in real-time and presented on graphs. Both transceiver components act as transmitter/receiver. The one connected to the PC confirms received data to the one mounted in the surfboard. This solution helps to determine the data transfer success rate and provide a more accurate representation of collected signals. It is possible to count data packages not received by the system connected to the PC. Sparkfun nRF24L01+ breakout board was used in the experiment. Figure 2.24A presents photography of a transceiver module. Furthermore, Table 2.24 depicts the specification of the unit.

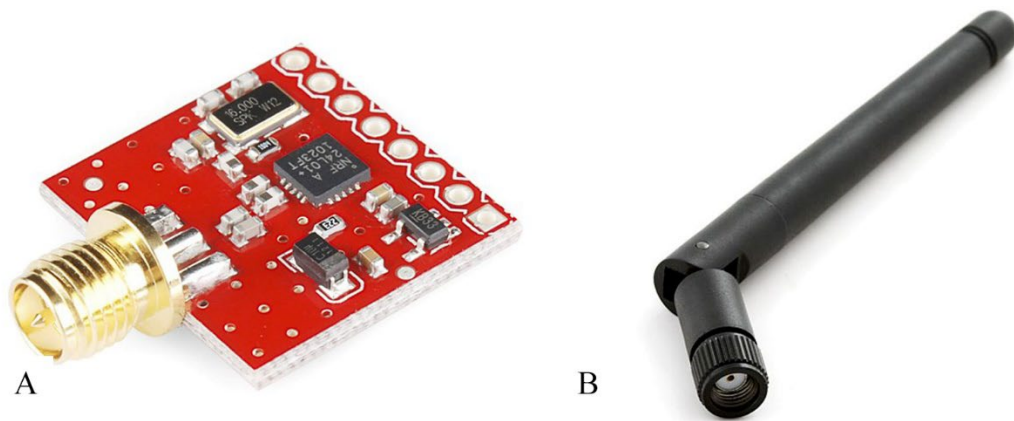


Figure 2.24: A) picture of a Sparkfun nRF24L01+ transceiver module [74]. B) picture of a Sparkfun 2.4GHz Duck Antenna RP-SMA [75].

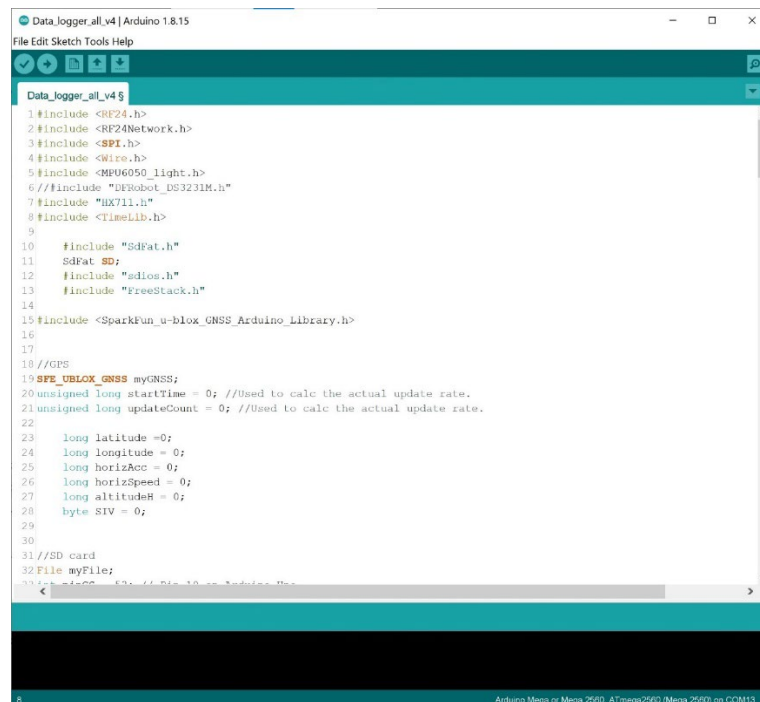
Table 2.23: General specification of used transceiver module.

Specification	
Brand	Sparkfun
Model	nRF24L01+
Antenna connector	Reverse polarized SMA
Antenna	2.4 GHz antenna
Range	Up to 100 m at 250 kbps
Data rate	250 kbps to 2 Mbit
Input voltage	5 V
Communication	SPI
Software selectable channel	From 2400 MHz to 2525 MHz
Dimension	26.4 x 20.4 mm
Weight	0.005 kg

In combination with mentioned transceiver module, Sparkfun 2.4GHz Duck RP-SMA antenna was used. It provides a balance between size and performance. Figure 2.24B depicts photography of a used antenna. The brand, model, connector type, dimensions, and weight of the antenna are Sparkfun, 2.4GHz Duck Antenna 2.2dBi, reverse polarized - SMA RF, 10 (width mm) x 106 (length mm), and 0.006 kg, respectively.

2.9. Arduino IDE and software solution

The electronics system was programmed through Arduino Integrated Development Environment (IDE). Figure 2.25 depicts the Arduino IDE work environment. The whole code used in both modules is presented in the Appendix 1 to this work.



```
1 #include <RF24.h>
2 #include <RF24Network.h>
3 #include <SPI.h>
4 #include <Wire.h>
5 #include <MPU6050_Light.h>
6 // #include "DFRobot_DS3231M.h"
7 #include "HX711.h"
8 #include <TimeLib.h>
9
10 #include "SdFat.h"
11 SdFat SD;
12 #include "adfos.h"
13 #include "FreeStack.h"
14
15 #include <SparkFun_u-blox_GNSS_Arduino_Library.h>
16
17
18 //GPS
19 SFE_UBLOX_GNSS myGNSS;
20 unsigned long startTime = 0; //Used to calc the actual update rate.
21 unsigned long updateCount = 0; //Used to calc the actual update rate.
22
23 long latitude = 0;
24 long longitude = 0;
25 long horizAcc = 0;
26 long horizSpeed = 0;
27 long altitudeH = 0;
28 byte SIV = 0;
29
30
31 //SD card
32 File myFile;
33
34
35
36
37
38
39
40
41
42
43
44
45
46
47
48
49
50
51
52
53
54
55
56
57
58
59
60
61
62
63
64
65
66
67
68
69
70
71
72
73
74
75
76
77
78
79
80
81
82
83
84
85
86
87
88
89
90
91
92
93
94
95
96
97
98
99
100
```

Figure 2.24: Screenshot of an Arduino IDE work space.

2.10. Characterisation

Samples and sensor fin were tested on the so-called pandemic tool, and Shimadzu EZ-S mechanical analyser. Figure 2.26 depicts photography of a mechanical analyser. Machine specification is detailed in Table 2.24.

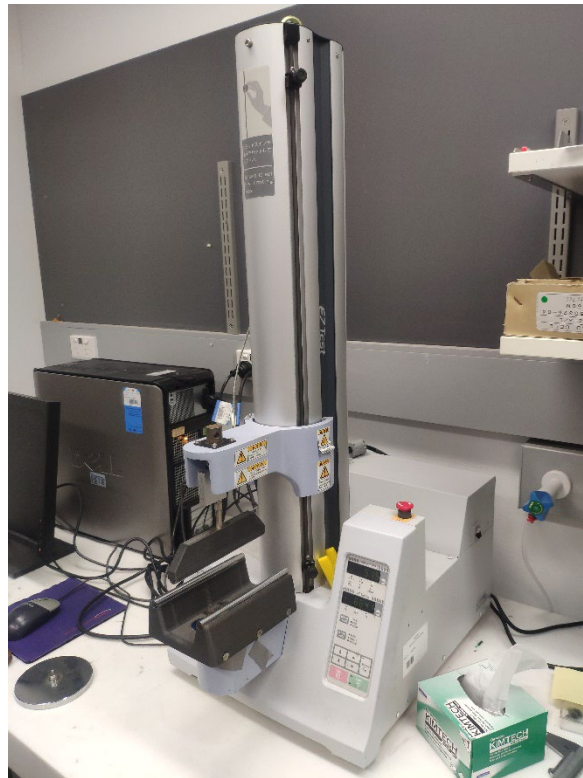


Figure 2.26: Picture of the Shimadzu EZ-S mechanical tester.

Table 2.24: General specification of used Shimadzu EZ-S.

Specification	
Brand	Shimadzu
Model	EZ-S
Load capacity	500 N
Load method	constant-speed strain control method via ball-screw drive
Force measurement accuracy	Within ± 1 % of cell indicated value Conforms to JIS B7721 Grade 1, ISO 7500-1 Class 1, EN10002-2 Grade 1, and ASTM E4
Crosshead speed range	0.05 mm/min. to 1000 mm/min.
Crosshead speed accuracy	± 0.5 % of the test speed or 0.05 mm/min., whichever is greater
Gap between crosshead and jig attachment surface	159 mm to 659 mm (travel distance 500 mm)

Crosshead position detection:	Optical encoder measurement / digital display (resolution: 0.01 mm) Accuracy within ± 1 % of indicated value, or ± 0.01 mm, whichever is greater
Dimensions	371 x 538 x 927 mm
Weight	38 kg

Figure 2.27A presents photography of the Agilent 34410A device. Table 2.25 depicts the specification of the unit. A multimeter was used to measure voltage and resistance response from the sensors mounted in the instrumented fin.



Figure 2.27: A) picture of a Agilent 34410A digital multimeter [76]. B) picture of a Powertech MP-3087 power supply [77].

Table 2.25: General specification of used Agilent 34410A.

Specification	
Brand	Agilent / Keysight
Model	34410A
Resolution	6½ digit
Basic accuracy	0.0030 % DC, 0.06 % AC
Sampling speed	50000 Hz at 4½ digits direct to PC 10000 Hz at 5½ digits direct to PC 1000 Hz at 6½ digits direct to PC
Communication	LAN, USB, GPIB
Data type	DCV, ACV, DCI, ACI, 2-wire and 4-wire Resistance, Frequency, Period, Continuity, and Diode Test
Dimensions	261 x 303 x 104 mm
Weight	3.72 kg

Powertech MP-3087 power supply was used to provide power to the sensors. Figure 2.27B depicts photography of a used device. Table 2.26 presents a detailed specification of the device.

Table 2.26: General specification of used Powertech MP-3087.

Specification	
Brand	Powertech
Model	MP-3087
DC voltage range	0-32 V
DC current rating	3 A
Ripple and noise	<1 mV
Number of outputs	2
Dimensions	260 x 185 x 400 mm
Weight	10 kg

2.10.1. Sample testing

Sample testing was first performed during the COVID-19 lockdown period with the use of the custom-designed so-called pandemic tool. The device was used for a three-point bend test in order to measure samples deflection under load. 0.5 kg weights were added at a rate of 3 per 10 s of a hold time up to 20 kg in total load. During hold time data from the dial indicator was collected. The unloading cycle was characterised by the same rate of weight deduction with a 10 s hold period. Collected data was used to create the function of applied force (converted from kg to N) and deflection. Subsequently, evaluation of the modulus of elasticity in bending E_f , flexural stress σ_f , flexural strain ϵ_f and the flexural stress–strain response was possible. Samples were tested up to 3 loading-unloading cycles in approximately 30 min intervals. Figure 2.28AB presents a CAD model of a pandemic tool setup with a sample position relative to the device. Figure 2.28C depicts photography of a used 3D printed three-point bend test solution.

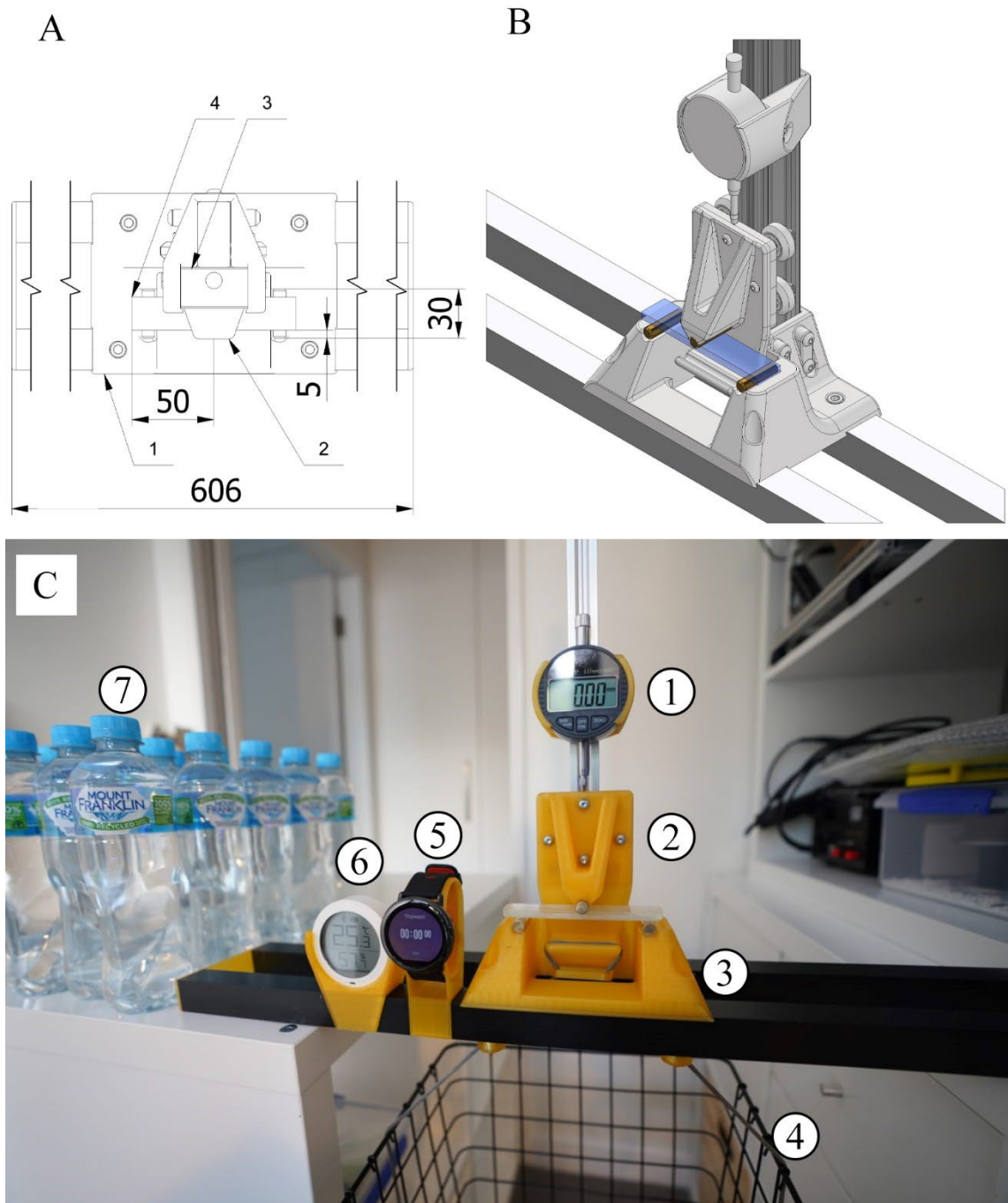


Figure 2.28: CAD model of pandemic tool head position relative to sample. A) top view. B) isometric view. C) photography of 3D printed three-point bend test solution. Numbers 1-4 in A depicts base, tool head, dial indicator, and sample, respectively. Numbers 50, 5, 30, and 606 in A indicate midpoint of the sample (mm), distance between sample, and pins (mm), pins length (mm), and length (mm), respectively. Numbers 1-7 in C indicate depth gauge, tool head, tool base, basket for weights, timer, thermometer and hygrometer, and 500 g weights, respectively.

When the first lockdown ended, mechanical analysis of the same set of samples was performed again. Shimadzu EZ-S tester in combination with 3D printed three-point bend test adapter tool were used. The load was applied up to 450 N at a rate of 10 mm/min continuously with 5 s hold time at a maximum of the range. The unloading cycle was characterised by the same rate of 10 mm/min. When samples were not able to perform to the presented range, the test was redone with custom chosen maximum load. Force was applied in three loading-unloading cycles in approximately 30 min intervals between cycles. Similarly to the previous experiment, collected data was used to create the function of applied force and deflection as well as to determine the modulus of elasticity in bending E_f , flexural stress σ_f , flexural strain ϵ_f , and the flexural stress-strain response of researched materials. Figure 2.29AB presents a CAD model of adapter probe position relative to a sample. The tested specimen was positioned in the middle of an adapter with the use of a positioner. Then the probe was lowered to start position and the positioner could be released. Figure 2.29C presents photography of the Shimadzu EZ-S mechanical analyser with a 3D printed adapter tool mounted and prepared for measurements.

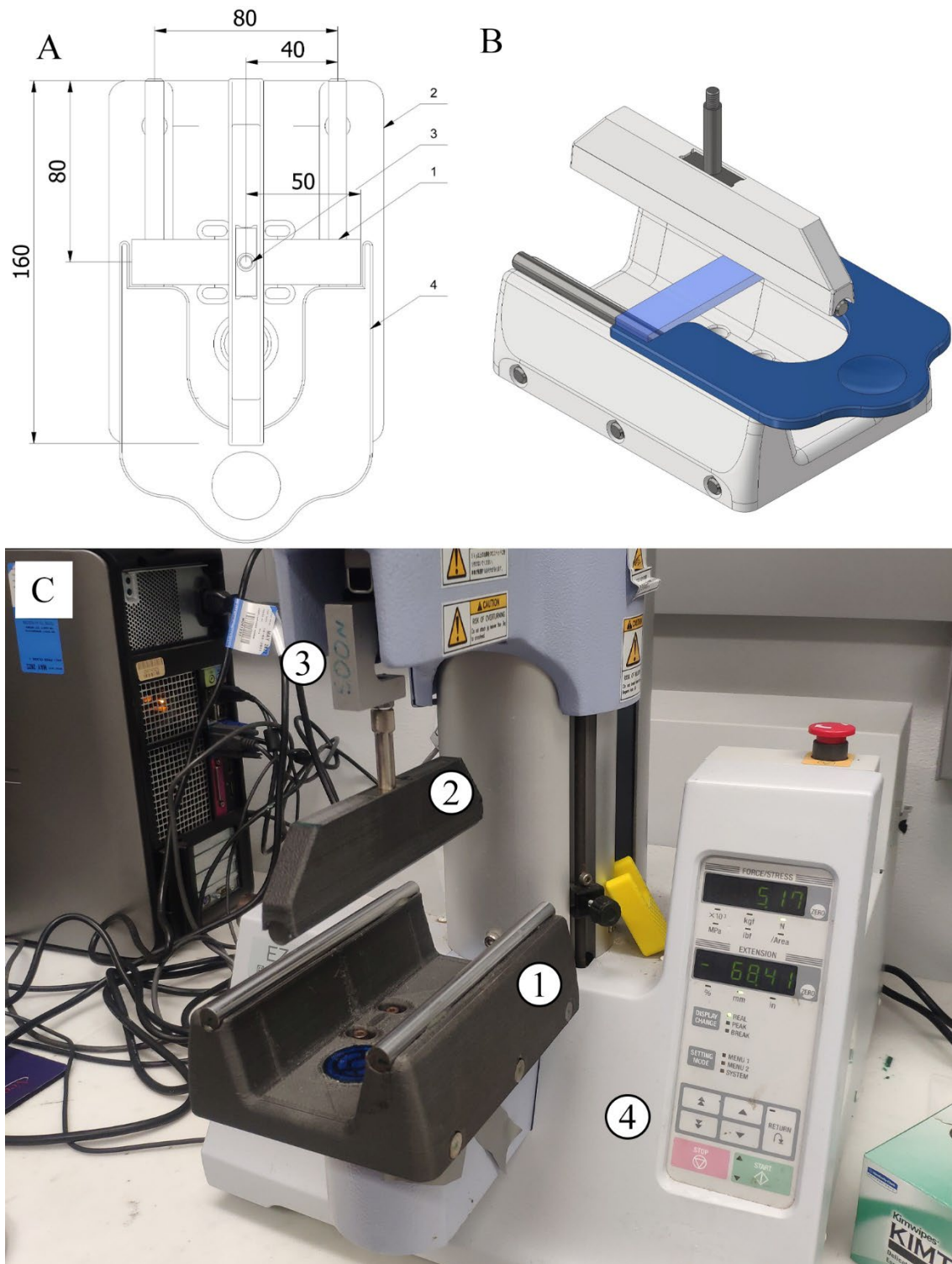


Figure 2.29: A) CAD model of Shimadzu adapter probe position relative to sample. B) picture of the Shimadzu EZ-S mechanical analyser with 3D printed adapter. Numbers 1-4 in A depicts sample, adapter base, press tool, and sample positioner, respectively. Numbers 160, 80, 80, 40, 50 in A indicate length (mm), midpoint length (mm), span (mm), distance between supporting pin and loading pin (mm), sample midpoint (mm), respectively. Number 1-4 in C indicate adapter base, press tool, 500 N load cell, and Shimadzu mechanical analyser, respectively.

2.10.2. Fin testing

Shimadzu EZ-S was also used without a 3D printed adapter to measure the flex of the instrumented surfboard fin. Figure 2.30A depicts a CAD model of the position of the mechanical analyser tool relative to the fin. For this purpose, a 10 mm in diameter Shimadzu press tool was used. Figure 2.30B presents photography of the Shimadzu EZ-S mechanical analyser with sensor fin setup. Fin was mounted in a surfboard fin box and surfboard was held by vice. Response of the sensors was obtained with the use of a custom-built setup consisting of Shimadzu EZ-S mechanical analyser (500 N load cell) and Agilent 34410A digital multimeter. Subsequently, data was depicted in TRAPEZIUMX and BenchVue software and could be saved for further analysis. A presented setup was used to measure the flex of the fin tip with perpendicularly applied force. Loading curve was characterised by 1 mm strokes at a rate of 10 mm/min with 5 s hold time on each step up to 10 mm. The unloading curve was designed in the same way. Instrumented fin was tested to 10 loading-unloading cycles with approximately 20 min intervals. Data was used to create force vs deflection, resistance vs deflection, resistance vs force, and resistance vs time curves for 3D printed sensor as well as Wheatstone bridge. Collected data provided information regarding the behaviour of 3D printed sensor in comparison to commercially available Wheatstone bridge as well as mechanical parameters of the tested 3D printed surfboard fin. Described setup was used to subject the Wheatstone bridge to tension, and 3D printed sensor to compression. Later, during comparison experiments between commercial and 3D printed fins, the whole setup was rotated 180 degrees in the vice to subject Wheatstone bridges to tension and compression.

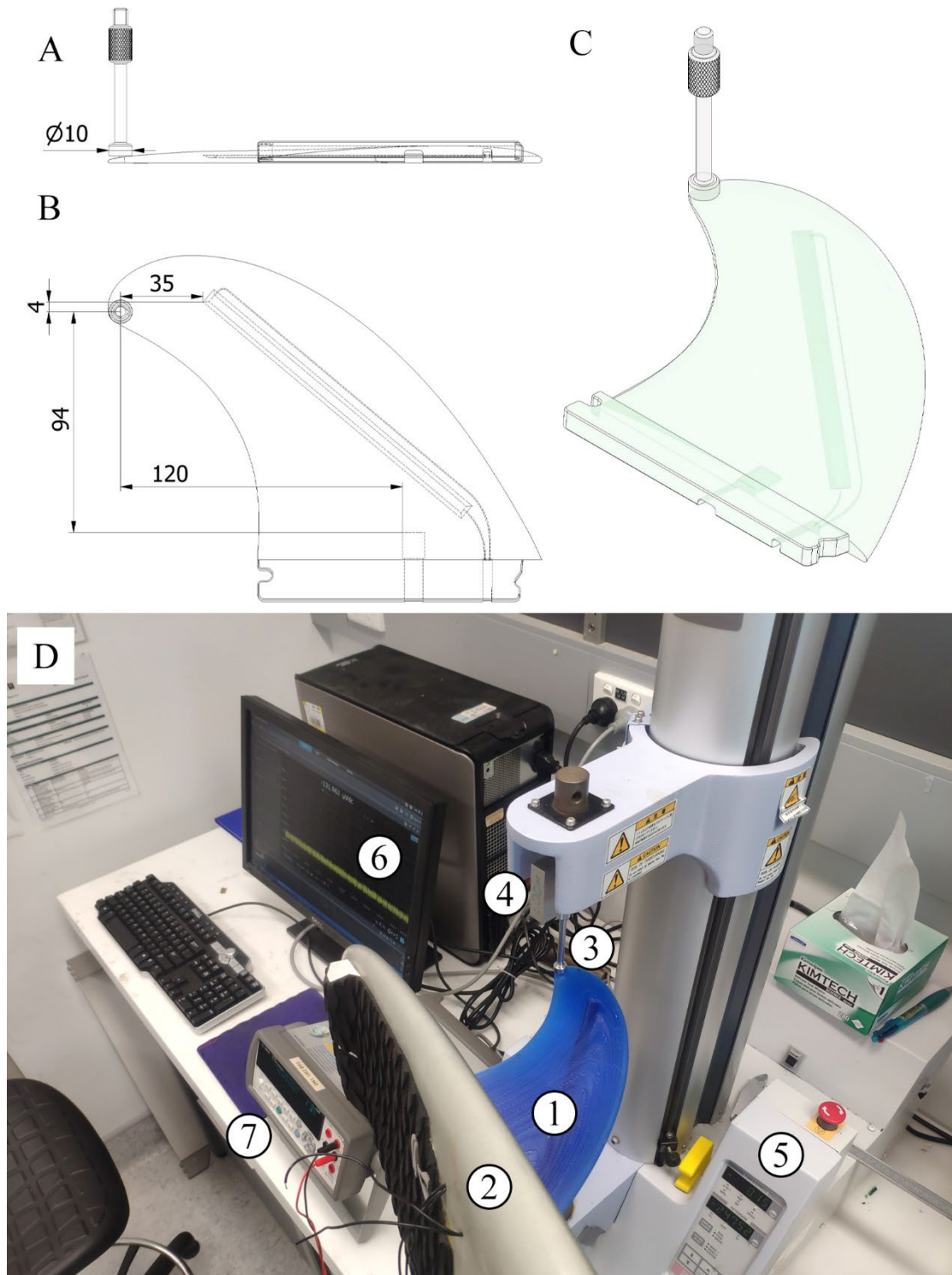


Figure 2.30: CAD model of Shimadzu EZ-S probe position relative to fin. A) side view. B) top view. C) isometric view. D) Picture of the Shimadzu EZ-S mechanical analyser with sensor fin setup. Numbers 4, 35, 94, and 120 indicate vertical distance between a 3D printed sensor and a tool (mm), horizontal distance between a 3D printed sensor and a tool (mm), vertical distance between a Wheatstone bridge, and a tool (mm), horizontal distance between a Wheatstone bridge and a tool (mm), respectively. Numbers 1-7 in D indicate: instrumented fin, surfboard, 10 mm press tool, 500 N load cell, mechanical analyser, PC, and digital multimeter, respectively.

Chapter 3: 3D printing and samples results

This chapter details the customisation of a 3D printer, parameters optimisation of a 3D printing process for 3D printing of rectangular samples, development of tools used for mechanical characterisation and optimisation of rectangular samples.

3.1. 3D printer customisation, process optimisation, and accuracy results.

FDM 3D printing technology is a complex process in which hardware parts and software parameters can be changed in order to improve the quality, accuracy and mechanical robustness of the printed parts. More important, hardware changes are necessary to allow for the printing of high-performance materials. For example, typically stock FDM printers are equipped with brass nozzles which excludes the use of filaments containing abrasive materials such as carbon fibre, graphene or wood additives. See chapter 2 for modifications of the 3D printer which allowed for the printing of abrasive materials during this project.

A first step was to establish if the used nozzle could withstand the printing of abrasive materials. Figure 3.1A shows a typical 3D printed rectangular sample (100 mm length, 20 mm width, and 5 mm height, respectively) using a Nylon 12 based filament with carbon fibre additives. Following the printing of rectangles, the nozzle was then examined under the microscope for any visible signs of use (Figure 3.1B). In the project, around 1 kg of abrasive materials was used and the nozzle was checked frequently. The nozzle did not exhibit any visible signs of use during the period of work. The chosen product proved to be a suitable tool for the task.

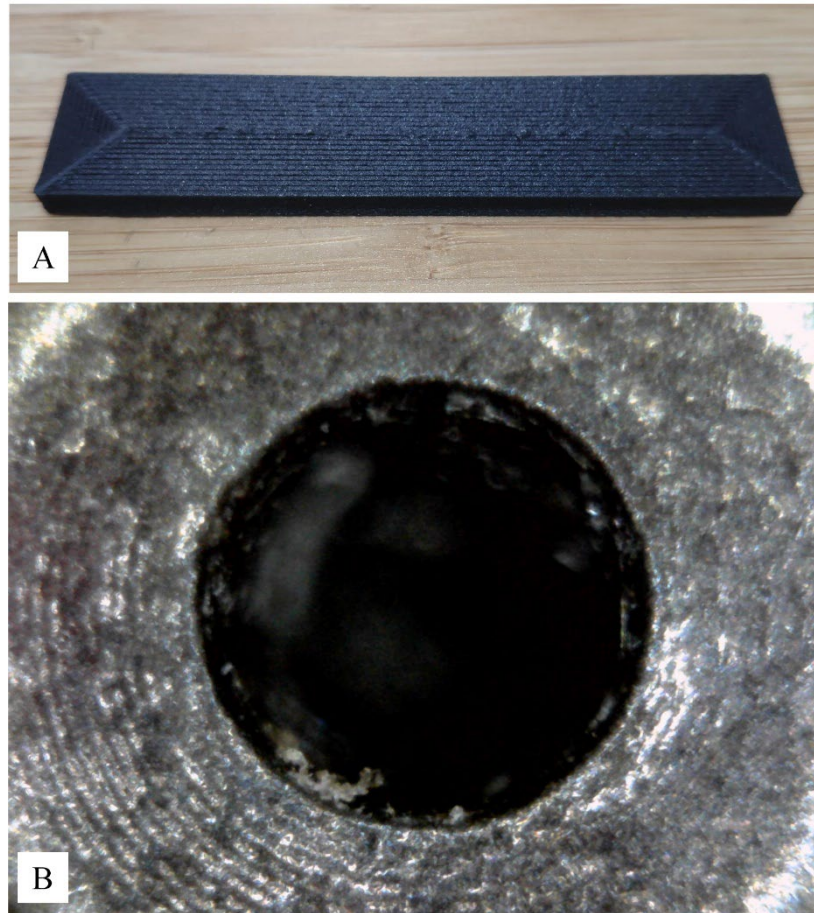


Figure 3.1: Photography of one of a 3D printed rectangular sample (A). Photography of a nozzle front opening after 3D printing of around 1 kg of abrasive materials (B).

The second step in printing process optimisation was to adjust parameters of the extrusion related to layer extrusion consistency and dimension accuracy. It was necessary as the extruder and type of extrusion system were changed. Single drive gear Bowden tube style extrusion system was modified to dual gear direct drive system in order to be able to 3D print conductive flexible materials. In Bowden style extruders this material was prone to nozzle clogging. E3D Hemera extruder system was chosen as it is characterised by high filament pushing force (100 N) and a short distance between gears and nozzle opening (39 mm) [61]. Additionally, the used in 3D printing thermoplastic materials exhibit different flow characteristics, therefore a trial

to determine the flow rate for each material used was necessary in order to achieve reasonable accuracy of the samples dimensions and layer extrusion consistency. There were two ways to adjust the flow rate in a presented 3D printing process. The first was to change the 3D printer's motherboard software parameter of a number of steps per mm of a stepper motor connected to an extruder. Accordingly, to the E3D Hemera datasheet, software parameters used for extruder E axis should equal 409 steps/mm for 1/16th microstepping. It is a base value that can be finely adjusted further by slicer software. The Cura slicer software provides flow rate parameter as a percentage value of the parameter mentioned above. It can be adjusted without the necessity of changing the 3D printer's motherboard software. For example trial for Nylon 12 based carbon fibre filament started from printing a rectangular sample with a 100 % flow rate parameter (Figure 3.2A). Surface finish quality indicated over extrusion of the filament as subsequent lines of a top layer pattern overlap each other. It was visible that the extruder was introducing too much of a material. Another sample was 3D printed with 80 % of a flow rate parameter (Figure 3.2B). This sample exhibited a smooth and consistent finish on the top layer. The extruder was able to squeeze subsequent lines close to each other. Additionally, layer extrusion consistency was even as can be seen on a side wall of a rectangular sample (Figure 3.2D). Moreover, the dimensions of rectangular samples were closer to the intended design. The last sample was produced with 70 % of the flow rate parameter (Figure 3.2C). Subsequent lines in the top layer pattern do not touch each other which was caused by under extrusion of the tested filament. It was determined that the parameter of 80 % flow rate (327 steps/mm) was optimal for layer consistency, and dimension accuracy for used Nylon 12 with carbon fibre filament.

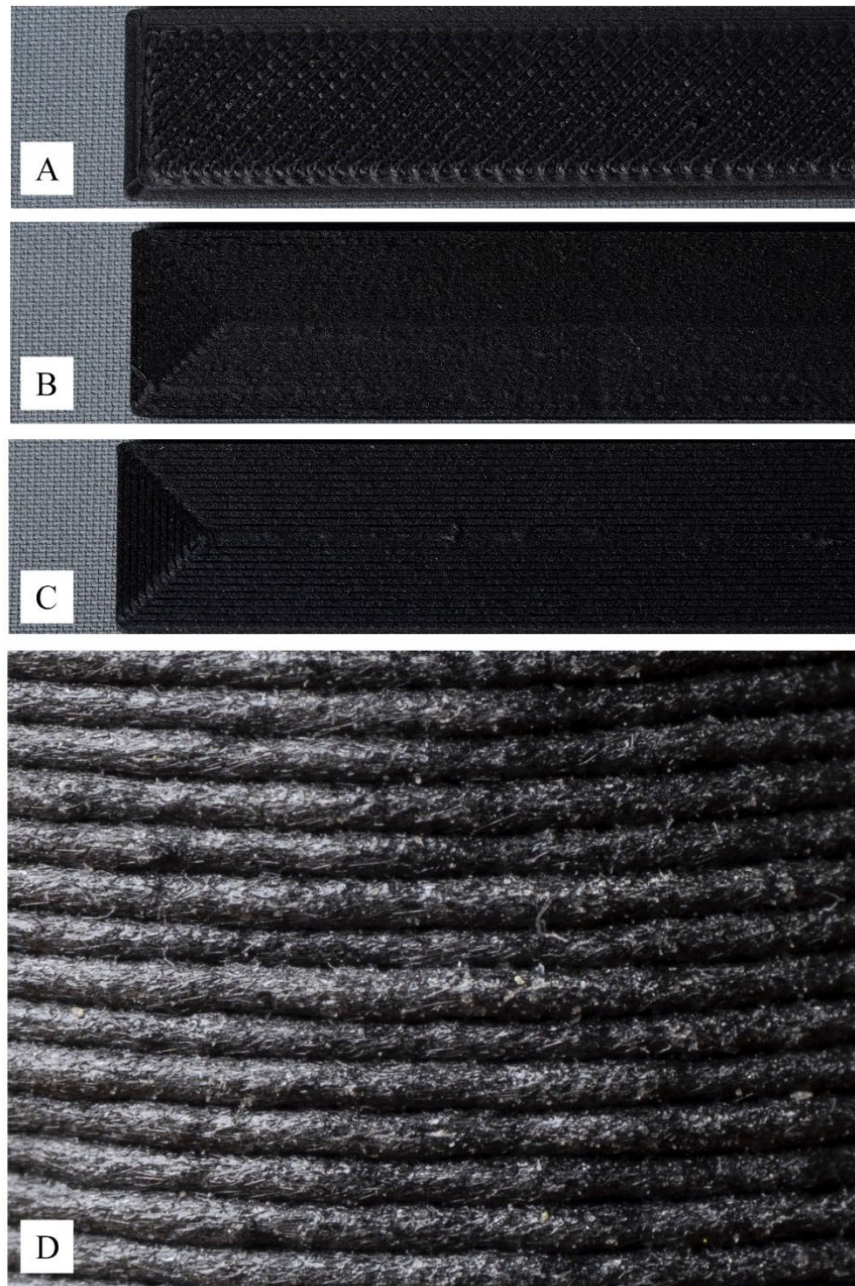


Figure 3.2: Photography of samples of Nylon 12 with carbon fibre filament with different Cura slicer software flow rates parameters, 100 % (A), 80 % (B), 70 % (C), and close up photography of a side wall of a 3D printed rectangular sample.

Table 3.1 presents the dimensions results yielded with different flow rate parameters. The sample produced with a 100 % flow rate had a zig-zag pattern on the top layer instead of a concentric pattern to prevent clogging of a nozzle (Figure 3.2A).

Table 3.1: Summary of flow rate calibration sample parameters for PA12-CF.

Flow rate	Steps/mm	Length [mm]	Width [mm]	Thickness [mm]
70 %	286	99.7 ± 0.1	19.8 ± 0.1	4.6 ± 0.1
80 %	327	99.9 ± 0.1	19.9 ± 0.1	4.8 ± 0.1
100 %	409	100.6 ± 0.1	20.9 ± 0.1	5.5 ± 0.1

A third step in improving the 3D printing process was to develop a dry box solution for hygroscopic materials such as Nylon 6 or Nylon 12. It was necessary as conducted tests of 3D printing of rectangular samples with saturated Nylon 12 based filament were unsuccessful. Tested material was exposed to environmental conditions for 24 h, and 3D printing resulted in nozzle clogging and failed printing process. Therefore dry box solution was developed. It was based on a food container equipped with 3D printed parts allowing to mount filament spool connected with the 3D printer's extruder via PTFE tube. The design is presented in chapter 2 of this project. In order to lower the humidity silica gel and calcium chloride pellet were used. It resulted in lowering the humidity inside the dry box from 54 ± 1 % to 28 ± 1 %, which proved to be enough to successfully manufacture rectangular samples, tools and fins. The design demonstrated to be a viable option for long term storage and 3D printing of hygroscopic filaments.

The subsequent step after 3D printer calibration and introduction of dry box solution was to produce rectangular samples with chosen materials. The aim of rectangular samples production was to determine the combination of materials with optimal relation between mechanical parameters, and weight suitable for surfboard fin production. Each combination of used material, resin, and fabric was produced in 1 set and measured in 3 cycles. Rectangular samples made from Nylon 12 based and Nylon 6 based with carbon fibre additives filaments wrapped with three layers of prepreg carbon fibre were produced in sets of 5 samples of each and tested in 3 cycles. Table 3.2 shows

the dimensions of prepared samples without resin and fibre cloth. The results indicate that there is a reasonable dimensions accuracy after calibrating the 3D printer. The table with all samples dimensions after the introduction of resin and reinforcement materials used can be found in appendix 2.

Table 3.2: Summary of mean values of rectangular samples dimensions. PA6-CF indicates as prepared Nylon 6 with carbon fibre additives material. PA12-CF indicates as prepared Nylon 12 with carbon fibre additives material. PA12-GF indicates as prepared Nylon 12 with glass fibre additives material. PETG indicates as prepared poly(ethylene terephthalate glycol-modified) material. PETG-CF indicates as prepared PETG with carbon fibre additives material. PLA indicates as prepared poly(lactic acid) material.

Material	Length [mm]	Width [mm]	Thickness [mm]
PA6-CF	99.8 ± 0.5	20.2 ± 0.3	4.6 ± 0.2
PA12-CF	100.1 ± 0.5	20.4 ± 0.3	5.0 ± 0.3
PA12-GF	100.1 ± 0.3	20.8 ± 0.1	5.2 ± 0.1
PETG	98.9 ± 0.9	20.1 ± 0.1	5.1 ± 0.2
PETG-CF	100.0 ± 0.4	20.4 ± 0.3	5.2 ± 0.1
PLA	99.5 ± 0.6	20.1 ± 0.3	5.2 ± 0.2

In conclusion combination of the E3D Hemera extruder system, and used nozzle provided the reliable, stable flow necessary to accurately produce the rectangular samples, tools, and surfboard fins. Calibration of the 3D printing process resulted in a reasonable dimension accuracy and layer consistency of produced parts. The consecutive stage of the project was the development of tools necessary to conduct three-point bend testing of rectangular samples.

3.2. Development of tools used for mechanical analysis.

The three-point bend test method was used to measure the mechanical parameters of the rectangular samples. Due to the COVID-19 pandemic related laboratory closure, two tools were developed. The first developed tool was a so-called pandemic tool which was then used in the home environment during the lockdown period. The second tool

was an adapter for Shimadzu mechanical analyser used in the laboratory. See chapter 2 for the design details of both tools.

Development of the pandemic tool started from the 3D printing of parts with PLA filament. Subsequently, two aluminium profiles (600 mm length), with the square cross-section (25 mm external dimensions, 1 mm thickness) were drilled to accommodate four screws. Then 3D printed base of the tool was assembled with square profiles via four M6 screws, ST6 washers, and M6 nuts. In the next step, profile covers were mounted at both ends of the square profiles. Subsequently, V-slot aluminium extrusion was connected with a tool base via eight M5 screws and M5 nuts. The next step was to assembly the gantry consisting of the tool head, top plate, eight 625-2Z ball bearings, four double bearings wheels, four M5 screws, four plate stands (2 off centre), four ST5 washers, four M5 nuts, and four M4 screws. Subsequently, 2 supporting pins and a loading pin were glued into the assembly with the use of Araldite Ultra Clear epoxy glue. In order to accurately set pins in relation to each other, a square mirror (300 mm width, and 2 mm thickness, respectively) was used. It was mounted between three pins during the epoxy glue curing process. The dial gauge was mounted on the tool with the use of a holder, three M5 screws, and three M5 nuts. Lastly, a wire mesh bin for weights was hung on a designed hook. Tool prepared in such a way was used to test rectangular samples. When the lockdown ended, a mechanical analyser adapter was developed for the Shimadzu EZ-S.

The Shimadzu mechanical adapter assembly started from the 3D printing of a base and Shimadzu tool sock from Nylon 12 carbon fibre filament. Subsequently, tool and rectangular samples positioners were 3D printed with the PLA filament. Then three 8 mm in diameter, 160 mm length, three 8 mm in diameter, 120 mm length, and six 8 mm in diameter, 35 mm length stainless steel pins were prepared. The tool was assembled

and aligned with the Shimadzu mechanical analyser and pins were glued into the base with the use of Araldite Ultra Clear epoxy glue. Similarly to the pandemic tool a mirror was used to accurately set pins in relation to each other. The tool prepared this way was then utilised for the three-point bend test of rectangular samples. Figure 3.4 depicts assembled Shimadzu adapter with a positioning tool.

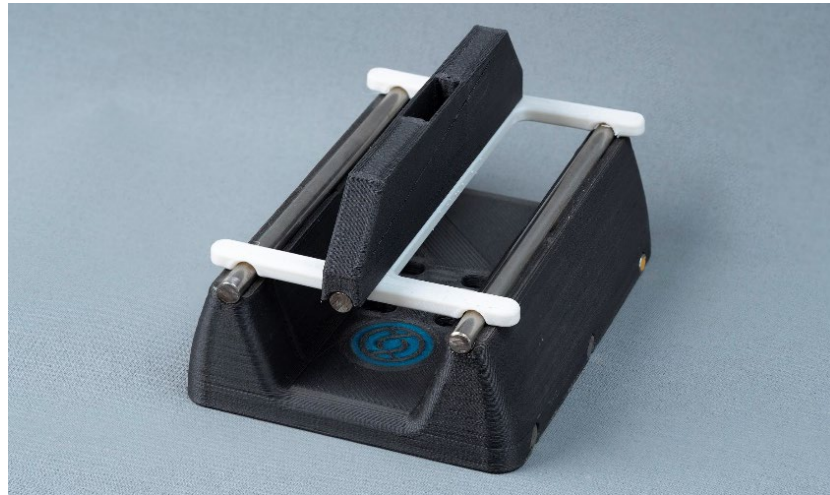


Figure 3.3: Photography of a 3D printed adapter base with PA12-CF.

Both tools were used to analyse the first 64 samples created in this project. The rest of the prepared rectangular samples (66 from 130) were measured using solely Shimadzu mechanical analyser. Comparison between tools and the results are presented in the next section of this chapter.

3.3. Samples mechanical analysis results

To determine composite materials with suitable robustness, 130 rectangular samples (100 mm length, 20 mm width, and 5 mm height, respectively) of different materials combinations were produced, post-processed and tested. See the table in appendix 2 for the full list of used materials. 3D printed rectangular samples were produced in a range of values of Cura slicer software infill rate parameter, from 35 % to 100% (65 samples with 35 %, 36 samples with 100 %, 1 sample with 50 %, and 1

sample with 40 % respectively). Samples with lower than 100% infill had no top layers. Therefore, there was a possibility to fill them with West System 105 epoxy resin (14 samples). Epoxy resin, and carbon fibre, fibreglass, basalt fibre, linen, or Kevlar reinforcement fabrics were added to 55 samples. Additionally, 50 samples were heat-treated in a range of temperatures, from 110 °C to 240 °C. Heat treatment as well as the addition of epoxy resin, and fabric reinforcement were introduced to improve mechanical parameters of rectangular samples.

Mechanical tests were conducted using three-point bend testing. It required the development of the so-called pandemic tool and Shimadzu mechanical analyser adapter mentioned in section 3.2 of this chapter. See chapter 2 for methods and design details of both tools. Figure 3.4 presents the loading-unloading cycle conducted on the 3D printed pandemic tool.

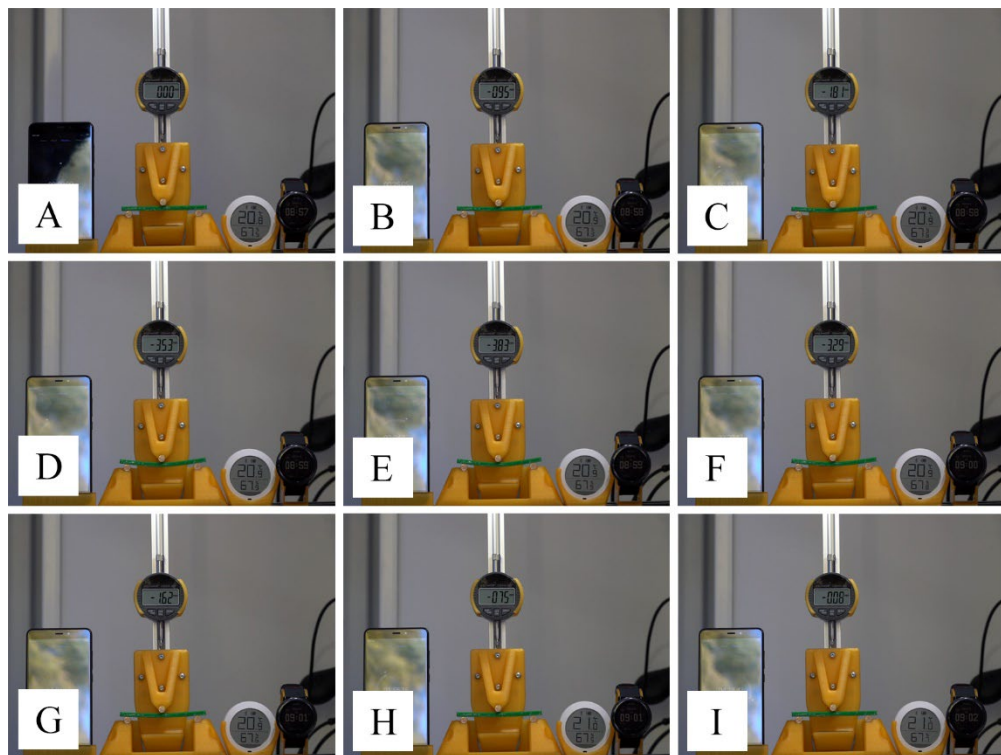


Figure 3.4: Response of a sample to loading-unloading cycle conducted on a 3D printed pandemic tool. Letters A-E indicate loading sequence: no load (A), 5 kg load (B), 9.5 kg load (C), 18.5 kg load (D), and 20 kg load (E) respectively. Letters F-I indicate unloading cycle: 18.5 kg (F), 9.5 kg (G), 5 kg (H), and no-load (I) respectively.

3.3.1. Comparison between pandemic tool and Shimadzu mechanical analyser.

The trial started from gathering data from the pandemic tool and Shimadzu EZ-S (500N load cell) tests. Figure 3.5 presents three cycles of randomly chosen samples measured with the use of the pandemic tool. Figure 3.5C shows the mean value of calculated flexural modulus with 1 standard deviation error. Gathered data presents excellent repeatability of the device within measured materials samples.

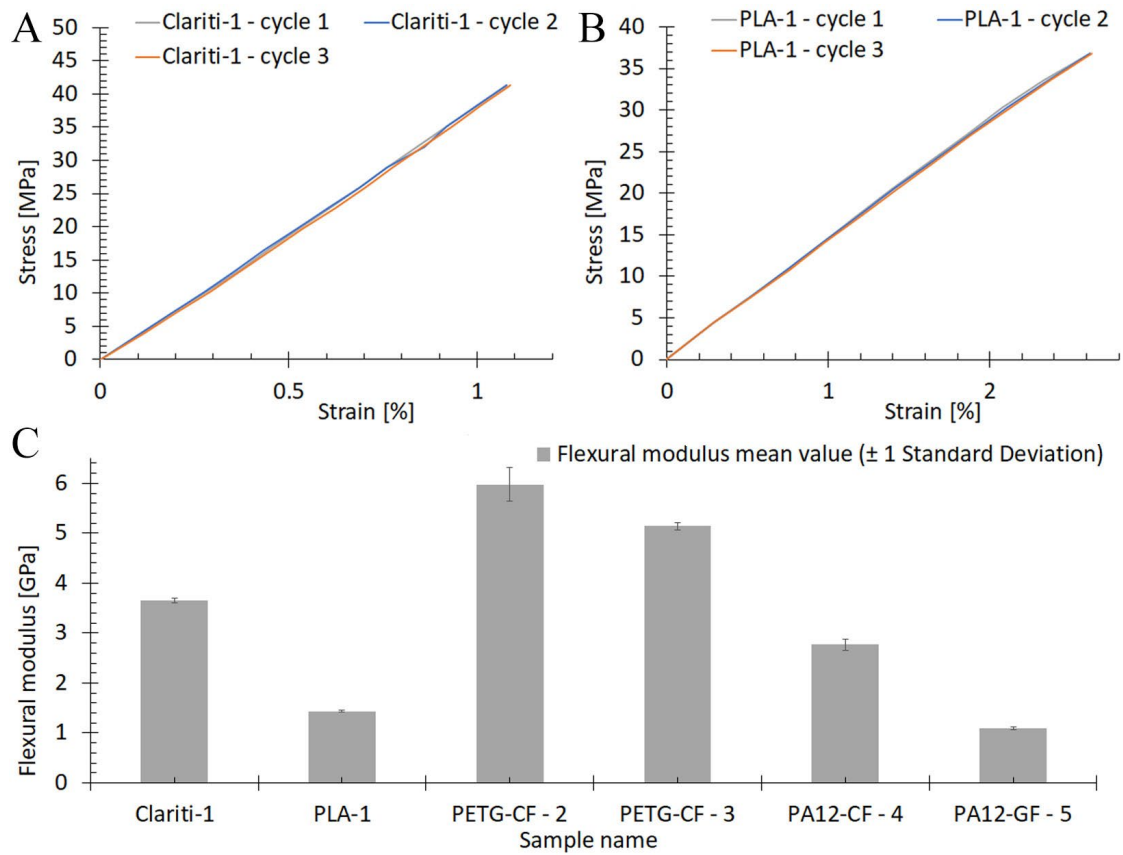


Figure 3.5: Presents characterisation data of the pandemic tool. A) stress-strain behaviour of the loading part of three cycles for Clariti - 1 (sample number 1). B) stress-strain behaviour of the loading part of three cycles for PLA - 1 (sample number 4). C) Obtained mean flexural modulus values with ± 1 Standard Deviation error.

Comparison between apparatuses was performed on 60 rectangles (sample numbers 1 to 64). See appendix 2 for details about used samples, and materials combination. For example, the comparison between the stress-strain behaviour of the loading part of the cycle for PETG-CF - 1 (sample number 3) indicates that the pandemic tool overestimated the values by around 26 % (Figure 3.6A). The second example (Figure 3.5B) of the stress-strain behaviour of the loading part of the cycle for PLA - 1 (sample number 4) depicts around a 3 % difference. Subsequently, a comparison of flexural modulus (Figure 3.6C), and the difference between flexural modulus obtained values (Figure 3.6D) of all samples was performed. The results indicate that there is a good agreement at around 20 % between measured values up to around 5 GPa. It seems that above the 5 GPa range, the pandemic tool is exponentially less accurate. For example, the difference in calculated flexural modulus for basalt fibre - 1 (sample no 64) is around 140 % between the pandemic tool and the Shimadzu EZ-S. Samples with higher flexural modulus, are characterised by smaller deflection under applied load in comparison to the Shimadzu EZ-S mechanical analyser. Studies indicate that the pandemic tool design was not stiff enough for these samples, which caused energy dissipation within the design. The applied load was not transferred efficiently to the samples. Data presented further in the mechanical analysis was obtained with the use of the Shimadzu EZ-S tool.

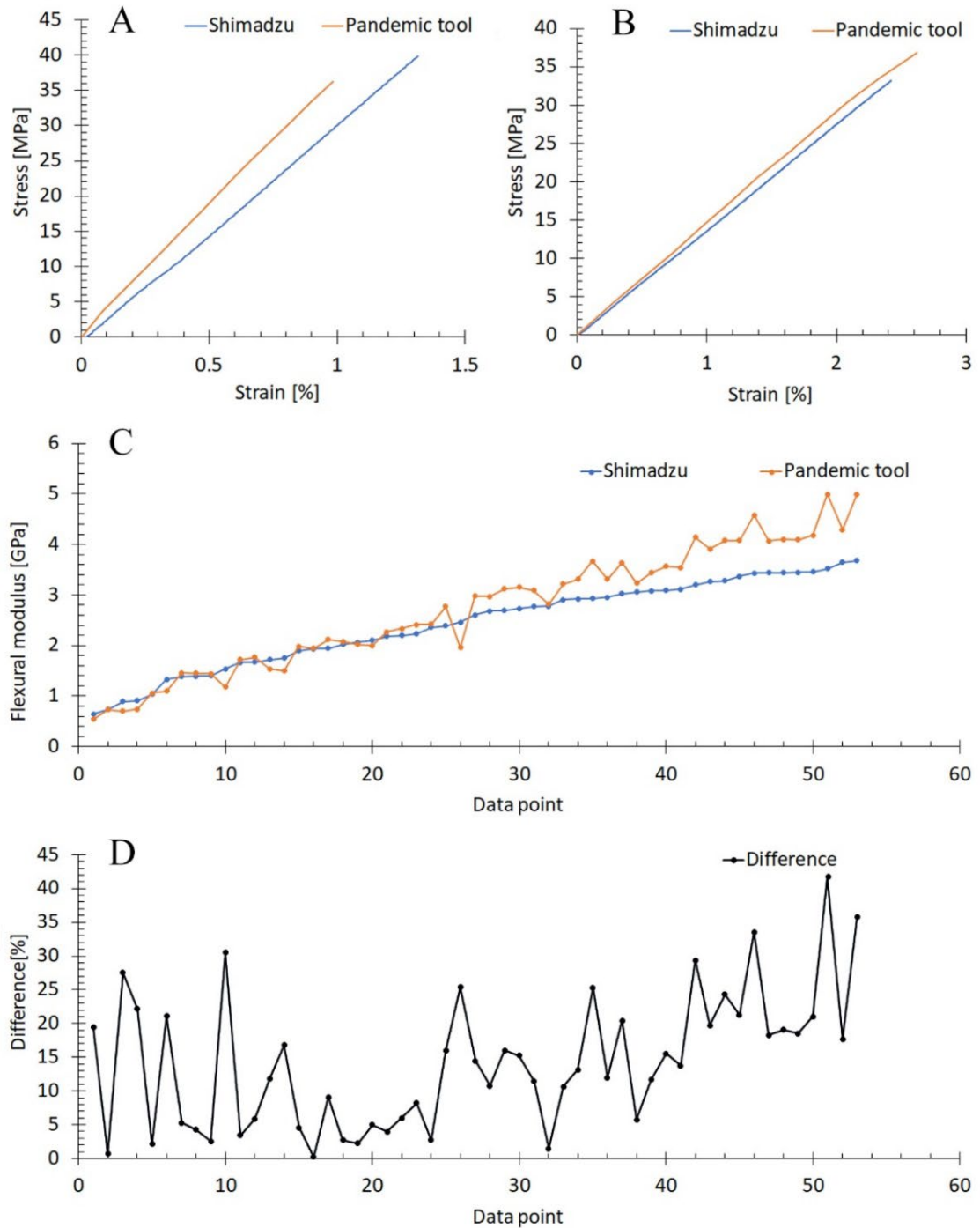


Figure 3.6: Presents comparison between so-called pandemic tool and Shimadzu mechanical apparatus. A) stress-strain behaviour of the loading part of the cycle for PETG-CF - 1 (sample number 3). B) stress-strain behaviour of the loading part of the cycle for PLA - 1 (sample number 4). C) Obtained flexural modulus using both tools up to about 5 GPa. D) Difference between determined Flexural modulus. For samples details check appendix 2. Orange and blue lines indicate testing concluded using the pandemic tool and the Shimadzu EZ-S, respectively.

3.3.2. Mechanical characterisation of samples without reinforcement materials

Data gathered during the three-point bend testing was divided into two groups consisting of samples as-prepared, and additionally reinforced with resin, and fabric mentioned in section 3.3. This section focus on the first group of rectangular samples analysis. Figure 3.7 presents the stress-strain behaviour of the loading part of the cycle of chosen samples of as-prepared composite materials determined with the use of Shimadzu EZ-S (500N load cell). Presented rectangular samples were manufactured from PLA, PETG, PA6, and PA12 with the addition of carbon fibre and fibreglass. Nylon 6 with carbon fibre additive (PA6-CF – 7, sample number 88) is characterised by the highest flexural modulus of all tested as-prepared materials with 5.9 ± 0.6 GPa. Heat treatment of Nylon 12 with carbon fibre additive in 240 ± 5 °C resulted in over 2 times improvement of flexural modulus from 2.5 ± 0.3 GPa (PA12-CF – 5, sample number 24) to 5.2 ± 0.5 GPa (PA12-CF – 18, sample number 72). Applied temperature caused a reduction in the internal humidity of the samples and sintered material. The impact of the humidity on Nylon 6 based material is presented in section 3.3.4 of this project. It was determined that humidity has a vast effect on the mechanical parameters of Nylon-based materials. Plain PLA (PLA – 3, sample number 11) is characterised by the third-highest stiffness from tested materials with 3.1 ± 0.3 GPa of flexural modulus value.

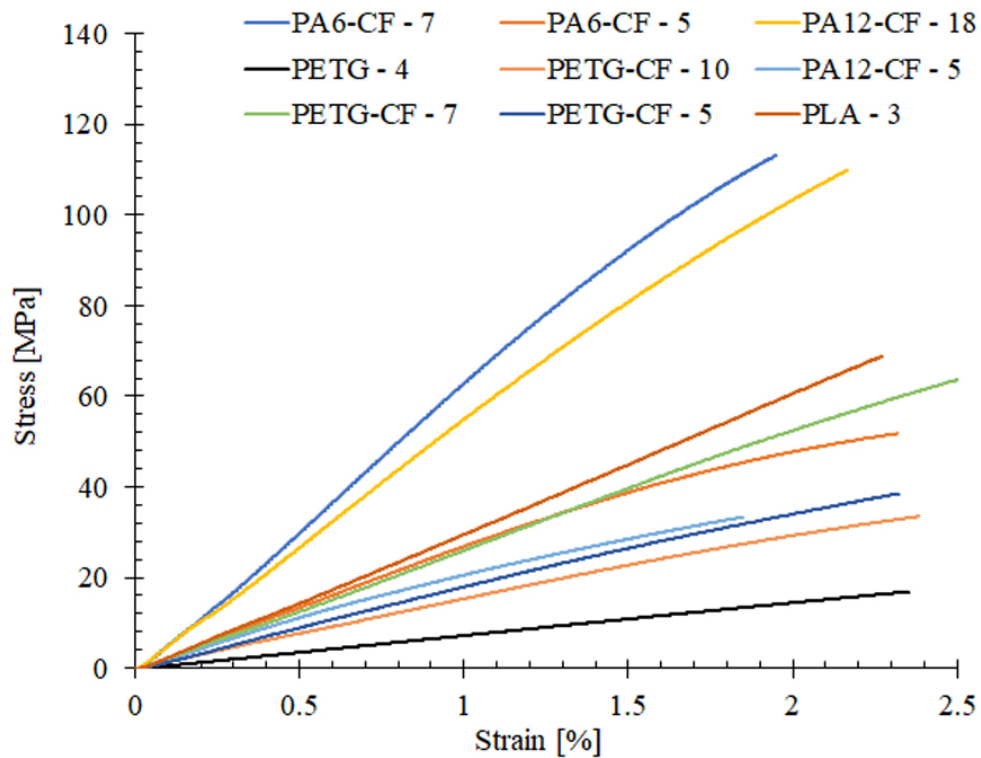


Figure 3.7: Stress-strain behaviour of the loading part of the cycle of as-prepared composite materials determined using the Shimadzu EZ-S (500N load cell). PA6-CF – 5, and PA6-CF - 7 indicate PA6-CF 3D printed with 35 % infill rate, and PA6-CF 3D printed with 100 % infill rate, respectively. PA12-CF – 5, and PA12-CF – 18 indicate PA12-CF 3D printed with 100 % infill, and heat-treated PA12-CF 3D printed with 100 % infill rate, respectively. PETG – 4 indicates a sample of PETG 3D printed with a 35 % infill rate. PETG-CF – 5, PETG-CF – 7, and PETG-CF – 10 indicate heat-treated PETG-CF 3D printed with 35 % infill rate, PETG-CF 3D printed with 100 % infill rate, and PETG-CF 3D printed with 35 % infill rate, respectively. PLA – 3 indicates PLA 3D printed with a 100 % infill rate.

Table 3.3 presents a summary of researched as-prepared composite materials. PA6-CF – 5 (sample number 85) produced with 35 % infill yielded higher flexural modulus than PETG-CF – 7 (sample number 20) and PA12-CF – 5 (sample number 24) 3D printed with 100 % infill rate Cura slicer parameter. The addition of carbon fibre to PETG base material resulted in improvement in flexural modulus from 0.7 ± 0.1 GPa (PETG – 4, sample number 41) to 1.7 ± 0.2 GPa (PETG-CF – 10, sample number 33) for samples 3D printed with a 35 % infill rate. Annealing in 140 ± 5 °C further improved flexural modulus to 1.9 ± 0.2 GPa (PETG-CF – 5, sample number 17).

Table 3.3: Summary of obtained results. Samples refer to table in appendix 2. PA6-CF – 5, and PA6-CF - 7 indicate PA6-CF 3D printed with 35 % infill rate, and PA6-CF 3D printed with 100 % infill rate, respectively. PA12-CF – 5, and PA12-CF – 18 indicate PA12-CF 3D printed with 100 % infill, and heat treated PA12-CF 3D printed with 100 % infill rate, respectively. PETG – 4 indicates a sample of PETG 3D printed with a w35 % infill rate. PETG-CF – 5, PETG-CF – 7, and PETG-CF – 10 indicate heat-treated PETG-CF 3D printed with 35 % infill rate, PETG-CF 3D printed with 100 % infill rate, and PETG-CF 3D printed with 35 % infill rate, respectively. PLA – 3 indicates PLA 3D printed with a 100 % infill rate.

Material	Sample no	Flexural modulus	Infill rate [%]	Heat treatment [°C]
		[GPa]		
PA6-CF – 5	85	2.9 ± 0.3	35	
PA6-CF – 7	88	5.9 ± 0.6	100	
PA12-CF – 5	24	2.5 ± 0.3	100	
PA12-CF – 18	72	5.2 ± 0.5	100	240
PETG – 4	41	0.7 ± 0.1	35	
PETG-CF – 5	17	1.9 ± 0.2	35	140
PETG-CF – 7	20	2.6 ± 0.3	100	
PETG-CF – 10	33	1.7 ± 0.2	35	
PLA – 3	11	3.1 ± 0.3	100	

3.3.3. Mechanical characterisation of samples with reinforcement

The second step of data analysis was to characterise the group of rectangular samples created with reinforced materials mentioned in section 3.3. Presented results depict samples manufactured in combination with the FDM technique, and with the use of CNC machined HDPE mould. The majority of samples were 3D printed and subsequently chosen reinforcement was applied. For comparison purposes, a few samples were made with the use of resin and fibre cloth only. Figure 3.8 presents the stress-strain behaviour of the loading part of the cycle created using the Shimadzu EZ-S tool. Eight materials combination with the highest flexural modulus registered are presented. Samples indicated as Kinetix R118 resin – 5, and Kinetix R118 resin - 6 refers to Kinetix R118 epoxy resin system, from which samples were produced, and reinforced with basalt, and carbon fibre 20 ± 1 mm chopped strands, respectively. The sample indicated as Basalt fibre - 1 was produced with the use of 25 layers

of basalt fibre cloth (plain weave, 200 gsm) and West System 105 epoxy resin. PA6-CF, and PA12-CF samples were reinforced with 3 layers of carbon fibre prepreg. Prepreg curing cycle process required 150 °C therefore samples wrapped in it were annealed during this process. The prepreg curing process is demonstrated in section 3.4.

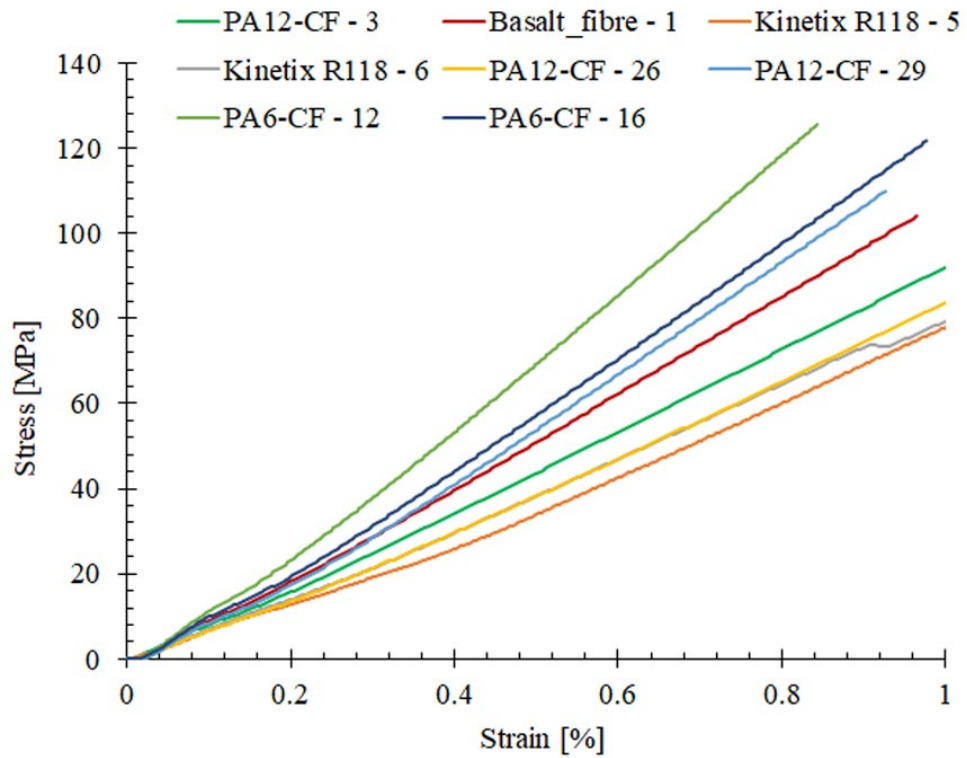


Figure 3.8: Stress-strain behaviour of the loading part of the cycle of reinforced composite materials tested using the Shimadzu EZ-S (500N load cell). Basalt fibre – 1 indicate 25 layers of basalt fibre, and West System epoxy resin. PA6-CF – 12, and PA6-CF - 16 indicate heat-treated 3D printed with 100 % infill rate prepreg reinforced PA6-CF, and heat-treated 3D printed with 35 % infill rate prepreg reinforced PA6-CF, respectively. PA12-CF – 3, PA12-CF – 26, and PA12-CF – 29 indicate 3D printed with 100 % infill rate carbon fibre reinforced PA12-CF, heat-treated 3D printed with 35 % infill rate prepreg reinforced PA12-CF, and indicate heat-treated 3D printed with 100 % infill rate prepreg reinforced PA12-CF, respectively. Kinetix R118 – 5, and Kinetix R118 – 6 indicate basalt fibre reinforced Kinetix R118 epoxy resin, and carbon fibre reinforced Kinetix R118 epoxy resin, respectively.

Results indicate that the addition of prepreg vastly improved the mechanical parameters of the samples. PA6-CF 3D printed with 100 % (PA6-CF – 11-15) and 35 % (PA6-CF – 16-20) yielded 12 ± 1 GPa and 11 ± 1 GPa respectively. PA12-CF (PA12-CF – 29-33) with prepreg and 25 layers of basalt fibre (Basalt fibre - 1) samples depicts

similar parameters, but the difference is in weight, 11 ± 0.1 g and 19 ± 0.1 g respectively. Samples produced with the resin and strands only are characterised by approximately half of the value of the flexural modulus of PA6-CF (PA6-CF – 16-20) with prepreg samples. Moreover, PA6-CF samples mean weight was 9 ± 0.1 g in comparison to 12 ± 0.1 g of resin samples. Table 3.4 presents a summary of chosen composites materials.

Table 3.4: Summary of obtained results Samples refer to table in appendix 2. Basalt fibre – 1 indicate 25 layers of basalt fibre, and West System 105 epoxy resin. Kinetix R118 – 5, and Kinetix R118 – 6 indicate basalt fibre reinforced Kinetix R118 epoxy resin, and carbon fibre reinforced Kinetix R118 epoxy resin, respectively. PA6-CF – 12, and PA6-CF - 16 indicate heat-treated 3D printed with 100 % infill rate prepreg reinforced PA6-CF, and heat-treated 3D printed with 35 % infill rate prepreg reinforced PA6-CF, respectively. PA12-CF – 3, PA12-CF – 26, and PA12-CF – 29-33 indicate 3D printed with 100 % infill rate carbon fibre reinforced PA12-CF, heat-treated 3D printed with 35 % infill rate prepreg reinforced PA12-CF, and heat-treated 3D printed with 100 % infill rate prepreg reinforced PA12-CF, respectively.

Material	Sample no	Flexural modulus [MPa]	Infill rate [%]	Heat treatment [°C]	Reinforcement / other
Basalt fibre - 1	64	10 ± 1	100		25 layers
Kinetix R118 – 5	104	6.5 ± 0.7			36 % by weight
Kinetix R118 – 6	108	7.3 ± 0.7			24 % by weight
PA6-CF – 11 - 15	121-125	12 ± 1	100	150	3 layers prepreg
PA6-CF – 16 - 20	126-130	11 ± 1	35	150	3 layers prepreg
PA12-CF – 3	19	8.6 ± 0.9	100		3 layers carbon
PA12-CF – 26	112	7.6 ± 0.8	35	150	5 layers prepreg
PA12-CF – 29 - 33	116-120	9.2 ± 0.9	100	150	3 layers prepreg

It was determined that PA6-CF with the addition of carbon fibre prepreg perform the best from all tested materials. Moreover, combinations of materials were one of the lightest. Next section of this project focus on the mechanical analysis of Nylon 6 with carbon fibre additive composite material.

3.3.4. Analysis of PA6-CF samples

The subsequent step of the data analysis was to focus on the best material tested. In section 3.3.3 it was determined that it was Nylon 6 with carbon fibre filament. Figure 3.8 represents a typical mechanical response of 3D printed in Nylon 6 with carbon fibre additive composite material rectangles samples (100 mm length, 20 mm width, 5 mm height, respectively). Response of the PA6-CF samples to deflection and force of loading-unloading cycle (Figure 3.9A) tested using the Shimadzu EZ-S (500N load cell) mechanical analyser, and stress-strain behaviour of the loading part of the cycle (Figure 3.9B).

Two samples were marked as “WET” (PA6-CF – 1, and PA6-CF - 2) were placed outside of the dry box for 24 h prior to measuring. Hygroscopic behaviour of the Nylon-based composite can be clearly seen as mechanical characteristics are impacted by water absorption, i.e. maximum load is reduced from 375 N to 290 N. The addition of three layers of prepreg carbon fibre cloth improved the mechanical robustness, i.e. 2 times increase in maximum load and a significant reduction in energy dissipation. It is suggested that prepreg composite sealed the surface of Nylon 6 based samples, preventing water absorption and reduction in mechanical robustness.

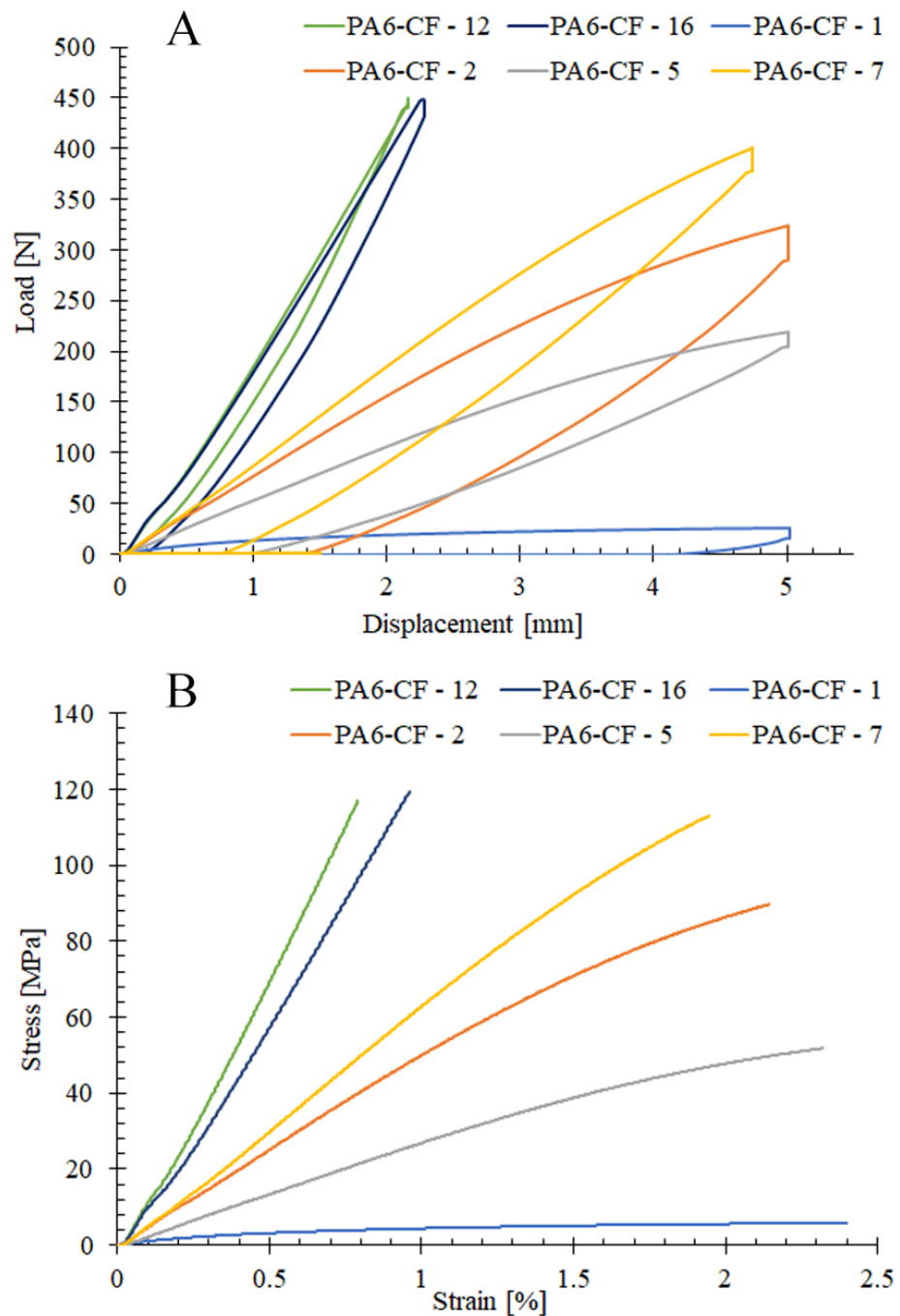


Figure 3.9: Typical mechanical response of 3D printed PA6-CF rectangles samples tested using Shimadzu EZ-S (500N load cell). A) loading-unloading cycle force-deflection. B) stress-strain behaviour of the loading part of the cycle. PA6-CF – 1, PA6-CF – 2, PA6-CF – 5, PA6-CF – 7, PA6-CF – 12, and PA6-CF - 16 indicate 3D printed with 35 % infill rate water-saturated PA6-CF, 3D printed with 100 % infill rate water-saturated PA6-CF, 3D printed with 35 % infill rate PA6-CF, 3D printed with 100 % infill rate PA6-CF, heat-treated 3D printed with 100 % infill rate prepreg reinforced PA6-CF, and heat-treated 3D printed with 35 % infill rate prepreg reinforced PA6-CF, respectively.

The data from the mechanical test were converted to moduli values and are displayed in Table 3.5. A composite consisting of Nylon 6 with carbon fibre additive and carbon fibre prepreg demonstrated the best mechanical characteristics out of 130 samples tested. For example, PA6-CF 3D printed at 100 % infill rate with prepreg yielded a flexural modulus value of 12 ± 1 GPa (PA6-CF – 11 - 15), which is more than double the value observed for Nylon 6 with carbon fibre additive 5.9 ± 0.6 GPa (PA6-CF – 7). Therefore it is suggested that this material combination would be suitable for use in the instrumented fins.

Table 3.5: Summary of obtained results for PA6-CF. Samples refer to table in appendix 2. PA6-CF – 1, PA6-CF – 2, PA6-CF – 5, PA6-CF – 7, PA6-CF – 11-15, and PA6-CF – 16-20 indicate 3D printed with 35 % infill rate water-saturated PA6-CF, 3D printed with 100 % infill rate water-saturated PA6-CF, 3D printed with 35 % infill rate PA6-CF, 3D printed with 100 % infill rate PA6-CF, heat-treated 3D printed with 100 % infill rate prepreg reinforced PA6-CF, and heat-treated 3D printed with 35 % infill rate prepreg reinforced PA6-CF, respectively.

Material	Sample no	Flexural modulus [MPa]	Infill rate [%]	Heat treatment [°C]	Reinforcement / other
PA6-CF – 1	65	0.6 ± 0.1	35		Wet sample
PA6-CF – 2	66	5.0 ± 0.5	100		Wet sample
PA6-CF – 5	85	2.9 ± 0.3	35		
PA6-CF – 7	88	5.9 ± 0.6	100		
PA6-CF – 11 - 15	121-125	12 ± 1	100	150	3 layers prepreg
PA6-CF – 16 - 20	126-130	11 ± 1	35	150	3 layers prepreg

3.3.5. Materials performance parameters analysis

Typically, high-performance surfboard fins are produced from fibreglass, basalt fibre, or carbon fibre cloth and poly(ester) or epoxy resin. In this study, the sample indicated as Basalt fibre - 1 was produced with the use of 25 layers of basalt fibre cloth (plain weave, 200 gsm) and West System 105 epoxy resin. It was used as an industry standard to compare the performance of 3D printed materials. Table 3.6 presents a summary of gathered data.

Table 3.6: Summary of obtained results. Samples refer to table in appendix 2. Basalt fibre – 1, PA6-CF – 7, PA6-CF – 11-15, PA6-CF – 16-20, PA12-CF – 18, PA12-CF – 29 – 33, and PLA - 3 indicate 25 layers of basalt fibre, and West System 105 epoxy resin, PA6-CF 3D printed with 35 % infill rate, heat-treated 3D printed with 100 % infill rate prepreg reinforced PA6-CF, and heat-treated 3D printed with 35 % infill rate prepreg reinforced PA6-CF, heat treated PA12-CF 3D printed with 100 % infill rate, heat treated 3D printed with 100 % infill rate prepreg reinforced PA12-CF, and PLA 3D printed with a 100 % infill rate, respectively.

Material	Weight	Flexural modulus	Flexural stress	Flexural strain	Reinforcement / other
		E_f	σ_f	ε_f	
	[g]	[MPa]	[MPa]	[%]	
Basalt fibre – 1	19 ± 0.1	10 ± 1	105 ± 10	1	25 layers
PA6-CF – 7	8 ± 0.1	5.9 ± 0.6	120 ± 12	2	-
PA6-CF – 11–15	11 ± 0.1	12 ± 1	133 ± 13	1	3 layers prepreg
PA6-CF – 16–20	9 ± 0.2	11 ± 1	136 ± 14	1	3 layers prepreg
PA12-CF – 18	9 ± 0.1	5.2 ± 0.5	111 ± 11	2	-
PA12-CF– 29–33	11 ± 0.3	9.2 ± 0.9	111 ± 11	1	3 layers prepreg
PLA – 3	12 ± 0.1	3.1 ± 0.3	70 ± 7	2	-

The obtained data indicate that 3D printed materials without reinforcement perform significantly lower than commercial solutions when it comes to flexural modulus. PA6-CF yielded flexural a modulus of 5.9 ± 0.6 MPa in comparison to 10 ± 1 MPa in the case of the basalt cloth-based sample. It is 41 % of a difference in flexural modulus. When reinforced with carbon fibre prepreg, 3D printed samples can exceed mechanical parameters of basalt fibre – 1 sample. For instance, PA6-CF - 11-15 reinforced with three layers of prepreg samples yielded a flexural modulus of 12 ± 1 MPa, which is 20 % more. The significant difference is related to the weight of the materials. Basalt fibre – 1 sample is the heaviest with 19 ± 0.1 g. In comparison, PA6-CF - 11-15 samples' mean weight is 11 ± 0.1 g. It is 42 % less than basalt cloth composite material. PA6-CF prepreg reinforced composite material exceeds commercially used solutions when it comes to flexural modulus and weight. The exact required material performance parameters are hard to determine as fins used in the surfboard industry are characterised by a wide range of mechanical parameters. Stiff

or flexible fins are used for different waves condition. In recent times it was presented that 3D printing is a viable option for rapid prototyping of custom fins for surfboards [29]. The research demonstrated that the mechanical properties of 3D printed fins are similar to commercially used solutions [29]. Field tests proved that participants were able to generate similar speed, yaw angle, duration, rotational speed, roll angle, pitch angle and bottom turn to cutback power.

3.4. Heat treatment

FDM 3D printing technology generates parts with various tensile strengths depending on printing direction. Interlayer performance in Z-axis is lower than X-axis and Y-axis hot-end printing plane. Additionally, it was determined that the addition of carbon fibre to base filaments lowers interlayer strength further. Increased melt viscosity impacts interlayer diffusion bonding [38]. Heat treatment proved to increase thermal and mechanical parameters and removed internal stresses of researched samples [38].

In this study, chosen samples of materials were annealed in 110 ± 5 °C and 140 ± 5 °C for 1 hour in an air environment. Additionally, selected rectangles were remelted in 240 ± 5 °C. In order to maintain the shape, samples were covered in salt.

Figure 3.10 depicts the prepreg curing curve. The side effect of the process was that materials used in conjunction with prepreg carbon fibre were annealed at the same time. Samples were cured in 80 ± 5 °C for 30 minutes and subsequently in 150 ± 5 °C for 2 hours. Then left in the oven to cool down.

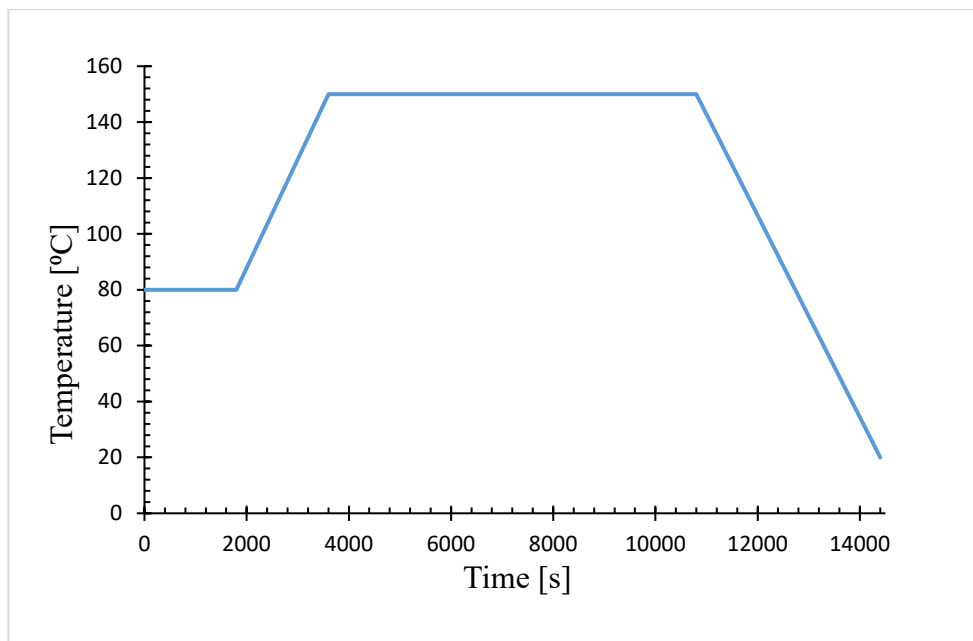


Figure 3.10: Prepreg datasheet optimal curing cycle.

Chapter 4: Instrumented fins and surfboard results

This chapter details the development of an instrumented fin and surfboard with a built-in electronic system.

4.1. Development of the touch probe and an instrumented fin.

The design of an instrumented fin was based on the Futures Twin T1 (Futures Fins) surfboard fins. The first step to develop the instrumented fin was to produce a touch probe tool able to measure discrete points on the surface of the Futures Twin T1. It was necessary as during pandemic related lockdown it was not possible to use the coordinate-measuring machine. A determined set of points was then used in CAD software (Inventor Professional) to create the design of an instrumented fin. See chapter 2 for tool and fin design details.

Development of the touch probe started from 3D printing of four parts with PLA material. Subsequently, three 4 mm in diameter, 16 ± 1 mm length brass pins, and 4 mm in diameter, 50 ± 1 mm length brass probe were prepared, and glue into the pin holder part. Then six 6 mm in diameter chrome steel balls were glued into the 3D printed bottom lid. The next step was to solder cables to connect steel balls in sets. Three M3 screws were used to connect the top lid with the case. The final step of the assembly process was to introduce the C-676 spring, and pin holder to the casing and connect the bottom lid with the casing via three M4 screws. The touch probe accuracy was then tested on a randomly chosen rectangular sample (100 mm length, 20 mm width, 5 mm height, respectively) used in chapter 3 of this project. The device was connected to a digital multimeter and the resistance of the circuit was measured (Figure 4.1A). Then the gantry of the CNC mill was moved in 0.01 mm increments. CNC machine coordinates were registered at the moment when a touch probe circuit stopped conducting current, and the resistance of the circuit could not be measured (Figure

4.1B). The test resulted in around 1 % accuracy between callipers and the touch probe. The device prepared this way was used to measure dimensions of the Futures Twin T1 fin. Then instrumented fin CAD model was developed.

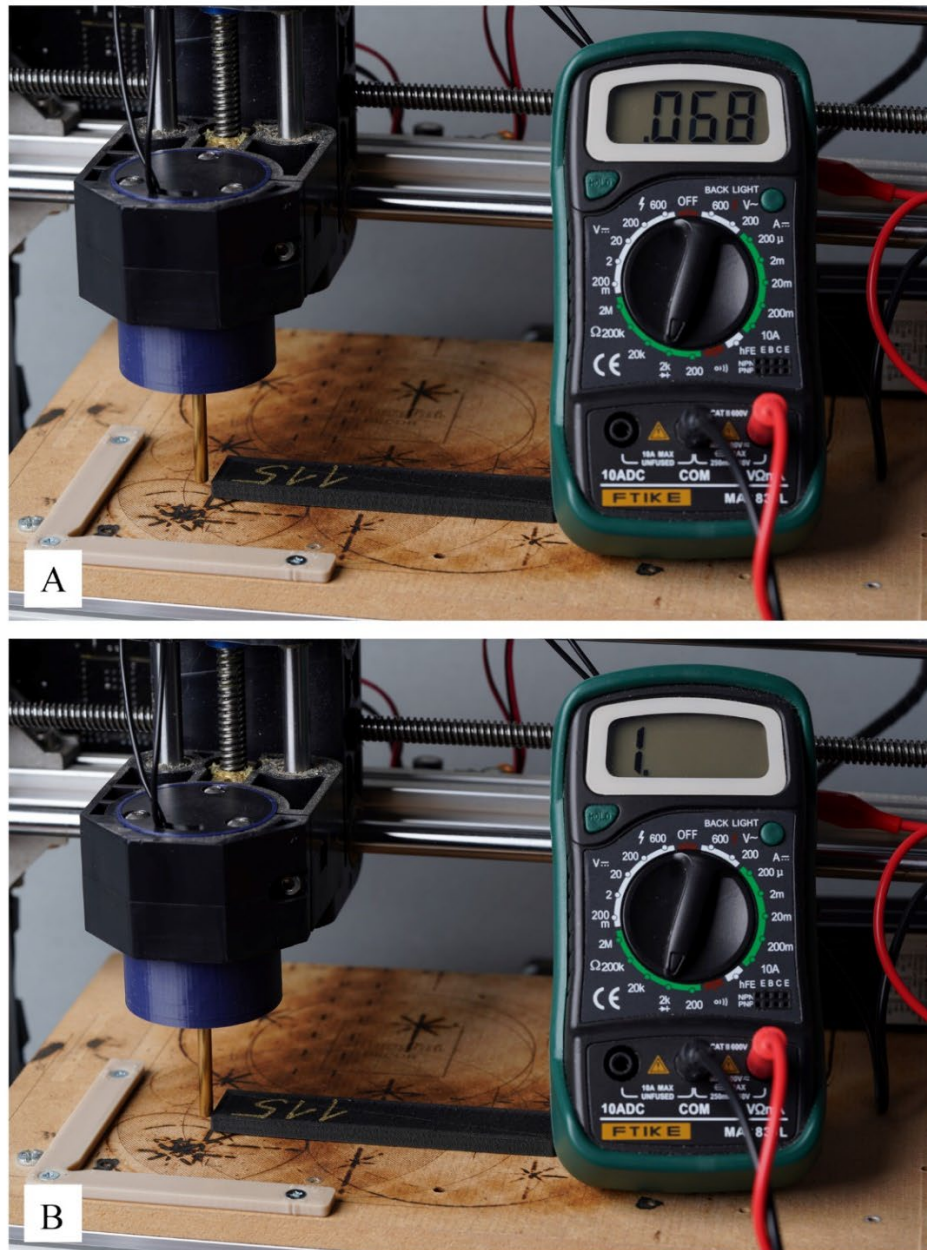


Figure 4.1: Photography of a typical touch probe set up used to measure discrete points of the Futures Twin T1 surfboard fin surface. An example of rectangular sample measurements. A) Touch probe was not touching the object, therefore the resistance of the circuit could be measured. B) Touch probe was touching the object, and the resistance of the circuit could not be measured which indicated breaking the electrical circuit, and machine coordinates could be registered.

The second step of an instrumented fin development was the optimisation of a 3D printing process. It required two stages during the manufacturing process. The first step was to 3D print the bottom part of the fin with trapezoidal prism shape space for a flex sensor. It was necessary as nozzle design exclude it from 3D printing of a rectangular shape in a 1 mm thick pocket. Then filament was changed for conductive TPU or PLA and a sensor was created. The used 3D printer has only one extruder therefore manual filament change and cleaning up after the use of conductive filaments during the printing process was necessary. The process was then continued and subsequent layers of filament covered 3D printed sensor. The second step was to glue in a commercially obtained Wheatstone bridge and cables with Araldite Ultra Clear epoxy glue. The rectangular pocket (11 mm length, 9.5 mm width, 0.4 mm height, respectively) was introduced into the design of the instrumented fin to accommodate the used Wheatstone bridge. When the glue was cured, 3D printed process was started again, and subsequent layers of filament sealed sensor inside the fin. The prototype was produced with transparent blue PLA material. This material was used for a proof of concept prototype to make sensors embedded inside the fin visible.

4.2. 3D printed sensor analysis

The 3D printed sensors were incorporated into rectangular samples (see Chapter 2.2.2) as they were too fragile to be tested independently. Samples were 3D printed in the PLA, PA12-CF, PA6-CF, conductive PLA and conductive TPU materials. The method of mechanical test was the same as in the case of a regular rectangular samples (see Chapter 2.10) and performed on the Shimadzu mechanical analyser. The only difference was the connection of probes on both sides of the material. The resistance was measured with Agilent 34410A digital multimeter.

The comparison between samples made with the same base PLA material with (indicated as PLA - 19) and without (indicated as PLA - 3) sensor is presented in Figure 4.2A. Results indicate that introduction of the sensor did not impact the mechanical characteristic of the tested samples. PLA - 19 - tension and PLA - 19 - compression indicate the same sample. The difference was in positioning the sample relative to the tool. Figure 4.2B presents the force vs time response of samples measured with a Shimadzu mechanical analyser. It is suggested that samples produced with the same base material performed similarly. Responses of sensors made with PLA and TPU are vastly different.

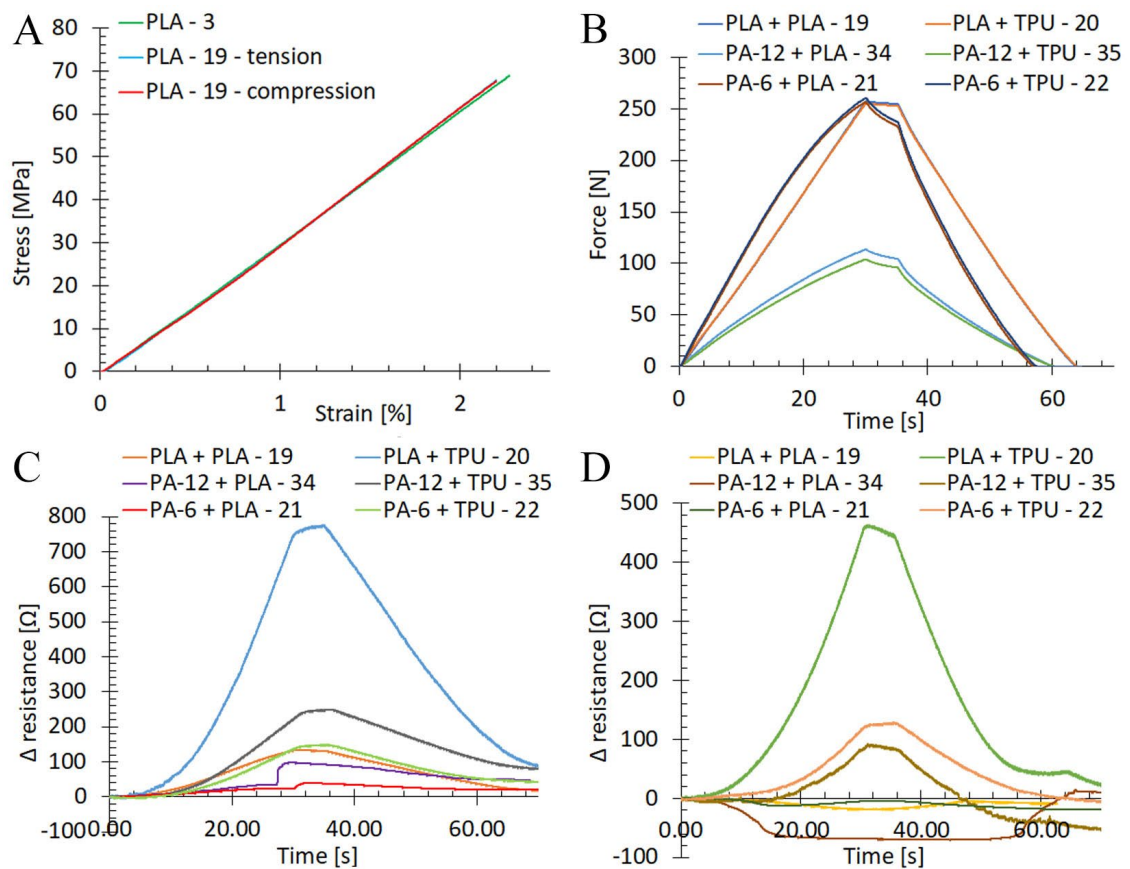


Figure 4.2: Charts of a typical response of an rectangular samples with 3D printed sensors for a loading-unloading cycle. A) stress vs strain. B) force vs time. C) Δ resistance vs time for tension. D) Δ resistance vs time for compression.

Figure 4.2C presents response of sensors to tension, TPU sensor (indicated as PLA + TPU – 20, PA-12 + TPU – 35, and PA-6 + TPU – 22, respectively) is characterised by greater change in resistance relative to sensors made with PLA material (indicated as PLA + PLA – 19, PA-12 + PLA – 34, and PA-6 + PLA – 21, respectively). Figure 4.2D presents the response of sensors to compression, TPU sensor is characterised by rise of resistance whilst the PLA sensor by fall of resistance. The sample indicated as PLA+TPU – 20 was made from PLA (base) and conductive TPU (sensor). It was subjected to tension and compression. Greater resistance change was observed in case of tension, up to 750 Ω in comparison to 470 Ω . Performed tests indicate a nonlinear characteristic of 3D printed sensors. Additionally, tested samples did not return to their starting point. In order to be able to accurately measure flex and force with 3D printed sensors, compensation curves should be applied.

4.3. Working prototype of an instrumented fin

The first prototype of an instrumented fin (Figure 4.2) was manufactured with the use of transparent blue PLA filament. The flex sensor (1) visible in Figure 4.2 was 3D printed with the use of conductive TPU with graphene additive composite material filament.



Figure 4.3: Image of the working prototype of an instrumented fin with visible 3D printed flex sensor (1), and commercial Wheatstone bridge (2).

Mechanical and sensor testing were conducted on a Shimadzu EZ-S mechanical analyser (500N load cell). The sensors were connected to Agilent 34410A multimeter. The surfboard with fin was mounted into a customised bench vice.

Figure 4.3AB presents a typical stroke response of an instrumented fin to an applied force. Response of an instrumented fin to a typical loading-unloading cycle (Figure 4.3 C) demonstrated that the load applied and deflection applied, scalar linearly without noticeable energy dissipation. Fin was deflected in an elastic region, therefore after unloading, instrumented fin returned to the original position. Figure 4.3D indicate that 3D printed sensor resistance vs stroke curve is characterised by a drop of resistance in the first 3 mm of deflection, then linear rise to around 8 mm and vast change in resistance from 8 to 10 mm. 3D printed sensor was mounted on the opposite side of the fin than commercial Wheatstone bridge. Therefore drop of resistance can

be observed as the sensor was initially compressed. Subsequent deflecting of the fin caused minor resistance rise from 5966Ω to 5971Ω . This would indicate the introduction of tension to 3D printed sensor. The fin flex can be calculated by dividing stroke by fin height. In the presented experiment, fin height was 130 mm and applied stroke was up to 10 mm, therefore maximum fin flex was $7.7 \pm 0.1 \%$. It is suggested that the linear behaviour of the Wheatstone bridge sensor makes it suitable to measure fin flex during surfing.

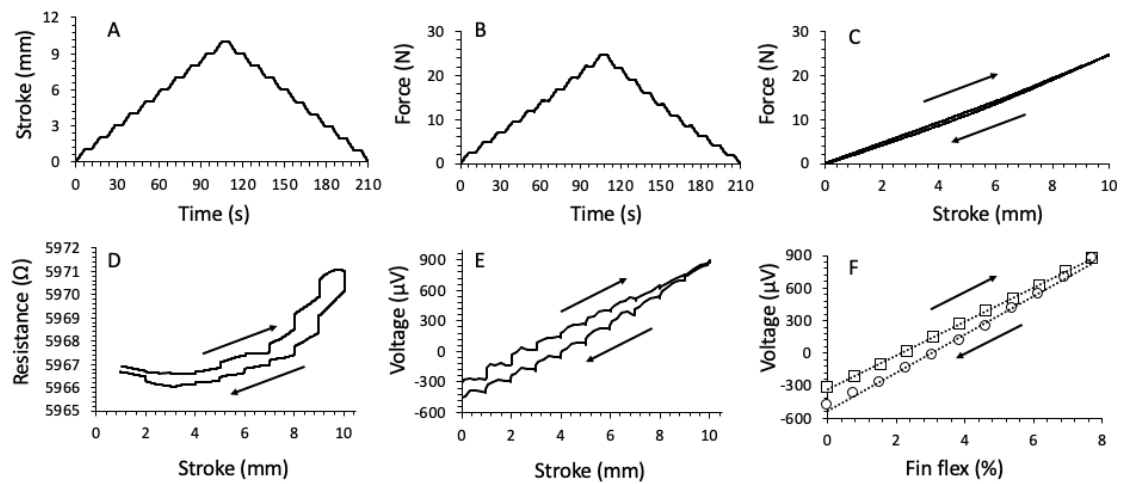


Figure 4.4: Charts of a typical response of an instrumented fin for a loading-unloading cycle. A) stroke vs time. B) force vs time. C) force vs stroke. D) resistance vs stroke. E) voltage vs stroke. F) average voltage vs fin flex response. Dotted lines are linear fits of the data. Arrows in C-F indicate the direction of loading and unloading of the instrumented fin.

Figure 4.5 presents data from three loading-unloading cycles of the instrumented fin. Gathered data indicate good repeatability and linear characteristic of the Wheatstone bridge (Figure 4.5A). 3D printed sensor is characterised by a high discrepancy in the first 80 s of loading cycles (Figure 4.5B). Further in the experiment, the discrepancy is decreasing. Figure 4.5CD presents the force vs time response of the fin measured with a Shimadzu mechanical analyser. It is suggested that the fin performance is consistent across loading-unloading cycles.

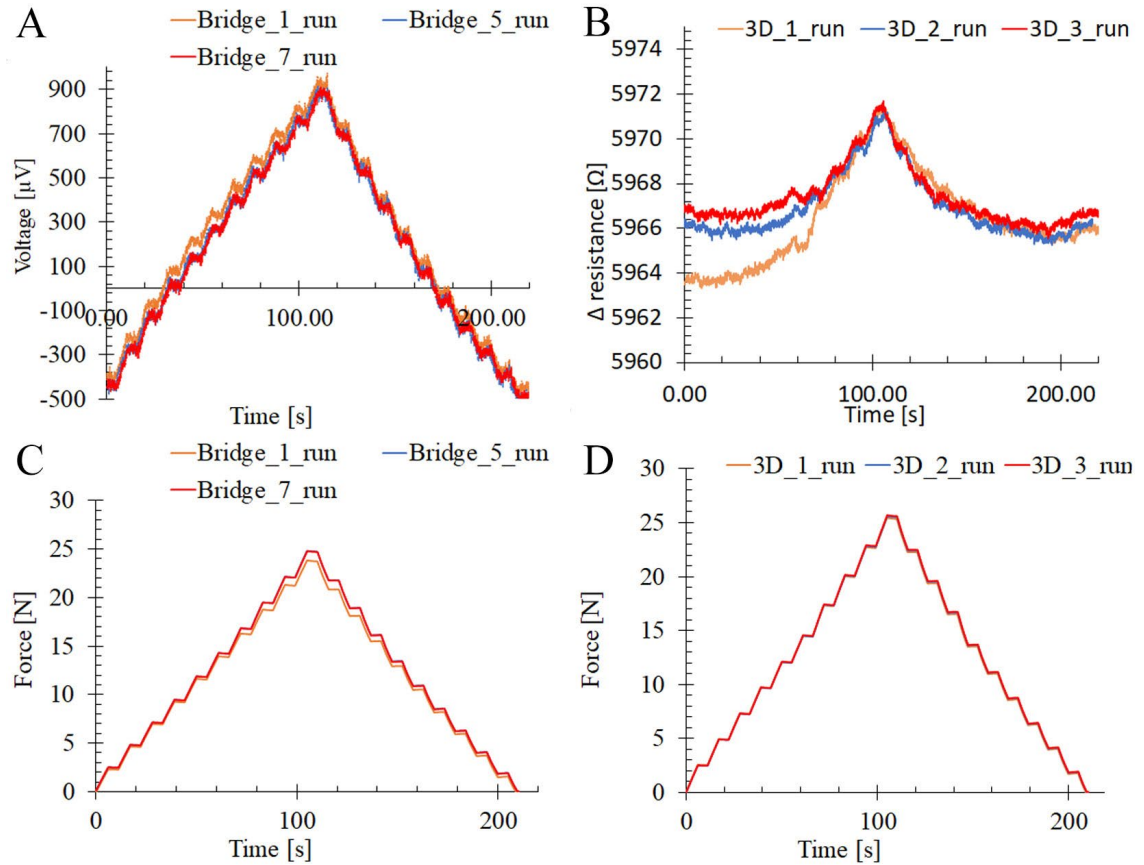


Figure 4.5: Charts of a response of an instrumented fin for a three loading-unloading cycles. A) voltage vs time for Wheatstone bridge. B) resistance vs time for a 3D printed sensor. C) force vs time. D) force vs time.

4.4. Comparison between Futures T1 Twin HC and 3D printed fins.

The first prototype of an instrumented fin (Figure 4.2) was tested against Futures T1 Twin HC fin. The commercial fin was CNC machined (Figure 4.6A) in order to accommodate the sensor. The same Wheatstone bridge as in the 3D printed fin was glued with epoxy glue. The positioning of the sensor was the same as in the case of a 3D printed fin (Figure 4.6BC).

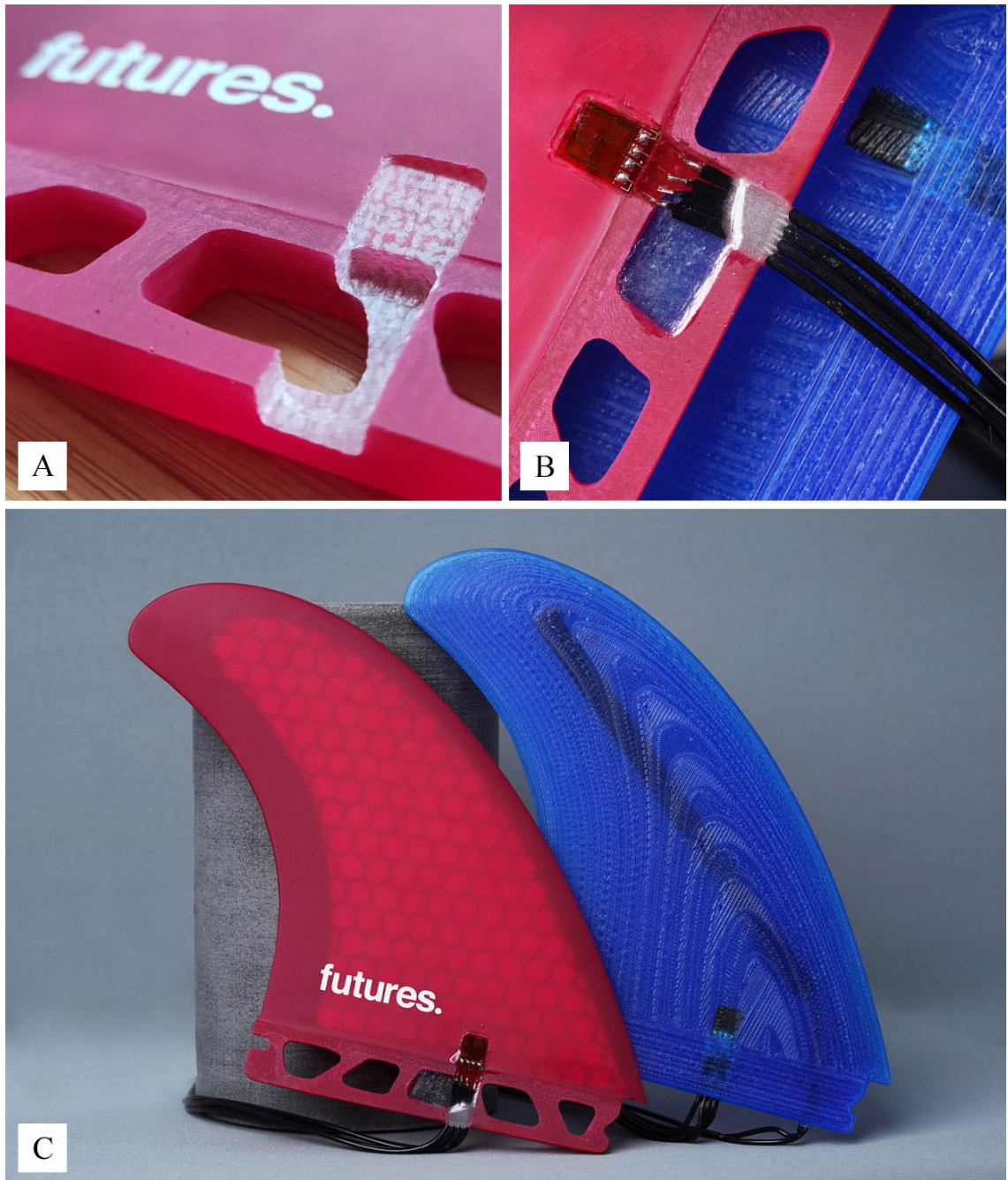


Figure 4.6: Picture of commercial and 3D printed fins. A) CNC machined pocket for a sensor. B) close up of two sensors. C) both fins.

Comparison was conducted on a Shimadzu EZ-S mechanical analyser (500N load cell). The sensors were connected to Agilent 34410A multimeter. The surfboard with fin was mounted into a customised bench vice. Fins sensors were subjected to tension

and compression. Figure 4.7AB presents loading-unloading cycle when sensors were subjected to tension, and compression, respectively.

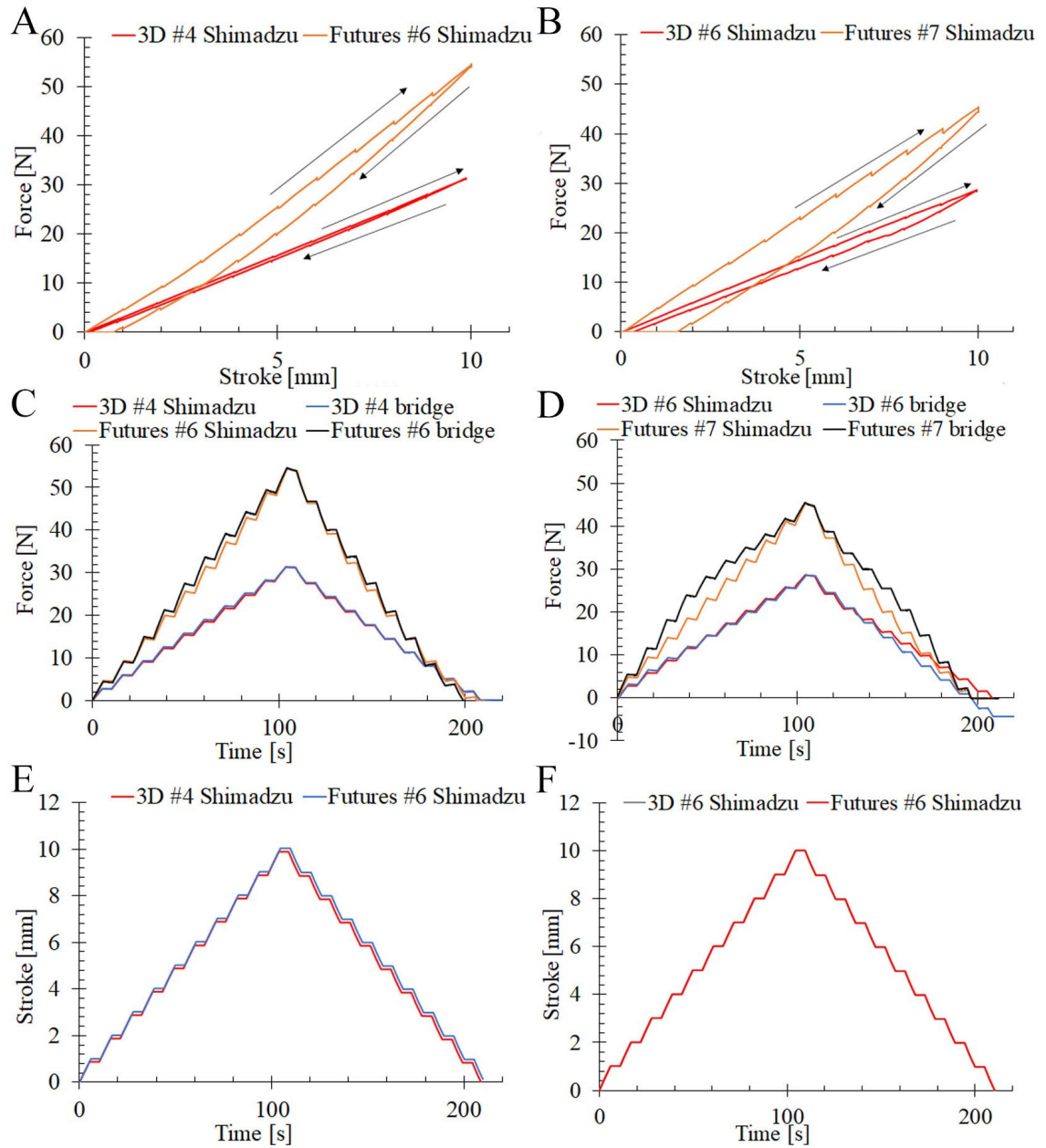


Figure 4.7: Charts of a typical response of a Futures T1 Twin HC and 3D printed fins equipped with Wheatstone bridge for a loading-unloading cycle. A) force vs stroke for tension. B)) force vs stroke for compression. C) force vs time for tension. D) force vs time for compression. E) stroke vs time for tension. F) stroke vs time for compression. Arrows in A-B indicate the direction of loading and unloading of the fins.

Gathered data indicate that fins performed differently, depending on the direction of the applied force. Futures fin yielded 55 N when force was applied on foil side and

45 N when force was applied on a “flat” side of the fin. It is around 18 % difference. 3D printed fin yielded 31 N (44 % less than Futures) when load was applied on a foil side and 29 N (36 % less than Futures) when force was applied on a “flat” side of the fin. Figure 4.7CD presents comparison between responses gathered by Shimadzu mechanical analyser and Wheatstone bridges mounted on fins. When sensors are subjected to tension, the signal representation is very accurate. In case of compression, drift between mechanical analyser and Wheatstone brides can be observed. When compressed, sensor mounted on commercial Futures fin is characterised by nonlinear behaviour.

Figure 4.8 presents teen cycles of loading-unloading cycles for Futures T1 Twin HC and 3D printed fins. Comparison between data collected from Wheatstone bridges mounted on fins and Shimadzu mechanical analyser indicate very good repeatability and accuracy of used sensors when fins are subjected to tension (Figure 4.8C). Presented force vs time responses for compression (Figure 4.8D) are characterised by a minimal drift.

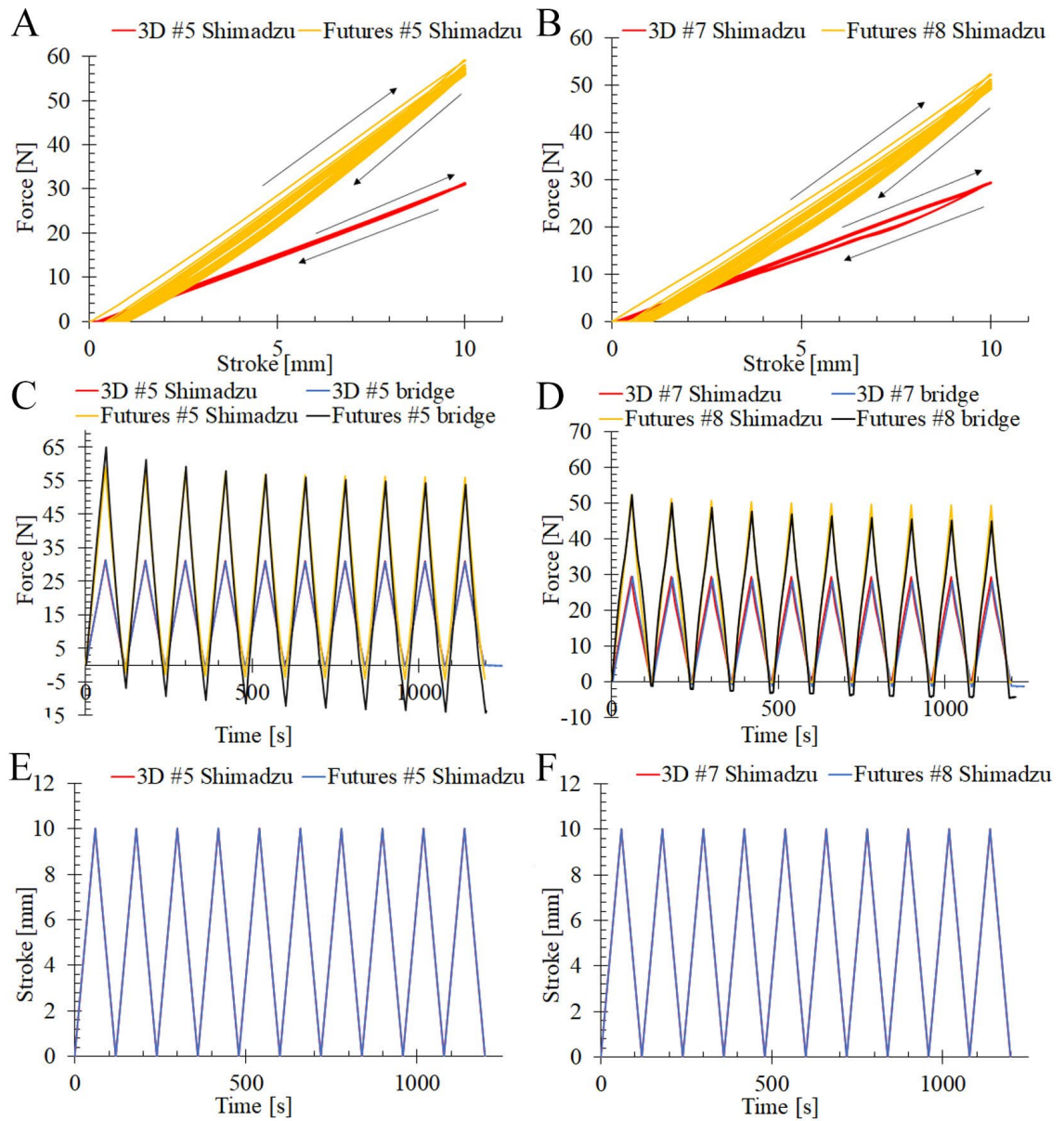


Figure 4.8: Charts of a typical response of a Futures T1 Twin HC and 3D printed fins equipped with Wheatstone bridge for a loading-unloading cycle. A) force vs stroke for tension. B)) force vs stroke for compression. C) force vs time for tension. D) force vs time for compression. E) stroke vs time for tension. F) stroke vs time for compression. Arrows in A-B indicate the direction of loading and unloading of the fins.

4.5. Surfboard with inbuilt measurement system and set of instrumented fins

The prototype of an instrumented surfboard was based on the Sanctum Mini Mal 7'4" (Sanctum Surfboards) epoxy resin surfboard. Electronic components were placed in the thickest and strongest section of the surfboard. Instrumented fins were connected

with electronics via a 6-way shielded computer data cable. West System's 105 epoxy resin with 207 hardener were used in prototype production. The process started from drilling holes in fins boxes to accommodate wires coming from instrumented fins and creating a drawing of the paths and position of the electronic box on the surfboard (Figure 4.9A). Subsequently, after determining the position, two-stage 3D printed templates were mounted on the surface (Figure 4.9B). Then, paths and casing cut-outs were made with the Makita DRT50Z router tool. The electronic box was custom fitted into the surfboard (Figure 4.9C), after creating space for cables and casing, wires were installed inside the box and glued with epoxy resin (Figure 4.9D). Moreover, the electronic box was coated with epoxy resin in order to seal the surface and prevent potential leaking caused by the imperfect 3D printing process (Figure 4.9E). Subsequently, after curing epoxy resin for 24 h, a gasket was produced with the use of Barnes M4642 silicone rubber characterised by Shore A37 hardness (Figure 4.9F).

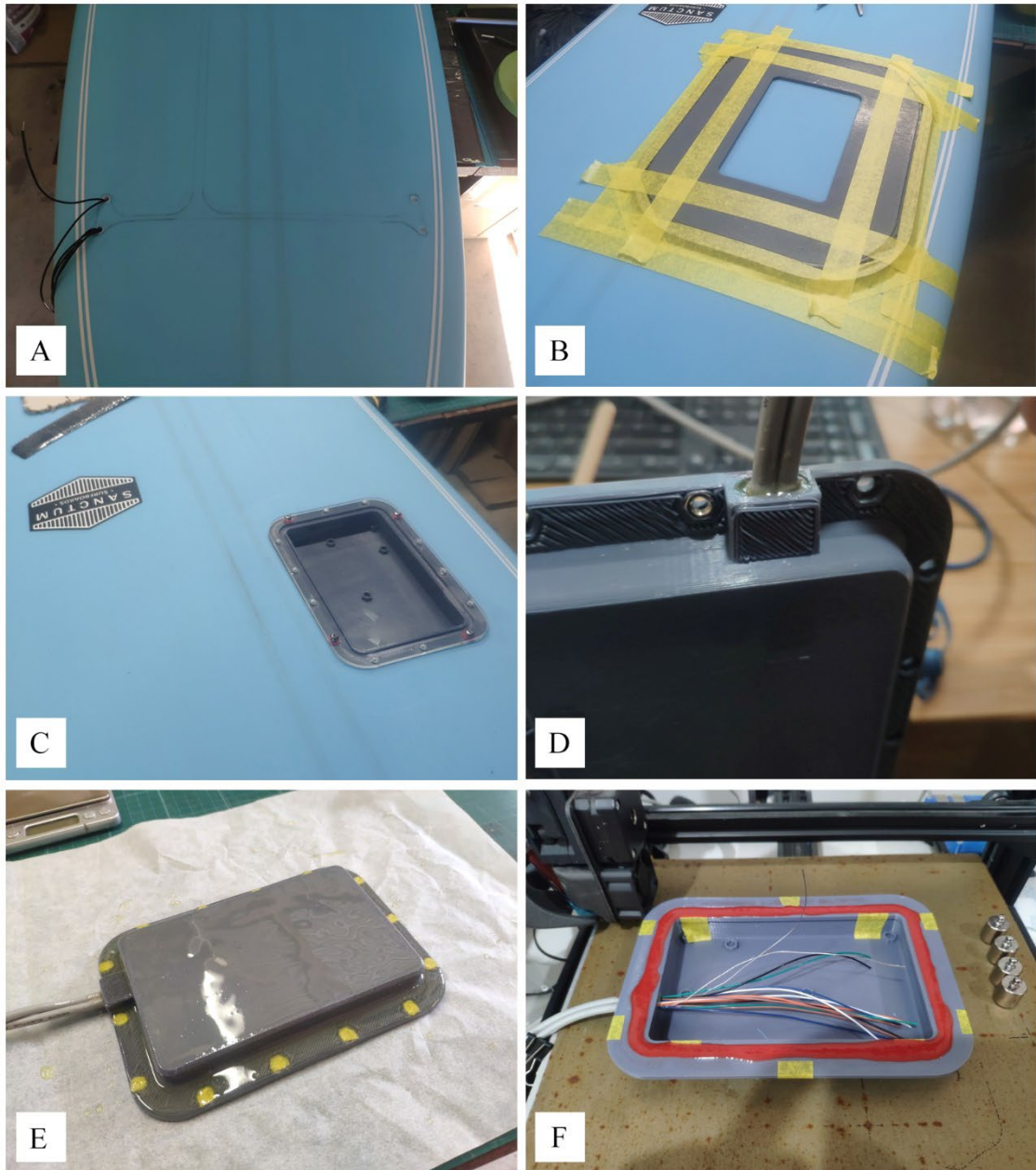


Figure 4.9: Pictures of subsequent stages of an instrumented surfboard prototype development. Letters A-F indicate: sketching of cut-outs (A), installing templates and cutting the surfboard (B), electronic box fitting (C), sealing cables hole with resin (D), coating box with a layer of epoxy resin (E), creating gasket (F), respectively.

The next step was to produce a cover from a 6 mm thick clear acrylic sheet with the use of a drill press, disk sander, and a jigsaw. Then the assembled electronic box was tested for leaking. The first try started by adding dyed water to the electronic box, and then the acrylic lid was mounted using fourteen M4 screws (Figure 4.10A). Then the assembly was moved around to check if water is escaping. The second test was characterised by placing the assembly 300 ± 1 mm submerged in water for up to 3 h (Figure 4.10B). Both tests resulted in no leaking, and the electronic box could be mounted into the prototype. Subsequently, instrumented fins wires were soldered and secured to electronic box cables (Figure 4.10C). Fibreglass cloth was used under the electronic box in order to create a stronger mechanical structure (Figure 4.10D). The casing was installed in the surfboard prototype with the use of epoxy resin (Figure 4.10E) and then weights were used to compress the electronic box, surfboard, and fibreglass cloth together (Figure 4.10F).

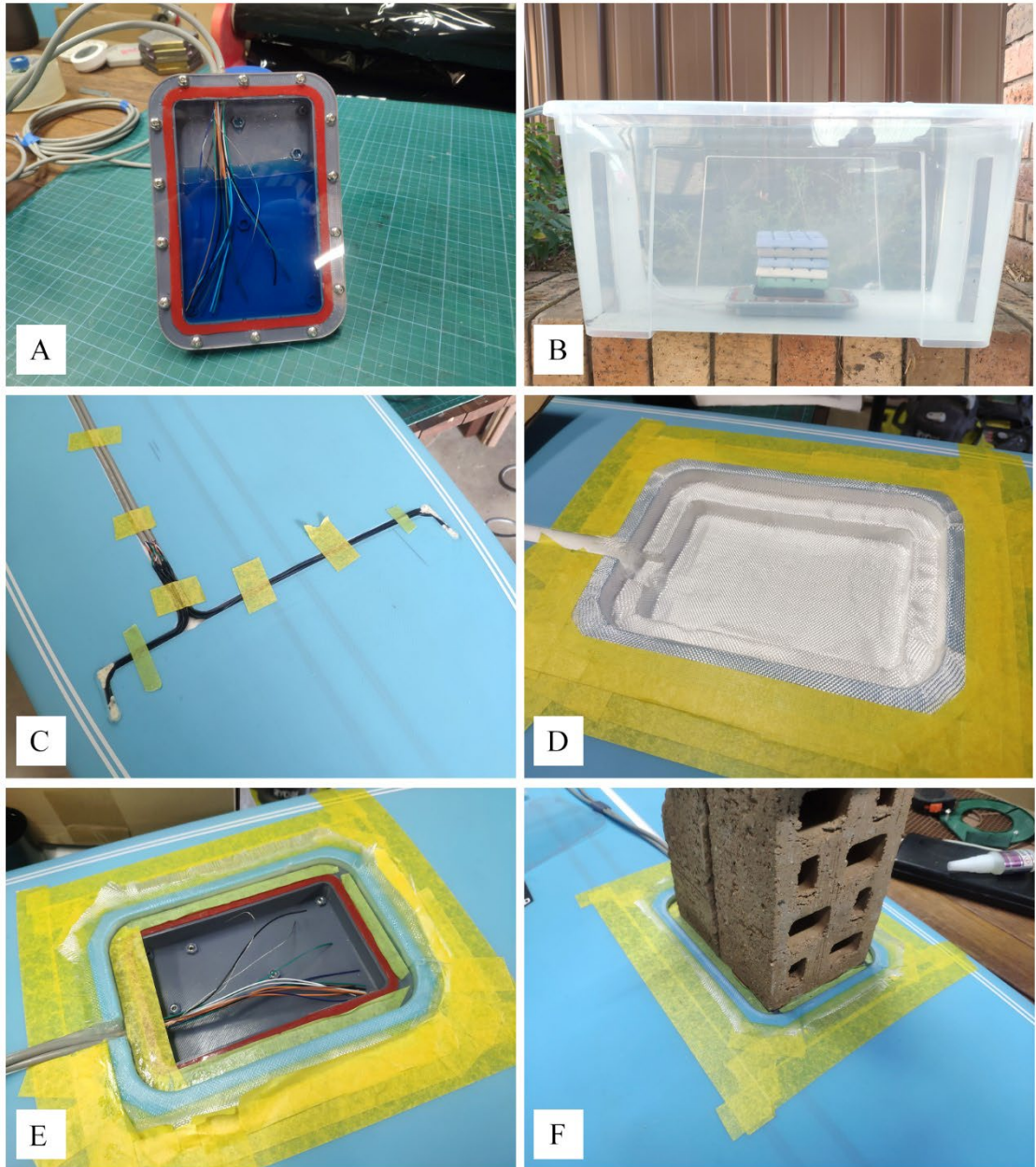


Figure 4.10: Pictures of subsequent stages of an instrumented surfboard prototype development. Letters A-F indicate: leak testing (A, B), soldering cables (C), installing a layer of fibreglass (D), electronic box glueing (E), compressing electronic box and fibreglass (F), respectively.

Figure 4.11. presents final stages of prototype assembly. The electronic components were connected to instrumented fins in order to test the connection before securing cables inside the surfboard prototype (Figure 4.11A). Then the telemetry visualisation software (discussed in detail in section 4.4) was utilised to test sensors mounted inside the fins (Figure 4.11B). Performed tests resulted in stable connection, and response from instrumented fins was observed. Therefore a decision was made to use fibre tapes to enclose cables and reinforce the electronic box section. For strengthening casing area 25 ± 0.1 mm width plain weave fibreglass tape was used, and 10 ± 1 mm overlap was introduced between cloth used under the electronic box and the fibre tape (Figure 4.11C). Cut-outs for cables were 12 ± 0.1 mm width around electronic box and 6 ± 0.1 mm width for instrumented fins wires respectively. For those two sections, 38 ± 0.1 mm width plain weave fibreglass with 20 ± 0.1 mm width unidirectional carbon fibre inlay tape was used (Figure 4.11D). Subsequently, tapes were glued with epoxy resin (Figure 4.11EF). The second layer of dyed epoxy resin was introduced after around 3 h of the curing process of the first layer of resin. Used epoxy resin was characterised by 4 days curing process in order to achieve optimal working strength. The final steps required hand sanding of a prototype which resulted in safe to use smooth surface finish. Figure 4.12A depicts the top side of the completed surfboard prototype. Figure 4.12B presents the bottom section of a finished instrumented surfboard.



Figure 4.11: Pictures of subsequent stages of an instrumented surfboard prototype development. Letters A-F indicate: connecting electronics (A), testing telemetry system (B), custom fit of fibreglass and carbon fibre tapes (C, D), glueing fibre tapes with epoxy resin (E, F), respectively.



Figure 4.12: Photography of a surfboard, and instrumented fins prototypes with inbuilt data telemetry unit. A) top view. B) bottom view.

Figure 4.13A presents the electronic components installed inside the surfboard prototype. The whole electronics assembly containing of electronic components, casing, acrylic lid, cables, fibre cloth, epoxy resin weights 572 ± 1 g. Complete surfboard with instrumented fins and electronics weight 5694 ± 1 g. Therefore electronics system makes up around 10 % of the total weight of the prototype.

Figure 4.13B depicts the telemetry system's PC/laptop module. See chapter 2 for design details, and used electronic components. The development process started from 3D printing of four parts with the use of black and transparent blue PLA filaments. Then the electronic components were mounted inside the casing using seven M3 screws. The laptop mount and cover were assembled using six M3 screws. The device prepared this way was used to wirelessly communicate with the surfboard and collect data from sensors in real-time. Subsequently, data was presented in form of graphs. More details about the telemetry system are presented in section 4.4. The transceiver box with electronics weight 101 ± 0.1 g.

Figure 4.13C depicts photography of a set of instrumented fins installed in a surfboard prototype. In order to recognise tested fins in future work, they were given reference names "Jimi" and "Hendrix". Detailed information was engraved on a layer of bamboo PLA filament 3D printed inside the fins.

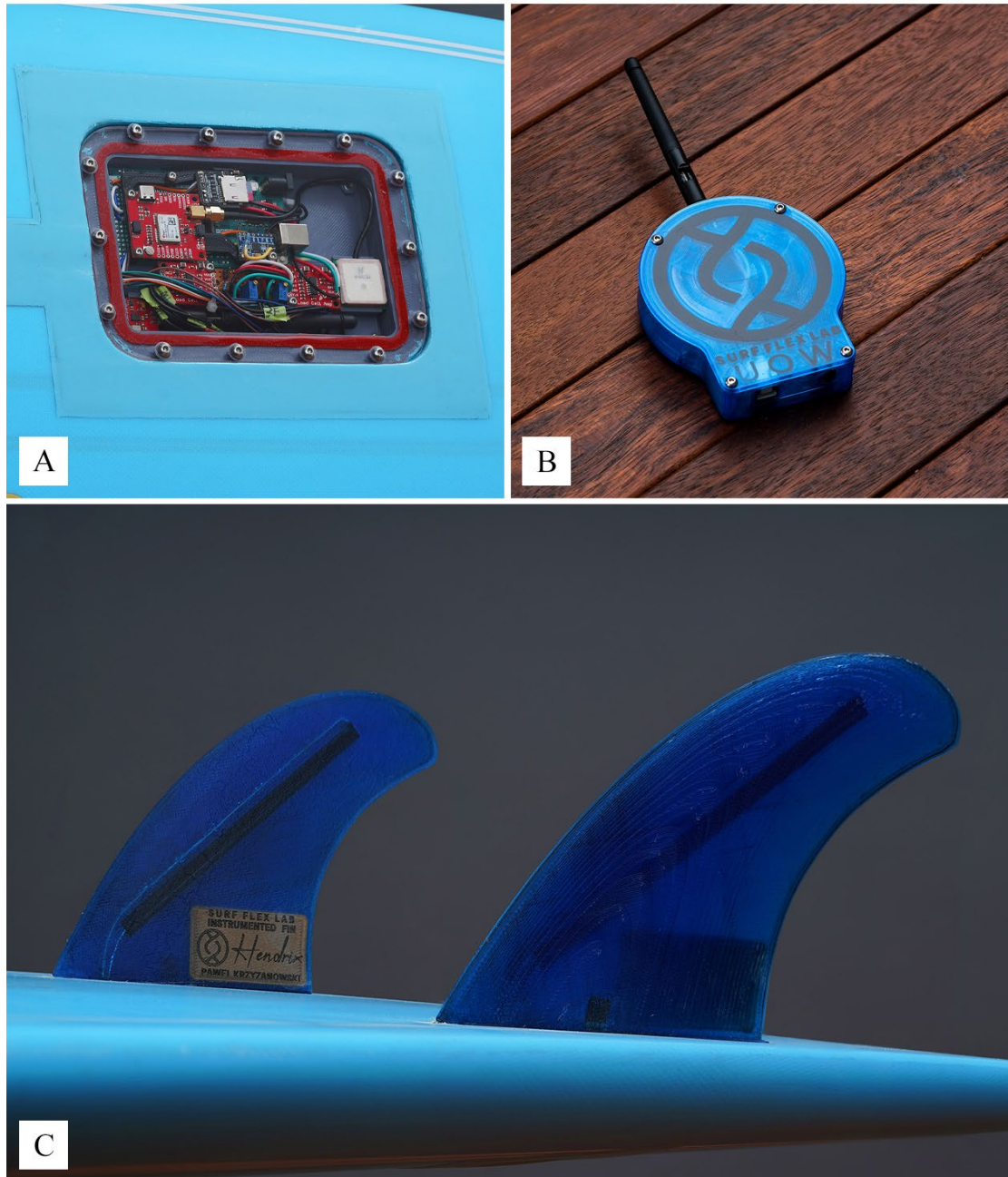


Figure 4.13: A) instrumented surfboard prototype electronics. B) photography of an assembled 3D printed transceiver. C) instrumented surfboard with a mounted set of “Jimi” and “Hendrix” instrumented fins.

4.6. Data telemetry visualisation

PC/Laptop data collection unit was based on an Arduino development board with an 8-bit microcontroller. Communication with the surfboard was performed with the set of two nRF24L01+ transceivers. The collection unit was connected to a PC/laptop via a USB port. Serial communication was utilised to transfer data to Telemetry Viewer software. Figure 4.14A depicts a data collection unit mounted on a laptop.

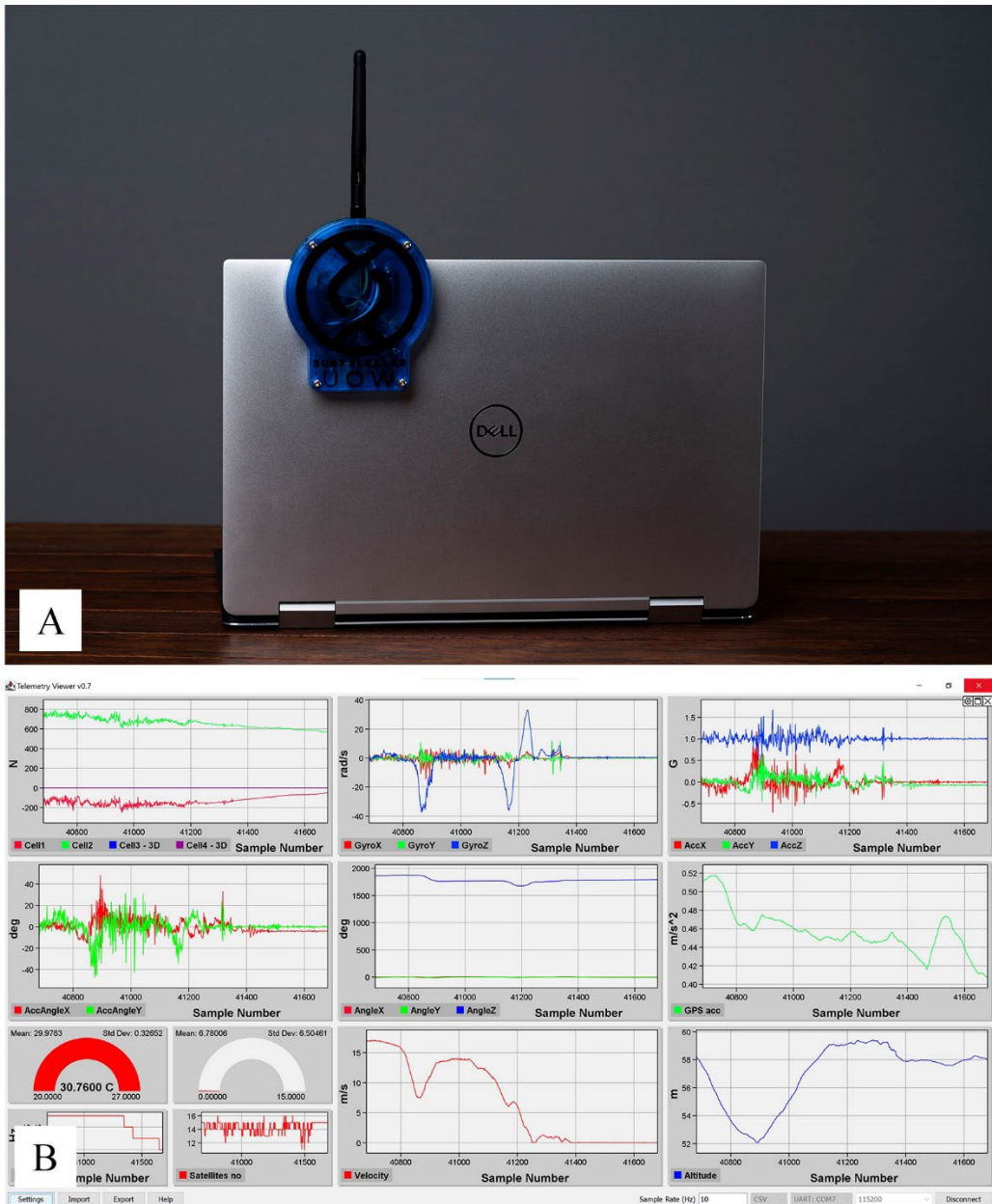


Figure 4.14: A) photography of a transceiver unit mounted on a data collection computer. B) typical data visualisation created in Telemetry Viewer software.

Data was collected from six sensors and presented in telemetry software. NEO-M9N GPS module was used to determine system's velocity (m/s), acceleration (m/s^2), latitude, longitude and altitude (m). MPU-6050 gyro/accelerometer module was utilised in order to collect X-axis, Y-axis, and Z-axis rotation accelerations (rad/s) and angles (deg), G force (g), X-axis, and Y-axis accelerations angles (deg) and temperature ($^{\circ}\text{C}$). Four HX711 load cell amplifiers were used to register Wheatstone bridges loads (N). 3D printed flex sensors were connected to a custom made full Wheatstone bridge setup consisting of three resistors and a flex sensor. Figure 4.14B presents a screenshot from a typical data collection session. The modularity of the system allows to choose sensors to read from, therefore sampling rate can be adjusted. Experiments showed that when all sensors are transmitting data, the sampling rate is around 13 Hz. This result proved to be satisfactory for the first prototype. The test of an average communication range was performed and characterised by moving ten times away from the surfboard in an open space (without any obstacles) until the transceiver connected to the laptop stop transmitting data. Then collected GPS data was used to determine the range at around 100 ± 2 m.

4.7. Preliminary results of an instrumented surfboard.

Preliminary data from the instrumented surfboard and fins were collected from field testing. The first field test involved driving with a car that had the instrumented surfboard mounted onto it. Data was then collected at various speeds (8 – 16 m/s) controlled using the car's cruise control system. The second field test involved paddling and walking the instrumented surfboard in a waveless part of the ocean (Gunnamatta Bay, NSW, Australia). In both trials, data was saved on the μSD card, while it was simultaneously transferred in real-time between the surfboard's electronics and the transceiver connected to the laptop. The resulting data was then compared to data

obtained from GoPro Hero 10 (action camera) and Poco F3 (Android operated cell phone).

4.7.1. GPS data

Data comparison started from visual observation of collected GPS information (Figure 4.15). The GPS paths overlays (solid red, yellow, and green lines indicate GoPro, Poco F3, and surfboard telemetry in Figure 4.15.BC, respectively.) indicate excellent accuracy of the surfboard's telemetry system. It seems that an action camera and a cell phone registered a drift when the first junction was approached (Figure 4.15B).

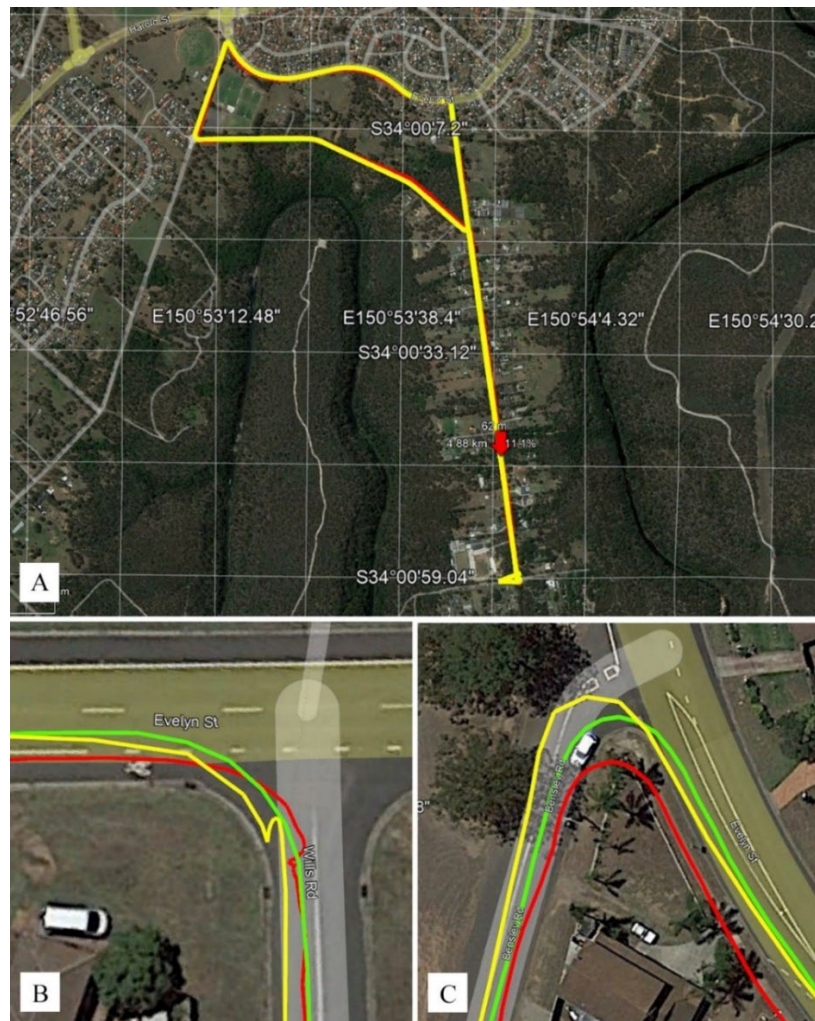


Figure 4.15: A) Path of the first GPS test. B) junction 1. C) junction 2. Red, yellow, and green solid lines indicate paths obtained using GoPro, Poco F3, and surfboard telemetry, respectively.

Data from the second junction (Figure 4.15C) indicate that the GoPro's GPS recorded (red line in Figure 4.15C) shortcutting of the corner, whilst Poco's GPS indicated overshooting of the corner. Only the telemetry unit (green line in Figure 4.15C) showed an accurate path of the car. The velocity (based on GPS data) was the second registered data set from devices. The results indicate the fastest response of the telemetry unit (brown line in Figure 4.16). GoPro's data (blue line in Figure 4.16) presents the biggest amplitudes of speed. It is suggested that it was not an accurate representation of the experiment (hence to cruise control). Poco F3 registered fairly similar data to the telemetry unit however, the noticeable difference was a response delay of the cell phone.

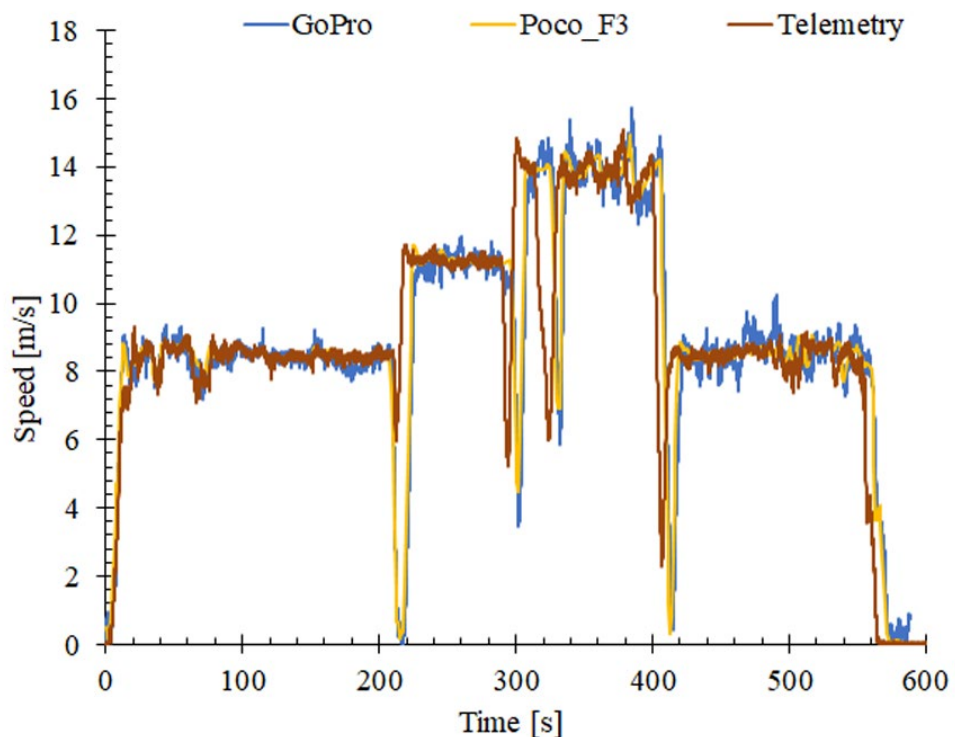


Figure 4.16: Speed vs time response of benchmarked devices. GoPro, Poco F3, and Telemetry indicate GoPro Hero 10 action camera, Poco F3 cell phone, and the telemetry unit built into the surfboard, respectively.

The second try was performed in the ocean. The GPS paths overlays (solid red, yellow, and green lines indicate GoPro, Poco F3, and surfboard telemetry in Figure 4.17 respectively.) indicate similar inaccurate behaviour of the action camera and the cell phone.

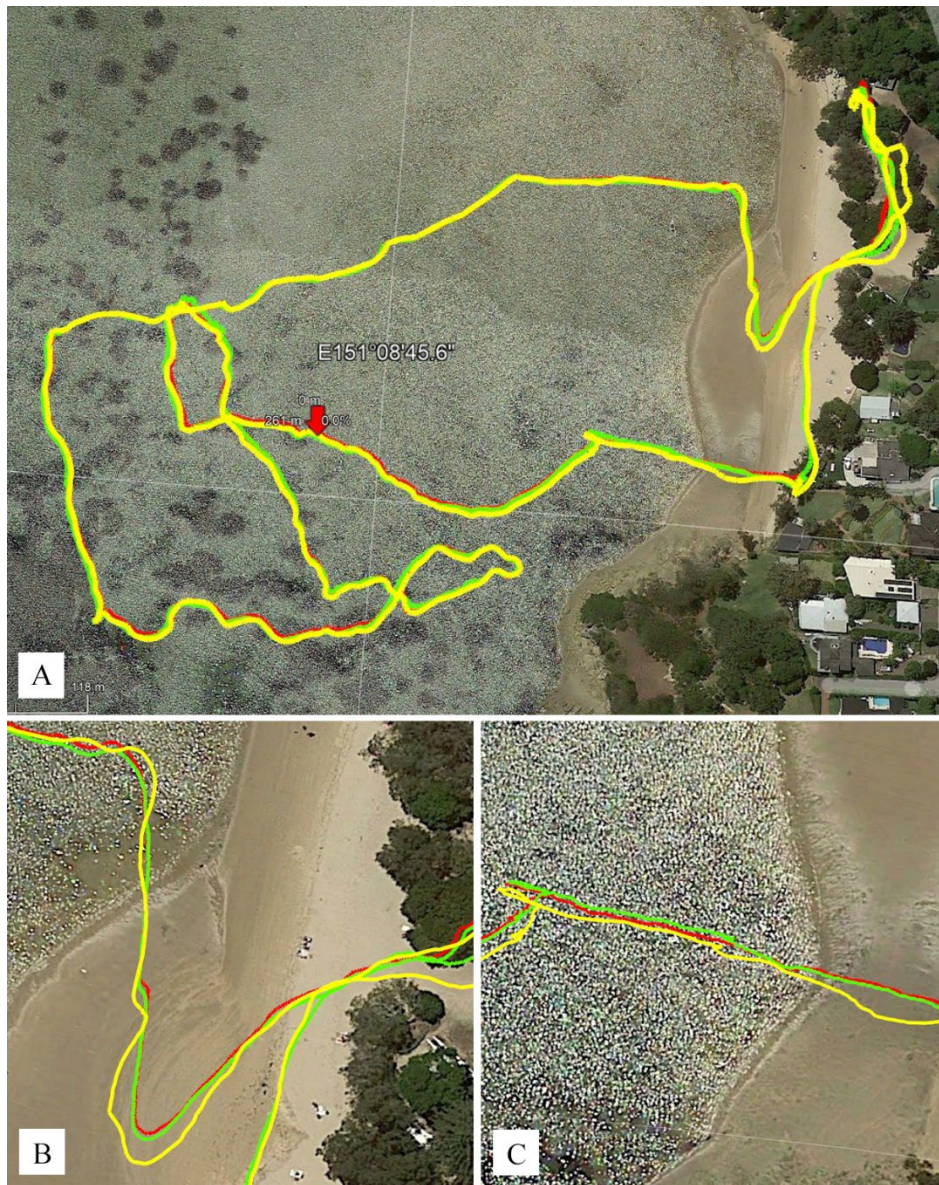


Figure 4.17: A) GPS path of the ocean test. B) event 1. C) event 2. Red, yellow, and green solid lines indicate paths obtained using GoPro, Poco F3, and surfboard telemetry, respectively.

The visual path observation (Figure 4.17BC) suggest that the telemetry system built into the surfboard was the most accurate representation of the experiment.

Accordingly, to the collected GPS data, the measured travelled distance was 1480 m, 1530 m, and 1480 m for GoPro, Poco F3, and the telemetry unit, respectively. The speed data obtained during the second test exhibit similarities to the first test. GoPro (red line in Figure 4.18) was characterised by the highest amplitudes of gained speed whilst Poco (yellow line in Figure 4.18) and the telemetry unit (green line in Figure 4.18) registered similar data.

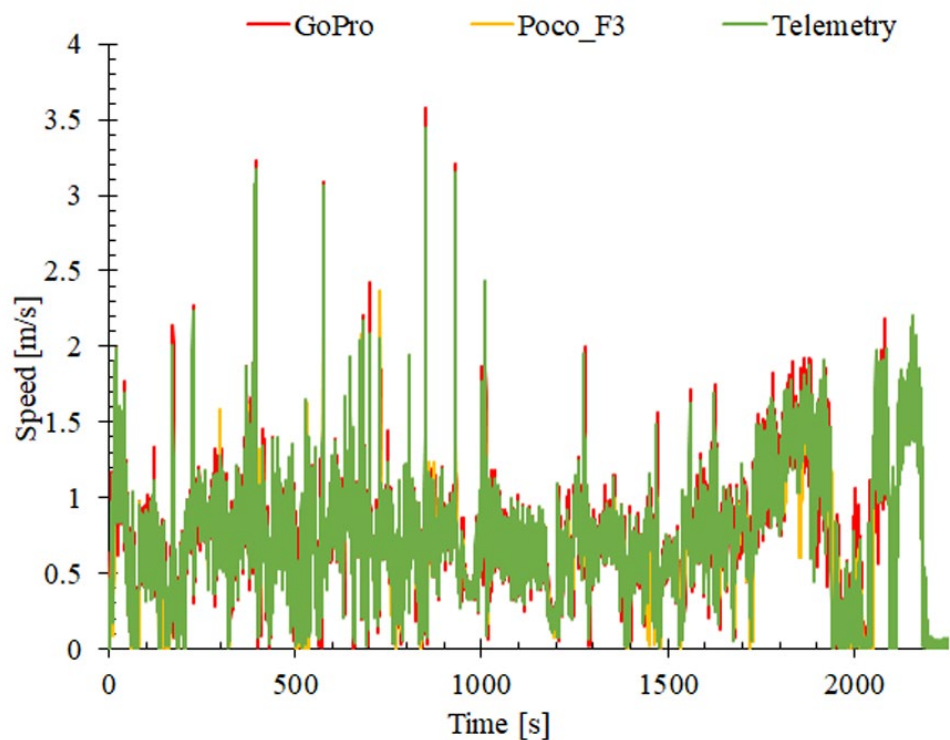


Figure 4.18: Speed vs time response of benchmarked devices. GoPro, Poco F3, and Telemetry indicate GoPro Hero 10 action camera, Poco F3 cell phone, and the telemetry unit built into the surfboard, respectively.

4.7.2. Accelerometer and gyroscope data

Accelerometer and gyroscope data were collected during two trials. Figure 4.19 presents a typical response of the sensor in the Z-axis (Figure 4.19AB), Y-axis (Figure 4.19CD), and X-axis (Figure 4.19EF) collected during the first test. Similarly to GPS data, GoPro recorded the highest amplitudes. During two trials, Poco F3 failed to record data after around 240 s. It seems that the data buffer in the cell phone has a limit.

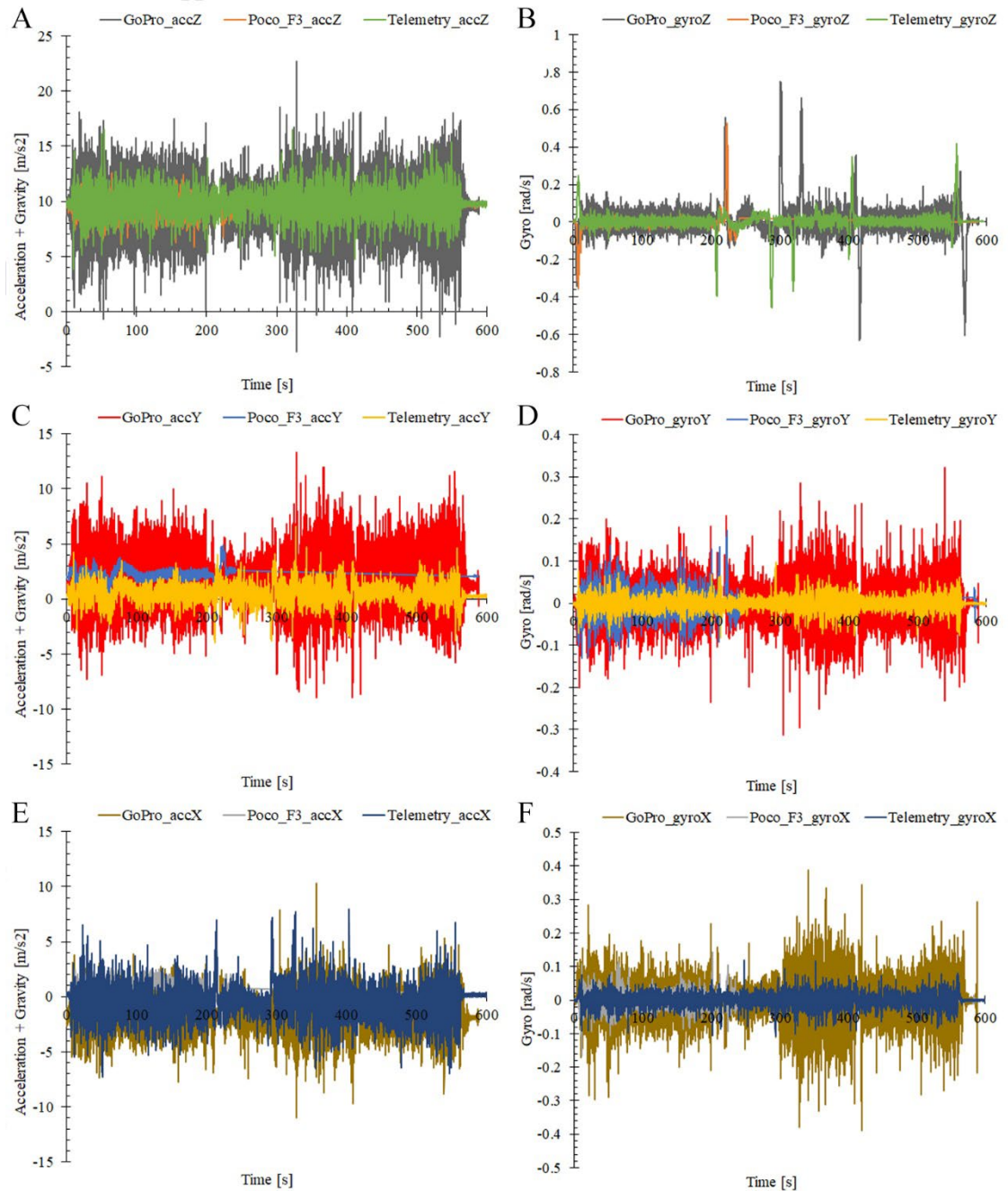


Figure 4.19: A typical response of an accelerometer and a gyroscope sensors. A) acceleration + gravity vs time response in Z-axis. B) gyro vs time response in Z-axis. C) acceleration + gravity vs time response in Y-axis. D) gyro vs time response in Y-axis. E) acceleration + gravity vs time response in X-axis. F) gyro vs time response in X-axis. GoPro_accZ, GoPro_accY, GoPro_accX, GoPro_gyroZ, GoPro_gyroY, GoPro_gyroX, indicate GoPro Hero 10 action camera. Poco_F3_accZ, Poco_F3_accY, Poco_F3_accX, Poco_F3_gyroZ, Poco_F3_gyroY, Poco_F3_gyroX, indicate Poco F3 cell phone. Telemetry_accZ, Telemetry_accY, Telemetry_accX, Telemetry_gyroZ, Telemetry_gyroY, Telemetry_gyroX, indicate telemetry unit inbuilt into surfboard.

4.7.3. Instrumented fins

During the first trial, instrumented fins worked in the air environment, and it turned out that it was not sufficient to deflect fins, therefore no data was recorded. Instrumented fins registered reactions during the second test (Figure 4.20). The response of commercially obtained Wheatstone bridges (Sensor 1 and Sensor 3 in Figure 4.20) was observed as fins were moving in the ocean. The raw data demonstrated noise which could be addressed in future work. Fins were not deflected enough to observe 3D printed sensors responses. Used fins require further calibration to accurately measure the loads. Nonetheless, the experiment turned out to be a success

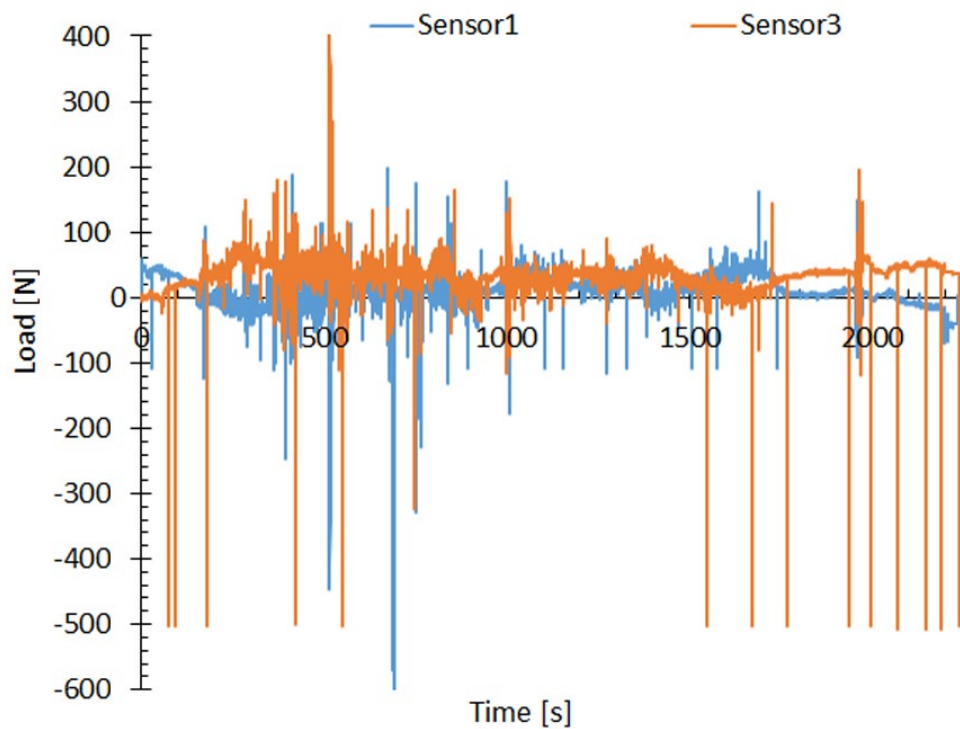


Figure 4.20: Load vs time response of instrumented fins sensors. Sensor 1, and Sensor 3 indicate commercial Wheatstone bridge in the first fin, and commercial Wheatstone bridge in the second, respectively.

4.7.4. Temperature

The temperature was measured using GoPro Hero 10 camera (blue line in Figure 4.21) and the telemetry system (orange line in Figure 4.21). In both tests, GoPro was operating at a significantly higher temperature due to video recording of the experiment. During the first test, the car was moving between 8 – 16 m/s and it caused cooling of both devices. In the second try, the telemetry system temperature was around 50 °C whilst GoPro overheated after 2092 s of recording at around 70 °C and switched off.

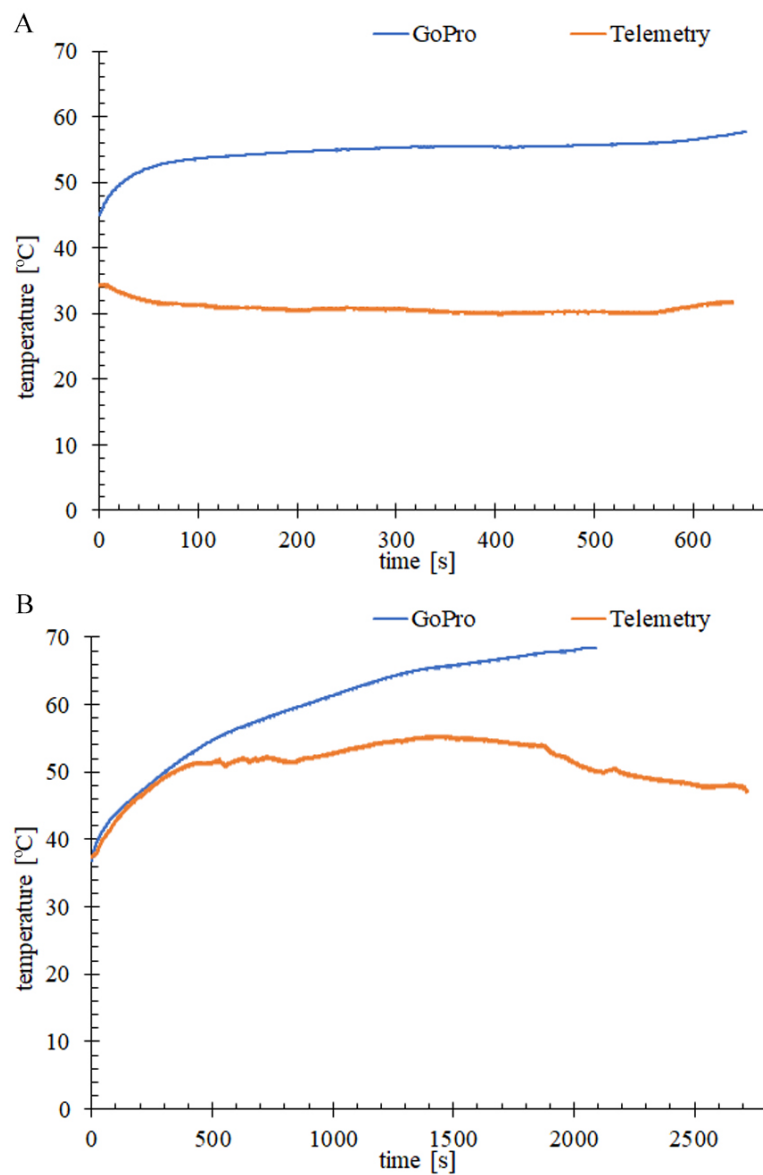


Figure 4.21: Temperature vs time response of benchmarked devices. A) the first test. B) the second test. GoPro and Telemetry indicate GoPro action camera, and telemetry unit built into the surfboard, respectively.

Chapter 5: Conclusions

Surfing is a highly competitive sport, where FDM additive manufacturing technology can be applied for product research and development. Until recent years, progress was based on the experience of shapers coupled with feedback from surfers or CFD studies of CAD designs. This project establishes the use of electronic components, in combination with 3D printing technology as a quantitative tool in the development process of surfboards and fins. The Covid-19 pandemic had a great impact on the timetable and the outcome of the project. During lockdowns periods the laboratory was closed. Tools were designed and developed to overcome challenges and to continue the work from home.

The main focus of this study was to design, develop, and test 3D printed surfboard fins with incorporated sensors integrated into an instrumented surfboard.

As part of Aim 1 (customisation of a 3D printer in order to 3D print with carbon fibre composites), a 3D printer was successfully customised. To enable the 3D printing of carbon fibre composites, it was demonstrated that this required changes to the nozzle, extruder, motherboard, stepper drivers, heat bed surface. Moreover, in order to be able to produce parts from hygroscopic materials such as PA12-CF or PA6-CF, a dry box was developed. The results showed that 3D printer modifications allowed the use of abrasive, and hygroscopic filaments. This resulted in an improved quality, and speed of the additive manufacturing process.

Aim 2 (3D printing of model samples and instrumented fins) was achieved on the customised 3D printer. 101 rectangular samples and six instrumented fins were 3D printed. The surfboard fin used in this study was CAD designed and it was based on commercially available Futures T1 Twin HC (Futures Fins) design. Two sensors were incorporated into the fin design. The first was 3D printed trapezoidal prism with

conductive PLA, and TPU filaments. The second was a commercially obtained full 350 Ω Wheatstone bridge. In order to install sensors in the surfboard fin, the printing process was divided into a two-step. The first step was to 3D print the base of the fin and subsequently print the flex sensor with the use of conductive filaments. The second step was to pause the 3D printing process for Wheatstone bridge incorporation. It was glued with epoxy glue and the fin printing process was finished.

As part of Aim 3 (design, and manufacturing of moulds and tools used for mechanical analysis and data collection unit) so-called pandemic tool, Shimadzu EZ-S mechanical analyser adapter, touch probe, fin mould, mould for rectangular samples produced from HDPE material, and router templates were successfully developed. The so-called pandemic tool was designed in CAD software, 3D printed and assembled. The device proved to be satisfactory for testing rectangular samples. Subsequent tests in the laboratory showed inaccuracy and flaws in the design. It was determined that the accuracy of around 20 % in the range from 0 to 5 GPa of calculated flexural modulus was excellent compared to the universal mechanical analyser laboratory tool. The pandemic tool gave a possibility to distinguish materials with higher flexural modulus. The developed solution could be used in the future in schools as it makes flexural testing accurate to anyone with a 3D printer.

Aim 4 (mechanical analysis of model samples and fins) was achieved using the pandemic tool during the Covid-19 pandemic related lockdowns, and the Shimadzu EZ-S equipped with a 500 N load cell between lockdowns. In total, 130 materials combinations were tested. It was shown that carbon fibre reinforced Nylon 6 (CF-PA6) with prepreg composite exhibited the highest flexural modulus value (12 ± 1 GPa). It was more than double the value observed for samples of the same material (CF-PA6) without prepreg (5.9 ± 0.6 GPa). Moreover, heat treatment of rectangular samples

improved the mechanical parameters of tested materials. For example, the flexural modulus of carbon fibre reinforced Nylon 12 (CF-PA12) exposed to 240 °C increased from 2.5 ± 0.3 GPa to 5.2 ± 0.5 GPa.

The last Aim (laboratory and field-testing of instrumented fins) was successfully addressed by laboratory testing of an instrumented surfboard and fins on Shimadzu EZ-S universal mechanical analyser and two trials in the field. In the laboratory tests, the fin was mounted in a surfboard which was installed in the bench vice. Sensors were connected to a digital multimeter. The fin flex was determined at 7.7 ± 0.1 %. It was demonstrated that the linear behaviour of the Wheatstone bridge sensor installed into the fin made it suitable to measure fin flex during surfing. The response of the 3D printed sensor was linear only over a part of the applied stroke.

One of the main outcomes of this project was the successful development and field-testing of a working prototype of a surfboard with inbuilt electronics and a set of instrumented fins. It was based on the Sanctum Mini Mal 7' 4" (Sanctum Surfboards) surfboard. The electronic box, mount, and laptop module were designed in CAD software and 3D printed with the use of PLA filament. The casing was successfully tested for leaks before installing it into the surfboard. Wireless communication between laptop and surfboard was successfully established with the set of two transceivers. Subsequently, field-testing was achieved in two trials. The first field test involved driving with a car that had the instrumented surfboard and fins mounted onto it. The second field test involved paddling and walking the instrumented surfboard and fins in a waveless part of the ocean (Gunnamatta Bay, NSW, Australia). Data from sensors installed in the surfboard and fins was saved on the μ SD card, while it was simultaneously transferred in real-time between the surfboard's electronics and the transceiver connected to the laptop. The resulting data was then compared to data

obtained from GoPro Hero 10 (action camera) and Poco F3 (Android operated cell phone). The preliminary data results indicate the excellent GPS and velocity accuracy of the telemetry unit in comparison to GoPro and Poco F3. The response of Wheatstone bridges mounted into instrumented fins was observed during the ocean test. 3D printed flex sensors did not register response as fins were not deflected enough. In both tests, the telemetry unit worked with a stable temperature.

The real-time telemetry data collection method has the potential to be used as a research and development tool in the surfing industry or as a way to help objectively judge surfers during competition. The sport of surfing made its debut at the Olympic Games in Tokyo 2020 and judging was based on five criteria such as commitment and degree of difficulty, innovative and progressive manoeuvres, variety of manoeuvres, the combination of major manoeuvres, and speed, power, and flow. The last criteria could be accurately measured with the presented telemetry system. It could potentially impact and raise the quality of the judging system. Additionally, data could be transferred in real-time to the spectators watching the competition raising the entertainment value of the spectacle. The presented project is the groundwork for this direction.

5.1. Future Work

Coming work should focus on the calibration of the surfboard prototype's sensors (3D printed and Wheatstone bridges) in the laboratory and further field tests. Subsequently, instrumented fins could be developed with the use of the prepreg lay-up process, and 3D printed PA6-CF cores and sensors. Gathered data could be used for analysis and improvement of the future solution.

This research established the way of the use of electronics in combination with 3D printing in the surfing industry. Future research could help to develop and rapid

prototype more solutions in order to be capable of measuring desired mechanical parameters in surfboards and fins.

The presented in this thesis research could help in the development of wearable electronics and mechatronics surfboards with moveable and reactive parts. Future research could utilise magnetorheological fluids to control the flexibility of the surfboards and fins.

List of references

- [1] S. Falk, S. Kniesburges, R. Janka, R. Grosso, S. Becker, M. Semmler, M. Döllinger, Computational hydrodynamics of a typical 3-fin surfboard setup. *Journal of Fluids and Structures* 90 297–314 (2019).
- [2] R. Buckley, Surf tourism and sustainable development in indo-pacific Islands. 1. the industry and the Islands. *Journal of Sustainable Tourism* 10 (5), 405–424 (2002).
- [3] S. Mc Cagh, *The Surfboard Book: How Design Drives Performance*. McCagh O’Neill Pty Ltd. (2013).
- [4] Developing R&D tools for the surfing industry. URL <https://www.linkedin.com/pulse/developing-rd-tools-surfing-industry-marc-in-het-panhuis/> (accessed May 11, 2021)
- [5] Composite materials industry overview. URL <http://compositeslab.com/composites-101/composites-industry-overview/> (accessed Apr. 21, 2021)
- [6] H. Dirk, J.A. Lukaszewicz, C Ward, K. D. Potter, The engineering aspects of automated prepreg layup: History, present and future. *Composites Part B: Engineering* Volume 43, Issue 3, 997-1009 (2012).
- [7] Lack of wind curtails racing in America’s Cup prelude. URL <https://apnews.com/article/mlb-sailing-auckland-sports-asia-new-zealand-edb3704cefe5d9dc43cd19e39eb0268a> (accessed Apr. 26, 2021)

- [8] L. W. McKeen. The Effect of Radiation on Properties of Polymers. *Plastics Design Library*, 393-408 (2020)
- [9] How to Make Prepreg Carbon Fibre Moulds Using Tooling Prepreg. URL <https://www.easycomposites.co.uk/learning/how-to-make-prepreg-carbon-fibre-moulds>
(accessed Apr. 28, 2021)
- [10] Wikipedia.com, Computer aided design
URL https://en.wikipedia.org/wiki/Computer-aided_design
(accessed Oct. 10, 2021)
- [11] A. Probst, M. Ebner, M. Schön, D. Gerhard, PDM Field Study in Collaborative Engineering Education – Results from 2016/17. *International Journal of Online and Biomedical Engineering (iJOE)* 15(04):127 (2019).
- [12] Wikipedia.com, Computer-aided manufacturing
URL https://en.wikipedia.org/wiki/Computer-aided_manufacturing
(accessed Oct. 10, 2021)
- [13] EUKLID
URL <https://www.euklid-cadcam.com/en/software-en/euklid-cadcam/cam/simulation/cutting-simulation.html>
(accessed Oct. 12, 2021)
- [14] S.S. Knudsen, Sail Shape Optimization with CFD. Technical University of Denmark, Master Thesis (2013).
- [15] R. Azcueta, N. Rousselon, CFD Applied to super and mega yacht design, in design. In: *Construction and Operation of Super and Mega Yachts Conference* (2009).

- [16] H.J. Mørch, M. Perić, J. Röper, E. Schreck, CFD-Supported Design of Lifeboats. Wiesbaden (2009).
- [17] D. Shormann, L. Oggiano, M. in het Panhuis. Numerical CFD Investigation of Shortboard Surfing: Fin Design vs. Cutback Turn Performance. Presented at the 13th conference of the International Sports Engineering Association, Online, 22–26 June 2020.
- [18] P.A. Brandner, G.J. Walker, Hydrodynamic performance of a surfboard fin. In: 15th Australasian Fluid Mechanics Conference (2004).
- [19] D. Shormann, M. in het Panhuis, L. Oggiano. Field Research and Numerical CFD Analysis of Humpback Whale-Inspired Shortboard Fins. Presented at the 13th conference of the International Sports Engineering Association, Online, 22–26 June 2020.
- [20] D. Shormann, L. Oggiano, M. in het Panhuis. Numerical CFD Investigation of Shortboard Surfing: Fin Design vs. Cutback Turn Performance. Presented at the 13th conference of the International Sports Engineering Association, Online, 22–26 June 2020.
- [21] N. Lavery, G. Foster, D. Carswell, S. Brown, CFD Modelling of the effect of fillets on fin drag. Reef Journal 1 (1), 93–111 (2009).
- [22] P. Gudimetla, N. Kelson, B. El-Atm, Analysis of the hydrodynamic performance of three- and four-fin surfboards using computational fluid dynamics. Australian Journal of Mechanical Engineering 7, 61–67 (2009).
- [23] K. Sakellariou, Z.A. Rana, K.W. Jenkins, Optimisation of the surfboard fin shape using computational fluid dynamics and genetic algorithms. Journal of Sports Engineering and Technology 231 (4), 344–354 (2017).

- [24] M.S. Macneill, Bio-Inspired Optimal Fin Shape and Angle for Maximum Surfboard Stability. Michigan Technological University (2015).
- [25] L. Oggiano, Numerical comparison between a modern surfboard and an alaiia board using computational fluid dynamics (CFD). In: Proceedings of the 5th International Congress on Sport Sciences Research and Technology Support. pp. 75–82 (2017).
- [26] L. Oggiano, F. Pierella, CFD For surfboards: Comparison between three different designs in static and manoeuvring conditions. Proceedings 2 (6), 309 (2018).
- [27] N.D. Barnett, E.G. Miravete, A study of planing hydrodynamics. In: Proceedings of the COMSOL Conference 2009 Boston (2009).
- [28] T. J. Horn, O. L. A. Harrysson, Overview of current additive manufacturing technologies and selected applications. Science Progress 95(3), 255-282 (2012).
- [29] R. Gately, S. Beirne, G. Latimer, M. Shirlaw, B. Kosasih, A. Warren, J. R. Steele, M. in het Panhuis. Additive Manufacturing, Modeling and Performance Evaluation of 3D Printed Fins for Surfboards. MRS Advances 2 913-920 (2017).
- [30] Wikipedia.com, fused filament fabrication
URL https://en.wikipedia.org/wiki/Fused_filament_fabrication
(accessed Apr. 23, 2021)
- [31] M.Heidari-Rarani, M.Rafiee-Afarani, A.M.Zahedi, Mechanical characterization of FDM 3D printing of continuous carbon fiber reinforced PLA composites. Composites Part B: Engineering, Volume 175 (2019)
- [32] S.W. Kwok, K. H.H. Goh, Z.D. Tan, S.T.M. Tan, W.W. Tiju, J.Y. Soh, Z.J.G. Ng, Z. Chan, H.K. Hui, Electrically conductive filament for 3D-printed circuits and sensors. Applied Materials Today 9 167–175 (2017).

- [33] Y. Moua, Y. Zhang, H. Cheng, Y. Peng, M. Chen, Fabrication of highly conductive and flexible printed electronics by low temperature sintering reactive silver ink. *Applied Surface Science* 459 249–256 (2018).
- [34] Nanowerk Spotlight 3D-printed, fully integrated wireless sensor devices
URL <https://www.nanowerk.com/spotlight/spotid=46930.php>
(accessed Apr. 21, 2021)
- [35] Wikipedia.com, mikrokontroler
URL <https://pl.wikipedia.org/wiki/Mikrokontroler>
(accessed Oct. 12, 2021)
- [36] Wikipedia.com, ATmega328
URL <https://en.wikipedia.org/wiki/ATmega328>
(accessed Oct. 12, 2021)
- [37] Wikipedia.com, Load Cell
URL https://en.wikipedia.org/wiki/Load_cell
(accessed Oct. 12, 2021)
- [38] Michigan Scientific Corporation
URL <https://www.michsci.com/what-is-a-strain-gauge/>
(accessed Oct. 14, 2021)
- [39] Wikipedia.com, Wheatstone bridge
URL https://en.wikipedia.org/wiki/Load_cell#/media/File:Wheatstone_bridge.jpg
(accessed Oct. 14, 2021)
- [40] Sprakfun.com, gyroscope
URL <https://learn.sparkfun.com/tutorials/gyroscope/all>
(accessed Oct. 14, 2021)

- [41] ASD Reports, The Key Players in The Global MEMS Gyroscope Market 2015-2019
URL:<https://www.asdreports.com/news-6900/key-players-global-mems-gyroscope-market-20152019>
(accessed Oct. 14, 2021)
- [42] M. Tilli M. Paulasto-Krockel M. Petzold H. Theuss T. Motooka Ve.Lindroos, Handbook of Silicon Based MEMS Materials and Technologies (Third Edition), Elsevier (2020)
- [43] Sprakfun.com, accelerometer
URL <https://learn.sparkfun.com/tutorials/accelerometer-basics>
(accessed Oct. 14, 2021)
- [44] Politecnico di Milano, Department of Civil and Environment Engineering
URL <http://www.mems.polimi.it/accelerometers.html>
(accessed Oct. 17, 2021)
- [45] European Space Agency
URL https://gssc.esa.int/navipedia/index.php/GPS_User_Segment
(accessed Oct. 17, 2021)
- [46] U.S. government GPS information webpage
URL <https://www.gps.gov/systems/gps/>
(accessed Oct. 17, 2021)
- [47] Wikipedia.com, Transceiver
URL <https://en.wikipedia.org/wiki/Transceiver>
(accessed Oct. 17, 2021)
- [48] Sprakfun.com, nRF24L01+ transceiver webpage
URL <https://www.sparkfun.com/products/691>

(accessed Oct. 17, 2021)

- [49] Gizmodo.com, All the Sensors in Your Smartphone, and How They Work

URL <https://gizmodo.com/all-the-sensors-in-your-smartphone-and-how-they-work-1797121002>

(accessed Oct. 18, 2021)

- [50] Wikipedia.com, C++

URL <https://en.wikipedia.org/wiki/C%2B%2B>

(accessed Oct. 17, 2021)

- [51] R. Meyers, Encyclopedia of Physical Science and Technology (Third Edition).

Academic Press (2001).

- [52] S. Bhandari, R. A. Lopez-Anido, D. J. Gardner, Enhancing the interlayer tensile

strength of 3D printed short carbon fiber reinforced PETG and PLA composites via annealing. Additive Manufacturing Volume 30 (2019).

- [53] J. Nagler. Failure Mechanics of Multi Materials Laminated Systems Review

Analysis-Based Project.

- [54] W. Harizia, J. Anjoula, V.A. Acosta-Santamaría, Z. Aboura, V. Briand,

Mechanical behavior of carbon-reinforced thermoplastic sandwich composites with several core types during three-point bending tests. Composite Structures Volume 262 (2021).

- [55] What is Bend Testing?

URLd <https://www.instron.com/en/our-company/library/test-types/flexure-test>

(accessed Feb. 17, 2022)

- [56] Siemens_PLM_Software, STAR-CCM+ Documentation Version 11.06, 2016.

- [57] F.R. Menter, M. Kuntz, R. Langtry, Ten years of industrial experience with

the SST turbulence model. Heat Mass Transfer 4 (4), 625–632 (2003).

- [58] Ebay.com, dial indicator
URL <https://www.ebay.com.au/itm/203540863191>
(accessed Nov. 17, 2021)
- [59] Gearbest.com, Mijia temperature and humidity meter
URL <https://www.gearbest.com/community/SanfL4>
(accessed Nov. 17, 2021)
- [60] Xiaomitoday, Xiaomi Amazfit Pace A1612
URL <https://www.xiaomitoday.com/2018/10/29/amazfit-pace-a1612-smartwatch-review>
(accessed Nov. 17, 2021)
- [61] Banggood.com, 3018 CNC mill
URL <https://au.banggood.com/3018-3-Axis-Mini-DIY-CNC-Router-Standard-Spindle-Motor-Wood-Engraving-Machine-Milling-Engraver-p-1274569.html>
(accessed Nov. 17, 2021)
- [62] E3D, Nozzle X webpage
URL <https://e3d-online.com/products/v6-nozzles>
(accessed Nov. 17, 2021)
- [63] E3D, Hemera extruder webpage
URL <https://e3d-online.com/products/e3d-hemera-direct-kit-1-75mm>
(accessed Nov. 17, 2021)
- [64] Aliexpress FYSETC shop, spring steel sheet webpage
URL <https://www.aliexpress.com/item/4000080043625.html>
(accessed Nov. 19, 2021)
- [65] Aliexpress BIGTREETECH shop, SKR V1.4 turbo
URL <https://www.aliexpress.com/item/4000470048293.html>

(accessed Nov. 19, 2021)

[66] Aliexpress FYSETC shop, TMC-2130 StepStick

URL <https://www.aliexpress.com/item/1005003301971580.html>

(accessed Nov. 19, 2021)

[67] Bunnings, PVA glue

URL https://www.bunnings.com.au/tarzan-s-grip-250ml-pva-wood-glue_p1210338

(accessed Nov. 19, 2021)

[68] Arduino, Mega 2560

URL <https://docs.arduino.cc/hardware/mega-2560>

(accessed Nov. 19, 2021)

[69] Core-electronics, DFRobot μ SD card reader

URL <https://core-electronics.com.au/microsd-card-module-for-arduino.html>

(accessed Nov. 20, 2021)

[70] Sparkfun, NEO-M9N GPS

URL <https://www.sparkfun.com/products/17285>

(accessed Nov. 20, 2021)

[71] Core-electronics, DFRobot MPU6050

URL <https://core-electronics.com.au/6-dof-sensor-mpu6050.html>

(accessed Nov. 20, 2021)

[72] Sparkfun, HX711

URL <https://www.sparkfun.com/products/13879>

(accessed Nov. 20, 2021)

[73] Wheatstone bridge

URL <https://www.aliexpress.com/item/1005002819318020.html>

(accessed Nov. 20, 2021)

[74] Sparkfun, nRF24L01+

URL <https://www.sparkfun.com/products/705>

(accessed Nov. 21, 2021)

[75] Sparkfun, 2.4GHz Duck Antenna RP-SMA

URL <https://www.sparkfun.com/products/145>

(accessed Nov. 21, 2021)

[76] KEYSIGHT, 34410

URL <https://www.keysight.com/au/en/product/34410A/digital-multimeter-6-digit.html>

(accessed Nov. 21, 2021)

[77] Jaycar, Powertech MP-3087

URL <https://www.jaycar.com.au/0-to-32vdc-dual-output-dual-tracking-laboratory-power-supply/p/MP3087>

(accessed Nov. 20, 2021)

Appendices

Appendix 1

1. Code used for data logger collection system:

Receiver code:

```
#include <SPI.h>      // libraries used for receiver code
#include <RF24.h>
#include <RF24Network.h>
#define LED 5        // defining pin used for LED diode
#define LED2 6

RF24 radio(7, 8);    // nRF24L01(+) radio attached using Getting Started board

RF24Network network(radio); //
const uint16_t this_node = 00; // Address in Octal format of the used node
const uint16_t other_node = 01; // Address in Octal format of the other node

struct payload_t { // Structure of used payload
    unsigned long ms; // 4 bytes
    unsigned long counter; // 4 bytes
    float AccX; // 4 bytes
    float AccY; // 4 bytes
    float AccZ; // 4 bytes
    float GyroX; // 4 bytes
    float GyroY; // 4 bytes
    float GyroZ; // 4 bytes
    float AccAngleX; // 4 bytes
    float AccAngleY; // 4 bytes
    float AngleX; // 4 bytes
    float AngleY; // 4 bytes
    float AngleZ; // 4 bytes
    float tempC; // 4 bytes
    int LCell1; // 2 bytes
    int LCell2; // 2 bytes
    int LCell3; // 2 bytes
    int LCell4; // 2 bytes
    long lati; // 4 bytes
    long longi; // 4 bytes
    long odom; // 4 bytes
    byte SIV; // 1 byte
```

```

    long acc;                // 4 bytes
    long alti;              // 4 bytes
};                          // 85 bytes in total

unsigned long startTime = 0;
unsigned long updateCount = 0;
byte LEDstatus=0;
void setup(void) {
    Serial.begin(115200);
    SPI.begin();

    pinMode(LED, OUTPUT);
    pinMode(LED2, OUTPUT);

    Serial.print("Hi, there");
    if (!Serial) {
        // some boards need this because of native USB capability
    }
    Serial.println(F("RF24Network/examples/helloworld_rx/"));

    if (!radio.begin()) {
        Serial.println(F("Radio hardware not responding!"));
        while (1) {
            // hold in infinite loop
        }
    }
    network.begin(90, this_node);

    radio.setPALevel(RF24_PA_MAX); //- power set (RF24_PA_MIN, RF24_PA_LOW,
RF24_PA_HIGH and RF24_PA_MAX)
    radio.setDataRate (RF24_250KBPS); // - 250KBPS, 1MBPS, 2MBPS, data rate

}

void loop(void) {

    network.update();        // network availability checker

    while (network.available()) {

        RF24NetworkHeader header;
        payload_t payload;
        network.read(header, &payload, sizeof(payload));

```

```

/*char counter_text[30];
dtostrf(payload.AccX, 10, 10, counter_text);
char counter_text2[30];
dtostrf(payload.AccY, 10, 10, counter_text2);
char counter_text3[30];
dtostrf(payload.AccZ, 10, 10, counter_text3);

char text[32];
snprintf(text, 32, "%s,%s,%s", counter_text,counter_text2,counter_text3);
Serial.print(text);

char text2[22];
snprintf(text2, 22, "%d,%d,%d,%d,%d", payload.LCell1, payload.LCell2,
payload.LCell3, payload.LCell4, payload.SIV);
Serial.print(text2);

//Serial.print("Received packet #");
Serial.print(",");
Serial.print(payload.counter);
Serial.print(",");
Serial.println(payload.ms);
*/
//Serial.print(" ");

Serial.print(payload.AccX);
Serial.print(" ");
Serial.print(payload.AccY);
Serial.print(" ");
Serial.print(payload.AccZ);
Serial.print(" ");
Serial.print(payload.GyroX);
Serial.print(" ");
Serial.print(payload.GyroY);
Serial.print(" ");
Serial.print(payload.GyroZ);
Serial.print(" ");
Serial.print(payload.AccAngleX);
Serial.print(" ");
Serial.print(payload.AccAngleY);
Serial.print(" ");
Serial.print(payload.AngleX);
Serial.print(" ");

```

```

Serial.print(payload.AngleY);
Serial.print(" ");
Serial.print(payload.AngleZ);
Serial.print(" ");
Serial.print(payload.tempC);
Serial.print(" ");
Serial.print(payload.LCell1);
Serial.print(" ");
Serial.print(payload.LCell2);
Serial.print(" ");
Serial.print(payload.LCell3);
Serial.print(" ");
Serial.print(payload.LCell4);
Serial.print(" ");
Serial.print(payload.lati);
Serial.print(" ");
Serial.print(payload.longi);
Serial.print(" ");
Serial.print(payload.odom);
Serial.print(" ");
Serial.print(payload.SIV);
Serial.print(" ");
Serial.print(payload.acc);
Serial.print(" ");
Serial.print(payload.alti);
Serial.print(" ");

updateCount++;

//Calculate the actual update rate
//Serial.print(F(" Rate: "));
Serial.println( updateCount / ((millis() - startTime) / 1000.0), 2);
//Serial.println(F("Hz"));

int check = LEDstatus;
if (LEDstatus == 1){
digitalWrite(LED, HIGH); // Turn the LED on
digitalWrite(LED2, LOW);
LEDstatus = 0;}
else{
digitalWrite(LED, LOW); // Turn the LED on
digitalWrite(LED2, HIGH);
LEDstatus = 1;
}

```



```
}  
}
```

Transmitter code:

```
#include <RF24.h>  
#include <RF24Network.h>  
#include <SPI.h>  
#include <Wire.h>  
#include <MPU6050_light.h>  
#include "HX711.h"  
#include <TimeLib.h>  
  
#include "SdFat.h"  
SdFat SD;  
#include "sdios.h"  
#include "FreeStack.h"  
  
#include <SparkFun_u-blox_GNSS_Arduino_Library.h>  
  
//GPS  
SFE_UBLOX_GNSS myGNSS;  
unsigned long startTime = 0; //Used to calc the actual update rate.  
unsigned long updateCount = 0; //Used to calc the actual update rate.  
long latitude = 0;  
long longitude = 0;  
long horizAcc = 0;  
long horizSpeed = 0;  
long altitudeH = 0;  
byte SIV = 0;  
//SD card  
File myFile;  
int pinCS = 53; // Pin 10 on Arduino Uno  
//Load cells  
HX711 scale;  
HX711 scale2;  
HX711 scale3;  
HX711 scale4;  
//Radio  
RF24 radio(7, 8); // nRF24L01(+)  
RF24Network network(radio); //  
const uint16_t this_node = 01; // Address in Octal format of the used node in  
const uint16_t other_node = 00; // Address in Octal format of the other node  
const unsigned long interval = 0;  
unsigned long last_sent;
```

```

unsigned long packets_sent;
//Gyro
MPU6050 mpu(Wire);
// Structure of our payload
struct payload_t {
    unsigned long ms;           // 4 bytes
    unsigned long counter;     // 4 bytes
    float AccX;                // 4 bytes
    float AccY;                // 4 bytes
    float AccZ;                // 4 bytes
    float GyroX;               // 4 bytes
    float GyroY;               // 4 bytes
    float GyroZ;               // 4 bytes
    float AccAngleX;           // 4 bytes
    float AccAngleY;           // 4 bytes
    float AngleX;              // 4 bytes
    float AngleY;              // 4 bytes
    float AngleZ;              // 4 bytes
    float tempC;               // 4 bytes
    int LCell1;                // 2 bytes
    int LCell2;                // 2 bytes
    int LCell3;                // 2 bytes
    int LCell4;                // 2 bytes
    long lati;                 // 4 bytes
    long longi;                // 4 bytes
    long odom;                 // 4 bytes
    byte SIV;                  // 1 byte
    long acc;                   // 4 bytes
    long alti;                 // 4 bytes
};                               // 85 bytes in total

void setup(void) {
    Serial.begin(115200);
    Wire.setClock(400000);
    Wire.begin();
    SPI.begin();
    scale.begin(62, 63);
    scale2.begin(64, 65);
    scale3.begin(66, 67);
    scale4.begin(68, 69);

//GPS initialisation
if (myGNSS.begin() == false) //Connect to the u-blox module using Wire port

```

```

    {
        Serial.println(F("u-blox GNSS not detected at default I2C address. Please check
wiring. Freezing."));
        while (1);
    }

myGNSS.setI2COutput(COM_TYPE_UBX);
myGNSS.setNavigationFrequency(25);
uint8_t rate = myGNSS.getNavigationFrequency();
Serial.print("Current update rate: ");
Serial.println(rate);
startTime = millis();
// SD Card Initialization
pinMode(pinCS, OUTPUT);
if (SD.begin())
{
    Serial.println("SD card is ready to use.");
} else
{
    Serial.println("SD card initialization failed");
    return;
}
//Gyro initialization
byte status = mpu.begin();
mpu.calcOffsets(true,true); // gyro and accelero
    if (!Serial) {
        // some boards need this because of native USB capability
    }
Serial.println(F("RF24Network/examples/helloworld_tx/"));
if (!radio.begin()) {
    Serial.println(F("Radio hardware not responding!"));
    while (1) {
        // hold in infinite loop
    }
}
network.begin(90, this_node);
//Radio adjustments
radio.setPALevel(RF24_PA_MAX); //- power set (RF24_PA_MIN, RF24_PA_LOW,
RF24_PA_HIGH and RF24_PA_MAX)
radio.setDataRate (RF24_250KBPS); // - 250KBPS, 1MBPS, 2MBPS, data rate
// HX711 Sesnors calibartion values
scale.set_scale(466); // this value is obtained by calibrating the scale with known
weights;
scale.tare(); // reset the scale to 0

```

```

scale2.set_scale(466); //scale2.set_scale(17416);
scale2.tare();
scale3.set_scale(466); // this value is obtained by calibrating the scale with known
weights;
scale3.tare(); // reset the scale to 0
scale4.set_scale(466); //scale4.set_scale(17416);
scale4.tare();
}
void loop() {
network.update(); // Check the network regularly
mpu.update();
int ww = (int)(scale.get_units());
int ww2 = (int)(scale2.get_units());
int ww3 = (int)(scale3.get_units());
int ww4 = (int)(scale4.get_units());
unsigned long now = millis();

Serial.print(F(" Rate: "));
Serial.print(updateCount / ((millis() - startTime) / 1000.0), 2);
Serial.print(F("Hz "));
updateCount++;

latitude = myGNSS.getLatitude();
longitude = myGNSS.getLongitude();
horizAcc = myGNSS.getHorizontalAccEst();
horizSpeed = myGNSS.getGroundSpeed();
altitudeH = myGNSS.getAltitude();
SIV = myGNSS.getSIV();

payload_t payload = { millis(), packets_sent++, mpu.getAccX(), mpu.getAccY(),
mpu.getAccZ(), mpu.getGyroX(), mpu.getGyroY(), mpu.getGyroZ(),
mpu.getAccAngleX(), mpu.getAccAngleY(), mpu.getAngleX(), mpu.getAngleY(),
mpu.getAngleZ(), mpu.getTemp(), ww, ww2, ww3, ww4, latitude, longitude,
horizSpeed, SIV, horizAcc, altitudeH};
//SD card saving
myFile = SD.open("trip4.txt", FILE_WRITE);

if (myFile) {
myFile.print(payload.counter);
myFile.print(", ");
myFile.print(payload.ms);
myFile.print(", ");
myFile.print(updateCount / ((millis() - startTime) / 1000.0), 2);
myFile.print(", ");

```

```
myFile.print(payload.tempC);
myFile.print(" ");
myFile.print(payload.lati);
myFile.print(" ");
myFile.print(payload.longi);
myFile.print(" ");
myFile.print(payload.odom);
myFile.print(" ");
myFile.print(payload.acc);
myFile.print(" ");
myFile.print(payload.alti);
myFile.print(" ");
myFile.print(payload.SIV);
myFile.print(" ");
myFile.print(payload.AccX);
myFile.print(" ");
myFile.print(payload.AccY);
myFile.print(" ");
myFile.print(payload.AccZ);
myFile.print(" ");
myFile.print(payload.GyroX);
myFile.print(" ");
myFile.print(payload.GyroY);
myFile.print(" ");
myFile.print(payload.GyroZ);
myFile.print(" ");
myFile.print(payload.AccAngleX);
myFile.print(" ");
myFile.print(payload.AccAngleY);
myFile.print(" ");
myFile.print(payload.AngleX);
myFile.print(" ");
myFile.print(payload.AngleY);
myFile.print(" ");
myFile.print(payload.AngleZ);
myFile.print(" ");
myFile.print(ww);
myFile.print(" ");
myFile.print(ww3);
myFile.print(" ");
myFile.print(ww2);
myFile.print(" ");
myFile.println(ww4);
myFile.close();
```

```
    }
    else{
        Serial.println("error can't open the file");
    }
//Radio sending
Serial.print("Sending...");
RF24NetworkHeader header(other_node);
bool ok = network.write(header, &payload, sizeof(payload));
if (ok)
    Serial.println("ok.");
else
    Serial.println("failed.");
}
```

Appendix 2

1. Table of combination of used materials:

Sample no	Material	Infill rate	Heat treatment	Reinforcement cloth / other	Sample weight	Sample width	Sample length	Sample thickness	Support span	Max load	Max defl.	Gradient	Flexural stress	Flexural strain	Flexural modulus Shimadzu	Flexural modulus pandemic tool
		[%]	[°C]		[g]	[mm]	[mm]	[mm]	[mm]	[N]	[mm]	[N/mm]	[MPa]	[%]	[GPa]	[GPa]
1	Clariti resin	-	-	-	12.24	20.30	100.00	5.30	80	388.40	5.02	71.36	81.74	2.5	3.02	3.64
2	PA12-GF - 1	35	-	-	7.6	20.83	100.24	5.03	-	-	-	-	-	-	-	3.67
3	PETG-CF - 1	35	140	linen cloth	12.15	20.31	99.34	5.65	80	411.83	5.01	83.8	76.22	2.7	2.93	1.44
4	PLA - 1	35	-	-	7.7	20.26	99.74	5.18	80	152.03	5.02	30.9	33.56	2.4	1.40	4.09
5	PLA - 2	35	-	fibreglass	12.8	20.3	99.75	5.29	80	373.53	5.02	81	78.90	2.5	3.45	2.33
6	PA12-GF - 2	35	-	fibreglass	11.96	20.8	100.22	5.18	80	213.23	5.02	49.64	45.85	2.4	2.20	1.5
7	PA12-GF - 3	35	-	resin	10.97	20.75	100.64	5.02	80	155.7	5.02	35.92	35.73	2.4	1.75	5.6
8	PETG-CF - 2	35	140	carbon fibre	12.16	20.07	99.02	5.32	80	444.35	3.92	105.74	93.87	2.0	4.48	5.2
9	PETG-CF - 3	35	-	fibreglass	11.89	20.6	100.64	5.13	80	376.45	5.02	90.1	83.33	2.4	4.15	4.07
10	PETG-CF - 4	35	140	fibreglass	11.47	20.29	100.08	5.3	80	386.45	5.02	81.21	81.37	2.5	3.44	3.23
11	PLA - 3	100	-	-	12.07	20.54	100.55	4.86	80	281.48	5.02	56.27	69.62	2.3	3.05	4.99
12	PETG-CF - 5	35	140	kevlar/carbon	12.08	20.63	99.6	5.5	80	405	4.02	94.41	77.88	2.1	3.52	4.1
13	PLA-Cork - 1	35	-	carbon fibre	12.35	20.16	100.06	5.19	80	354.95	5.02	75.83	78.44	2.4	3.44	3.09
14	PETG - 1	35	-	fibreglass	12.43	20.34	99.82	5.17	80	275.76	5.02	60.9	60.87	2.4	2.77	3.57
15	PA12-CF - 1	35	-	fibreglass	11.27	20.84	100.57	5.21	80	288.38	5.02	71.13	61.17	2.5	3.09	2
16	PA12-CF - 2	35	-	resin	10.6	20.66	100.33	5.15	80	197.35	5.02	46.3	43.22	2.4	2.10	1.98
17	PETG-CF - 5	35	-	-	7.34	20.65	99.83	4.97	80	165.18	5.02	37.51	38.86	2.3	1.89	3.54
18	PETG-CF - 6	35	140	resin	11.26	20.7	99.73	5.07	80	307.05	5.02	65.6	69.25	2.4	3.11	13
19	PA12-CF - 3	100	-	carbon fibre	10.54	20.09	99.06	5.23	80	448.3	2.16	192.51	97.90	1.1	8.57	2.98
20	PETG-CF - 7	100	-	-	12.11	20.84	100.4	5.45	80	335.58	5.01	68.6	65.06	2.6	2.60	2.82

21	PA12-CF - 4	35	140	resin	11.5	20.69	100.85	5.2	80	272.88	5.02	63.18	58.53	2.4	2.78	2.41
22	PA12-GF - 4	35	140	fibreglass	12.09	20.86	99.89	5.46	80	277.85	5.01	59.09	53.62	2.6	2.23	1.96
24	PA12-GF - 5	100	-	-	6.55	19.47	99.76	3.95	80	84.98	5.02	23.04	33.57	1.9	2.46	2.12
25	PETG-CF - 8	-	-	hollow	5.04	20.07	99.94	5.4	80	143.28	5.02	47.99	29.38	2.5	1.94	1.54
27	PA6-CF + PA12-CF - 1	35	-	-	5.43	20.5	100.33	4.6	80	110.1	5.01	26.84	30.46	2.2	1.72	1.1
28	PA12-CF - 5	35	-	-	6.88	20.68	100.39	4.8	80	88.28	5.01	23.8	22.23	2.3	1.33	1.18
29	PA12-CF - 6	35	140	-	6.82	20.65	100.41	4.77	80	93.3	5.02	26.96	23.83	2.2	1.54	4.08
30	PETG-CF - 9	35	140	basalt fibre	11.46	20.47	99.8	5.26	80	315.2	4.02	76.39	66.78	2.0	3.28	0.74
31	PA12-CF - 7	35	140	-	5.99	20.45	100.05	4.86	80	69.2	5.02	16.58	17.19	2.3	0.90	0.7
32	PA12-CF - 8	35	-	-	5.89	20.47	100.04	4.91	80	67.88	5.01	16.9	16.51	2.3	0.89	0.7
33	PETG-CF - 10	35	-	-	7.68	20.91	100.56	5.1	80	152.8	5.02	36.03	33.71	2.4	1.66	3.15
34	PETG-CF - 11	35	-	resin	11.68	20.64	100.49	5.4	80	328.65	5.01	69.4	65.53	2.5	2.73	3.22
35	PLA - 4	35	110	resin	12.15	20.14	99.03	5.07	80	288.05	5.02	59.68	66.77	2.4	2.91	3.12
36	PETG - 2	35	140	fibreglass	12.46	20.2	98.61	5.33	80	293.3	4.66	64.26	61.33	2.3	2.69	2.42
37	PETG - 3	35	140	resin	12	20.03	98.1	5.08	80	234.63	5.01	48.34	54.47	2.4	2.36	4.14
38	PLA-HT - 1	35	110	fibreglass	13.1	20.17	99.31	5.49	80	350.2	5.02	83.45	69.13	2.6	3.20	3.44
39	PA12-CF - 9	35	-	fibreglass	10.42	20.56	100.08	5.03	80	245	5.02	62.96	56.52	2.4	3.08	4.99
40	PA12-CF - 10	35	-	carbon fibre	10.83	20.36	100.06	5.47	80	444.65	5.02	95.71	87.59	2.6	3.68	0.73
41	PETG - 4	35	-	-	7.47	20.24	99.7	5.03	80	72.53	5.01	14.79	17.00	2.4	0.73	2.02
42	PA12-CF - 11	35	-	resin	9.71	20.63	100.03	4.93	80	172.75	5.02	39.88	41.34	2.3	2.07	1.46
43	PLA - 5	35	110	-	7.21	20.02	99.05	4.93	80	128.6	5.02	25.99	31.71	2.3	1.39	2.77
44	PLA - 6	35	-	resin	12.68	20.17	99.71	5.42	80	293.88	5.01	59.89	59.52	2.5	2.39	4.08
45	PA12-CF - 12	35	140	fibreglass	11.8	20.68	100.9	5.23	80	348.83	5.01	77.78	74.00	2.5	3.37	3.91
46	PLA - 7	35	-	fibreglass	12.82	20.26	99.75	5.34	80	357.53	5.01	78.71	74.26	2.5	3.27	4.29
47	PLA-Bamboo - 1	35	-	carbon fibre	10.97	20.61	100.29	5.17	80	331.53	4.48	81.09	72.22	2.2	3.64	2.97
48	PA12-CF - 13	35	140	fibreglass	11.13	20.6	99.84	5.29	80	297.33	5.02	63.88	61.89	2.5	2.68	1.06
49	PETG - 5	35	140	-	7.38	19.93	97.35	4.71	80	83.7	5.01	16.89	22.72	2.2	1.04	2.27

50	PA12-CF - 14	35	140	resin	10.72	20.47	99.8	5.1	80	206.03	5.02	46.33	46.44	2.4	2.18	4.58
51	PLA - 8	35	110	fibreglass	12.73	20.14	98.27	5.34	80	407.45	5.02	82.16	85.14	2.5	3.43	1.45
52	PLA - 9	35	-	-	7.51	20.15	99.91	4.94	80	126.93	5.02	26.39	30.98	2.3	1.39	0.54
53	PA12-GF - 6	35	140	-	7.54	20.79	99.97	5.14	80	60.3	5.02	14.23	13.17	2.4	0.65	1.94
54	PA12-GF - 7	35	140	resin	11.56	20.89	99.82	5.26	80	202.93	5.02	45.98	42.13	2.5	1.94	1.77
55	PLA - 10	35	110	-	7.68	20.01	97.93	5.16	80	175.7	5.01	35.9	39.57	2.4	1.67	3.31
56	PLA - 11	35	-	resin	12.5	20.23	99.85	5.2	80	324.2	5.02	65	71.12	2.4	2.92	4.18
57	PLA - 12	35	110	fibreglass	13.29	20.13	98.95	5.44	80	382.93	5.01	87.45	77.14	2.6	3.45	2.08
58	PETG - 6	35	-	resin	12.26	20.12	99.71	5.23	80	219.63	5.01	45.54	47.89	2.5	2.03	3.31
59	PLA - 13	35	110	resin	12.19	20.02	98.75	5.3	80	343.08	5.01	68.86	73.21	2.5	2.96	5.93
61	XPS foam - 1	-	-	kevlar	4.68	19.82	99.6	5.11	80	370.25	3.14	97.16	85.85	1.5	4.70	6.29
62	XPS foam - 2	-	-	basalt fibre	4.67	19.74	99.76	5.06	80	237.3	3.29	94.49	56.34	1.6	4.73	11.44
63	XPS foam - 3	-	-	carbon fibre	4.32	19.8	99.76	5.01	80	313	2.73	93.91	75.58	1.3	4.83	24.19
64	Basalt fibre - 1	-	-	25 layers	19.23	19.91	99.56	5.07	80	449.13	2.03	204.83	105.31	1.0	10.10	
65	PA6-CF - 1	35	-	wet	7.21	20.59	100.13	5.1	80	25.94	5.02	13.07	5.81	2.4	0.61	
66	PA6-CF - 2	100	-	wet	9.56	20.47	100.37	4.59	80	323.68	5.02	77.8	90.06	2.2	5.03	
67	PLA - 14	100	-	fibreglass tape	11.96	19.6	99.02	4.97	80	239.73	5.01	49.33	59.42	2.3	2.62	
68	PLA - 15	100	210	remelted	13.34	20.28	100	6.42	80	195.38	5.02	56.92	28.05	3.0	1.36	
69	PA12-CF - 15	100	-	fibreglass tape	9.49	20.99	100.79	4.97	80	253.05	5.01	56.86	58.57	2.3	2.82	
70	PETG-CF - 12	100	240	remelted	11.43	20.08	100.34	5.19	80	321.68	5.02	69.7	71.37	2.4	3.18	
71	PA12-CF - 16	100	-	fibreglass tape	10.12	20.82	100.56	5.03	80	215.63	5.01	57.23	49.12	2.4	2.76	
72	PA12-CF - 17	100	240	-	8.95	19.88	97.57	4.64	80	395.25	5.02	80.99	110.82	2.2	5.22	
73	PETG-CF - 13	100	-	fibreglass tape	11.64	20.19	99.86	5.19	80	364.68	5.02	78.79	80.47	2.4	3.57	
74	PA12-CF - 18	100	240	fibreglass tape	9.28	20.52	100.12	4.39	80	330.35	5.02	67.15	100.24	2.1	4.95	
75	PA12-CF - 19	100	-	fibreglass tape	9.4	20.91	100.72	4.87	80	203.45	5.02	52.82	49.23	2.3	2.80	
76	PA6-CF - 3	100	-	fibreglass tape	9.87	21.27	100.43	5.01	80	410.35	5.02	92.97	92.23	2.4	4.45	
77	PETG-CF - 14	100	240	fibreglass tape	11.68	20.06	99.86	5.41	80	386.13	5.01	71.68	78.92	2.5	2.89	
78	PLA-Cork - 1	100	210	remelted	11.85	19.89	100	6.16	80	159.58	4.4	46.26	25.37	2.5	1.27	

79	PLA - 16	100	210	remelted	12.98	20.32	100	5.64	80	288.58	4.54	59.34	53.58	2.4	2.08
80	PLA - 17	100	-	carbon fibre	12.01	19.88	99.05	4.85	80	254	5.02	47.14	65.18	2.3	2.66
81	PLA - 18	100	-	-	11.54	19.39	99.21	4.96	80	250.48	5.02	51.82	63.01	2.3	2.80
82	PA12-CF - 20	100	-	basalt fibre	9.15	20.89	100.66	4.84	80	208.6	5.02	46.69	51.15	2.3	2.52
83	PA6-CF - 4	100	-	carbon fibre	9.02	20.13	100.08	4.82	80	440.6	5.78	91.04	113.05	2.6	5.17
84	PA6-CF + PA12-CF - 2	35	-	-	5.14	20.42	100.24	4.58	80	83.4	5.01	20.57	23.36	2.2	1.34
85	PA6-CF - 5	35	-	-	7	20.57	100.24	4.96	80	219.08	5.01	56.66	51.95	2.3	2.89
86	PA12-CF - 21	100	-	70% flow rate	9.37	20.29	99.9	4.43	80	136.68	5.02	37.22	41.19	2.1	2.70
87	PA6-CF - 6	100	-	80% flow rate	7.79	20.27	100.08	4.72	80	402.13	4.65	94.69	106.86	2.1	5.69
88	PA6-CF - 7	100	-	70% flow rate	8.26	20.05	100.59	4.55	80	401.55	4.74	87.67	116.09	2.0	5.94
89	PA6-CF - 8	35	-	fibreglass	6.38	19.92	100	4.77	80	212.58	3.91	76.3	56.28	1.7	4.52
90	PA6-CF - 9	100	-	60% flow rate	7.13	19.78	99.75	4.34	80	291.95	4.26	80.57	94.03	1.7	6.38
91	PA6-CF - 10	35	-	80% flow rate	6	19.84	99.72	4.71	80	333	5.01	80.21	90.79	2.2	4.95
92	Kinetix R118 resin - 1	-	-	-	9.46	20.2	100	3.99	80	154.56	4.71	34.92	57.67	1.8	3.48
93	Kinetix R118 resin - 2	-	-	fibreglass	13.18	20.24	100.32	5.14	80	444.58	3.73	92.43	99.77	1.8	4.30
94	Kinetix R118 resin - 3	-	-	-	9.65	20.35	100	3.92	80	92.85	2.83	33.74	35.63	1.0	3.52
95	Clariti resin - 2	-	-	-	10.37	19.94	99.33	4.42	80	183.3	5.01	39.51	56.46	2.1	2.94
96	Kinetix R118 resin - 4	-	-	kevlar	11.45	21.08	100.54	5.11	80	351.55	5.02	67.61	76.64	2.4	3.08
97	Carbon fibre - 1	-	-	hollow	3.88	19.64	98.88	6.8	80	173.18	1.72	131.83	22.88	1.1	2.73
98	West System 105 - 1	-	-	fibreglass	9.1	19.97	99.55	3.65	80	180.75	5.01	34.03	81.53	1.7	4.49
99	PA12-CF - 22	50	-	carbon fibre	11.84	20.17	100.19	5.32	80	382.6	5.02	46.79	80.43	2.5	1.97
100	PA12-CF - 23	45	-	carbon fibre	11.98	20.26	100.53	5.23	80	442.5	5.01	91.62	95.82	2.5	4.05
101	PA12-CF - 24	35	-	carbon fibre	12.12	20.01	100.11	5.48	80	431.13	5.01	78.46	86.10	2.6	3.05
102	Clariti resin - 3	-	-	carbon fibre	4.87	20.44	99.8	1.94	80	207.53	5.01	41.73	323.73	0.9	35.79
103	West System 105 - 2	-	-	carbon fibre	10.33	19.9	99.62	5.06	80	442.5	5.68	77.33	104.22	2.7	3.84
104	Kinetix R118	-	-	basalt fibre	11.59	20.51	100.23	4.04	80	447.03	5.01	68.82	160.25	1.9	6.51

	resin - 5														
105	West System 105 - 3	-	-	basalt fibre	9.86	20.05	99.55	4	80	223.1	5.01	44.94	83.45	1.9	4.48
106	West System 105 - 4	-	-	-	11.39	20.1	99.6	4.8	80	254.75	5.02	51.79	66.01	2.3	2.98
107	Clariti resin - 4	-	-	-	11.17	19.94	99.54	4.99	80	230.55	5.02	44.97	55.72	2.3	2.32
108	Kinetix R118 resin - 5	-	-	carbon fibre	12.74	20.99	100.39	5.03	80	446.83	4.64	152.22	100.97	2.2	7.29
110	Prepreg - 1	-	-	hollow	8.43	23.05	100.62	4.94	80	447.45	2.51	153.61	95.46	1.2	7.08
111	PU foam - 1	-	-	prepreg	8.4	23.08	99.87	5.09	80	447.7	2.54	159.71	89.85	1.2	6.72
112	PA12-CF - 25	35	150	prepreg	11.76	22.71	99.75	5.27	80	449.9	2.04	197.28	85.60	1.0	7.60
113	PA12-CF - 26	35	150	prepreg	11.97	22.1	100.96	5.22	80	449.25	2.23	179.62	89.52	1.1	7.31
114	PA12-CF - 27	35	150	prepreg	9.97	22.4	100.67	5.25	80	448.58	2.31	165.47	87.19	1.1	6.53
116	PA12-CF - 28	100	150	prepreg	10.7	20.29	99.74	4.86	80	449.78	2.05	179.7	112.62	0.9	9.88
117	PA12-CF - 29	100	150	prepreg	10.54	20.04	100.15	4.89	80	447.7	2.23	166.72	112.11	1.0	9.11
118	PA12-CF - 30	100	150	prepreg	11.15	20.34	100.42	5.11	80	449.73	2.11	168.88	101.61	1.0	7.96
119	PA12-CF - 31	100	150	prepreg	10.34	20.02	98.24	4.92	80	449.13	2.29	166.33	111.21	1.1	8.93
120	PA12-CF - 32	100	150	prepreg	10.55	20.23	97.79	4.81	80	449.03	2.11	179.25	115.13	1.0	10.19
121	PA6-CF - 11	100	150	prepreg	10.5	19.97	99.66	4.49	80	449.68	2.2	169.05	134.03	0.9	11.97
122	PA6-CF - 12	100	150	prepreg	10.37	20.01	99.6	4.44	80	449.63	2.16	173.64	136.78	0.9	12.69
123	PA6-CF - 13	100	150	prepreg	10.44	20.19	100.15	4.52	80	448.08	2.17	175.12	130.35	0.9	12.02
124	PA6-CF - 14	100	150	prepreg	10.47	20	99.22	4.48	80	449.25	2.26	164.58	134.30	0.9	11.71
125	PA6-CF - 15	100	150	prepreg	10.56	20.06	99.47	4.53	80	450	2.2	172.05	131.18	0.9	11.81
126	PA6-CF - 16	35	150	prepreg	8.53	20.02	98.51	4.67	80	448.2	2.28	173.02	123.18	1.0	10.86
127	PA6-CF - 17	35	150	prepreg	8.74	20.06	98.87	4.67	80	449.05	2.2	184.51	123.17	1.0	11.56
128	PA6-CF - 18	35	150	prepreg	8.6	20.05	99.85	4.64	80	448.88	2.24	176.64	125.87	1.0	11.29
129	PA6-CF - 19	35	150	prepreg	8.12	20.2	99.45	4.16	80	447.4	2.74	129.88	159.66	1.0	11.43
130	PA6-CF - 20	35	150	prepreg	8.63	20.18	102.72	4.15	80	447.45	2.68	130.24	172.27	1.0	11.56
131	PLA - 19	100	-	PLA sensor	12.33	20.45	110.6	4.70	80	257.4	5.01	49.66	68.37	2.2	2.99
132	PLA - 20	100	-	TPU sensor	12.28	20.55	110.3	4.55	80	255.5	5.01	48.91	72.07	2.1	3.23

133	PA12-CF – 34	100	-	PLA sensor	9.55	20.3	110.3	4.79	80	113.4	5.01	29.85	29.22	2.3	1.71
134	PA12-CF – 35	100	-	TPU sensor	9.53	20.1	110.2	4.82	80	103.9	5.01	25.94	26.7	2.3	1.48
135	PA6-CF – 21	100	-	PLA sensor	9.36	19.88	109.7	4.92	80	256.6	5.01	64.71	63.99	2.3	3.50
136	PA6-CF – 22	100	-	TPU sensor	9.31	19.89	109.2	4.73	80	260.6	5.01	66.72	70.27	2.2	4.06

